CNTs based nanofluids over a stretchable surface

By

Shafiq Ahmad

Department of Mathematics

Quaid-i-Azam University
Islamabad, Pakistan
2021

CNTs based nanofluids over a stretchable surface

By

Shafiq Ahmad

Supervised By

Prof. Dr. Sohail Nadeem

Department of Mathematics
Quaid-i-Azam University
Islamabad, Pakistan
2021

CNTs based nanofluids over a stretchable surface

By

Shafiq Ahmad

A DISSERTATION SUBMITTED IN THE PARTIAL FULFILLMENT OF THE
REQUIREMENT FOR THE DEGREE OF

DOCTOR OF PHILOSOPHY

IN

MATHEMATICS

Supervised by

Prof. Dr. Sohail Nadeem

Department of Mathematics
Quaid-i-Azam University
Islamabad, Pakistan
2021

CERTIFICATE

CNTs based nanofluids over a stretchable surface

By

Shafiq Ahmad

A THESIS SUBMITTED IN THE PARTIAL FULFILLMENT OF THE
REQUIREMENTS FOR THE DEGREE OF THE

DOCTOR OF PHILOSOPHY IN MATHEMATICS

We accept this thesis as conforming to the required standard

1. _____
   Prof. Dr. Sohail Nadeem
   (Chairman)

2. _____
   Prof. Dr. Sohail Nadeem
   (Supervisor)

3. _____
   Dr. Rahmat Ellahi
   (External Examiner)

4. _____
   Dr. Noreen Sher Akbar
   (External Examiner)

Department of Mathematics, International
Islamic University, H-10, Islamabad.

Department of Basic Humanities CE&ME,
(NUST) Peshawar Road Rawalpindi

Department of Mathematics
Quaid-i-Azam University
Islamabad, Pakistan
2021

Certificate of Approval

This is to certify that the research work presented in this thesis entitled **CNTs based nanofluids over a stretchable surface** was conducted by **Mr. Shafiq Ahmad** under the kind supervision of **Prof. Dr. Sohail Nadeem**. No part of this thesis has been submitted anywhere else for any other degree. This thesis is submitted to the Department of Mathematics, Quaid-i-Azam University, Islamabad in partial fulfillment of the requirements for the degree of Doctor of Philosophy in field of Mathematics from Department of Mathematics, Quaid-i-Azam University Islamabad, Pakistan.

Student Name: **Shafiq Ahmad**   Signature:_____

External committee:

   a) **External Examiner 1**:   Signature:_____
      Name: **Dr. Rahmat Ellahi**
      Designation: Associate Professor
      Department of Mathematics, International Islamic University, H-10, Islamabad

   b) **External Examiner 2**:   Signature:_____
      Name: **Dr. Noreen Sher Akbar**
      Designation: Associate Professor
      Department of Basic Humanities CE&ME, (NUST) Peshawar Road Rawalpindi

   c) **Internal Examiner**   Signature:_____
      Name: **Prof. Dr. Sohail Nadeem**
      Designation: Professor
      Office Address: Department of Mathematics, QAU Islamabad.

   Supervisor Name: Signature:_____
   Prof. Dr. Sohail Nadeem

   Name of Dean/ HOD   Signature:_____
   Prof. Dr. Sohail Nadeem

Author's Declaration

I, **Shafiq Ahmad,** hereby state that my PhD thesis titled **CNTs based nanofluids over a stretchable surface** is my own work and has not been submitted previously by me for taking any degree from the Quaid-I-Azam University Islamabad, Pakistan or anywhere else in the country/world.

At any time if my statement is found to be incorrect even after my graduate the university has the right to withdraw my PhD degree.

Name of Student: **Shafiq Ahmad**

Date: **20-October-2021**

Plagiarism Undertaking

I solemnly declare that research work presented in the thesis titled "**CNTs based nanofluids over a stretchable surface**" is solely my research work with no significant contribution from any other person. Small contribution/help wherever taken has been duly acknowledged and that complete thesis has been written by me.

I understand the zero-tolerance policy of the HEC and **Quaid-i-Azam University** towards plagiarism. Therefore, I as an Author of the above titled thesis declare that no portion of my thesis has been plagiarized and any material used as reference is properly referred/cited.

I undertake that if I am found guilty of any formal plagiarism in the above titled thesis even afterward of PhD degree, the University reserves the rights to withdraw/revoke my PhD degree and that HEC and the University has the right to publish my name on the HEC/University Website on which names of students are placed who submitted plagiarized thesis.

Student/Author Signature

Name: **Shafiq Ahmad**

<u>ACKNOWLEDGEMENT</u>

Dedicated to

My Beloved Parents,

Brothers, Sister

And

Wife

Contents

List of Tables

List of Figures

4

Nomenclature

	Nomenclature		
u	velocity component along x-axis	x, y	Cartesian coordinates
v	velocity component along y-axis	N_1, N_2	Micro-rotation component in x, y direction.
$Q(x)$	volumetric rate of heat source	$f'(\eta), G'(\eta)$	Dimensionless velocity profiles
k_{nf}, k_{hnf}	thermal conductivity	$h_1(\eta), h_2(\eta)$	Dimensionless micro-rotation components
k^*	Mean absorption coefficient	$g(\eta)$	Dimensionless concentration profile
M	Magnetic parameter	$q'(\eta)$	Dimensionless induced magnetic field profile
n^*	Micro-gyration parameter	SWCNTs	Single wall carbon nanotubes
k_r	Reaction rate constant	MWCNTs	Multi wall carbon nanotubes
k	Boltzmann constant	H_2O	water
K^{**}	permeability of porous medium	ODE	Ordinary Differential Equations
F^{**}	non-uniform inertia coefficient	U_w, u_e	Velocity at boundary
K	Micropolar parameter	W_c	cell swimming speed
E	Activation energy	D_m	microorganism diffusivity
n_H	conjugate parameter	b^*	chemotaxis constant
u_e	free stream velocity of the fluid	S_b	bioconvection Schmidt number
$B(x)$	strength of magnetic field	P_e	bioconvection Peclet number
m, c, b_2, d, b_1, e	Constant	N_r	buoyancy ratio parameter
N_c	bioconvection Rayleigh number	**Greek symbols**	
D_c	Heat generation coefficient	β_T	volumetric thermal expansion
Pr	Prandtl number	β_C	volumetric concentration expansion
S_1, S_2	Thermal and solutal stratification parameter	ρ_{nf}, ρ_{hnf}	density of the nanofluid

A, B	Velocity and thermal slip parameter respectively	$(\rho C_p)_{nf}, (\rho C_p)_{hnf}$	Nanofluid heat capacity
Be	Bejan number	μ_{nf}, μ_{hnf}	dynamic viscosity
g^*	Gravitational acceleration	$\sigma_{hnf}, \sigma_{nf}$	Electric conductivity
S_c	Schmidt number	$\alpha_{nf}, \alpha_{hnf}$	modified thermal diffusivity
D_B	mass diffusivity	γ_{nf}	Spin gradient viscosity
j	Micro-rotation density	σ^*	Stefan Boltzmann constant
$N_1(x)$	Variable slip factor	δ	Temperature difference parameter
$D_1(x)$	Variable thermal factor	Ω^*	Wedge angle
Br	Brinkman number	κ	Coefficient of vortex viscosity
M_1	reciprocal magnetic Prandtl number	β_e, β_i	Hall and ion slip parameter
L	diffusive constant parameter	β	Hartree parameter
N_s	Entropy generation rate	α_2	Concentration difference parameter
P_m	Porosity parameter	ϕ_1, ϕ_2	Solid volume fraction
F_r	Inertia coefficient	θ_r	Variable viscosity
E_c	Eckert number	τ_T	Relaxation time factor
R_d	Thermal radiation	λ_m	Mixed convection parameter
C_f	surface drag force	λ	Wedge parameter
Nu_x	Local Nusselt number	γ_c	Thermal relaxation time parameter
Sh_x	Local Sherwood number	γ^*	Navier's slip length
Re_x	local Rayleigh number	μ_0	magnetic permeability
T_r	Temperature ratio parameter	τ_w	shear stress
T	Temperature field	$\theta(\eta)$	Dimensionless temperature profile
T_w, C_w	temperature and concentration at surface	ξ	critical shear rate
T_∞, C_∞	ambient temperature and concentration	ε_1	mass diffusivity parameter
R_c	Reaction parameter	μ_e	Magnetic diffusivity

1 Chapter1

Introduction

Nanofluid has wide range of application in several crucial areas such as transportation, microelectronics, microfluidics, medical, manufacturing, power saving; all of these elements minimize process time and increase heat ratings as well as extend the life span of machinery and so on. Nanofluids are being used as coolants in the thermal exchange systems of automobiles and nuclear reactors. Nanofluids are essentially a combination of suspended ultra-fine nanoparticles flooded into different regular fluids like oil, water, engine oil, ethylene glycol etc. The nano-sized particles are compose of single and multiple wall carbon nanotubes (SWCNTs, MWCNTs), metal (Cu, Al, Fe), carbide (SiC, and TiC), metal oxide (Al_2O_3, CuO), and some other nano-scale fluid droplets. The size of nanoparticles is commonly 1-100 nm, but it can contrast slightly as demonstrated by their size and shape. Choi and Eastman [1] was the first one to introduce the concept of nanofluids. In all these wide applications, nanofluids have found to be able to manage the significant critical issues by improving the efficient heat transfer capability of fluid material at lower cost. Nanotechnology is expected to serve as an efficient and effective heat transfer medium due to its flexible physical and thermo-physical features including, thermal conductivity or heat capacitance and effective density. Several studies in the field of nanofluid have participated after Choi, mention is made to some very relevant and significant studies. The numerical descriptions of various-shaped copper nanoparticles across a flat surface to increase rate of heat transfer were discussed by Saleem et al. [2]. Lu [3] scrutinized the carbon nanotubes (CNTs) with energy activation and heat generation and numerically solved by utilizing the shooting technique. Hussain et al. [4] using the rotating sheet to examine the water driven flow of carbon nanotubes (CNTs). He found that the impact of rotation causes the drag increase and declines the Nusselt number irrespective of the other related parameters. Shahzadi

et al. [5] discussed the influence of single wall carbon nanotube (SWCNT) in peristaltic flow past a permeable annulus. Sheikholeslami et al. [6] reported a detailed method for modeling melting acceleration by utilizing stretching sheet in the presence of copper oxide nanoparticles. In Borehole heat exchangers, Diglio et al. [7] propose a geophysical use of nanofluid as a heat transporter. In place of traditionally using liquids such as water and glycol mixtures, they performed a numerical analysis to test the procedure of various nanofluids. The goal of this thesis was to establish a medium that could effectively lessen the borehole thermal resistance. They researched the problem using a variety of solid materials, including alumina, copper, silver, and others, and observed that a copper-based nanofluid decreases the thermal resistance of boreholes significantly. One of the forms of solid nanoparticles which are widely used in the nanofluid as a solid component is carbon nanotubes. These nanoparticles are cylindrical nanostructures and have considerable implementations such as solar collection, drugs delivery system, catalyst supports, non-porous filters, vascular stunts, electrostatic dissipation, filtration devices for water and air, etc. In comparison to several other solid constituents of nonliquids, such materials have very specific thermo-physical properties. In contrast to metallic nanoparticles, carbon nanotubes (CNTs) are less dense, though they have greater thermal conductivity. Above all, all these items are environmentally friendly. Ahmed et al. [8] examine the CNT-based magneto-hydrodynamics (MHD) nanoliquid flow above a permeable shrinking surface with temperature dependent viscosity. Further expending the Keller box method, the numerical solution is acquired. Akbar et al. [9] discuss the stagnation point flow of CNTs with convective boundary condition and slip impact through a stretching sheet. Haq et al. [10] explore the feature of carbon nanotube nanofluid flow past a stretching sheet in the incidence of partial slip and magneto-hydrodynamics. Nasir et al. [11] addressed the novel phenomenon of Magneto hydrodynamic three-dimensional rotating nanofluid flow in the involvement of single wall carbon nanotubes

(SWCNT) via a stretch sheet. Saba et al. [12] utilized the shooting technique to solve the numerical solution of two-dimensional radiation nanofluid flow in the presence of carbon nanotubes through a curved sheet. Lately, a new group of nanofluids, known as hybrid nanofluids, have been developed and studied, which are formed by mixing different kinds of nanoparticles into the regular liquid. The purpose of implementing hybrid nanofluids is to get the constituent material properties. The thermal conductivity of hybrid nanofluid is improved analogous to individual nanofluids, chemical stability, physical strength, and mechanical resistance. An individual material does not acquire all the affirmative aspects needed for an appropriate objective; it may have specific rheological or thermal characteristics. In real applications, it is a mandatory trade-off between many characteristics and that is where hybrid nanofluids are used. Another important point about recent models (analog) is their validity and reliability. Chen et al. [13] discussed the hybrid nanoliquid by scattering nanoparticles i.e., MWCNT and Fe_2O_3 in water. Madhesh et al. [14] discussed the $Cu–TiO_2$ hybrid nanofluid rheological characteristic and convective heat transfer experimentally. Sundar et al. [15] have experimentally measured the friction drag and convective heat transfer for the produced turbulent flow of multi wall carbon nanotubes and Fe_3O_4 based hybrid nanofluids moving through a circular tube. Through an experimental analysis, Zadkhast et al. [16] created a new comparison to estimate MWCNT–CuO/water hybrid nanofluid's thermal conductivity. Nadeem et al. [17] used numerical simulations to scrutinize the characteristic of heat transfer in the existence of CNT based hybrid nanofluid. It should be realized that the solid volume fraction improves the temperature and velocity distribution. The attributes of heat transfer play a notable role in industrial processes, engineering and physics problems including space cooling, energy production, nuclear reactor cooling, biomedical applications, for example, heat conduction in tissues, magnetic drug targeting and so on and numerous others. Therefore, controlling the heat transfer rate can certainly build up the efficiency of

numerous processes deal in electronic cooling and heat exchangers. In such a manner, thermal relaxation time is a commonly used parameter which is implemented to control and evaluate the required time for transfer of heat from heated region. In previously mentioned works [18–19], the thermal relaxation time is generally taken as unchanged factor. However, realistic situations insist variable feature from this time factor. This time factor is inversely proportional to temperature. Cattaneo [20] studied comprehensively on conduction of heat transport in order to remove the shortage in Fourier's law of heat conduction. One of the crucial shortages in Fourier's law of heat conduction is that it creates a parabolic energy equation that means that the system under contemplation would suddenly be affected by an initial disturbance. So Cattaneo [20] presented the thermal relaxation time to modify the heat conduction law of Fourier, which tolerates the transference of heat with the assistance of thermal wave propagation followed by a limited velocity. Later, by evaluating the upper-convected derivative of Oldroyd's, Christov [21] provided a material invariant structure of the Cattaneo model. Shah et al. [22] used the Cattaneo–Christov heat flux approach to explore CNT-based nanofluid flow across a stretchable sheet. The analytic technique homotopy analysis method (HAM) was manipulated to resolve the highly nonlinear ordinary differentials equation. Han et al. [23] found the analytic solution for coupled flow in the presence of Cattaneo–Christov theory with velocity slip condition. The generalized Fourier law model application is shown in Refs. [24 – 31].

Non-Newtonian fluids have a great interest of scientists because of its several engineering and industrial applications. The flow dynamics of non-Newtonian liquids is the nonlinear affiliation among the shear stress to shear rate. The micropolar fluids are those fluids which have their microstructures and they have non-Newtonian liquid models. Micropolar liquid is to be part of non-symmetric stress tensor. Micropolar fluids are hanging in viscous medium having their own spin and rotation. The rotation

11

and shrinking are the micro size effects of micropolar fluid. In micropolar fluids, the small volume element of a rigid particle will spin around the centroid of the volume element. They are acceptable for animal blood, exocitic lubricants, bubby liquids, colloidal, certain biological fluids and liquid crystals. Kumari and Nath [32] have researched the time-dependent boundary layer flow of micropolar fluids at stagnation points. The impressive aspects of micropolar fluid application and theory can be identified with in works of Eringen [33] and Lukazewicz [34]. Nadeem et al. [35] analyzed the 3D micropolar nanoliquid flow with magnetic field through an exponential stretching sheet. Further, Nadeem et al. [36] discussed over a moving cylinder the micropolar nanofluid with axisymmetric stagnation flow. Balram and Sastry [37] analyzed over a parallel plate vertical channel the free convection flow of a micropolar fluids. Das [38] highlighted the impact of an MHD and partial slip on micropolar nanoliquid flow above a shrinking surface. The feature of heat transfer in non- Newtonian nanofluids is explained in Refs. [39–41].

The analysis of the magnetic properties and performance of electrically conducting liquids is magnetohydrodynamics (magneto-fluid dynamics or hydro-magnetics as well; MHD). Plasmas, salt water, liquid metals, or electrolytes consist of examples of such magneto-liquids. The term ''magneto-hydrodynamics'' is derived beyond magneto—meaning magnetic field, hydro—that means water, then dynamics that means movement. Alfvén [42] was first time in 1942 started the concept of magnetohydrodynamics (MHD) for which in 1970 he got the Nobel Prize in Physics. A few applications about the phenomena of hydro magnetic (MHD) might be viewed in [43–46]. Ishak et al. [47] investigate the heat transfer flow past stretching cylinder in the occurrence of MHD. Sheikholeslami et al. [48] explore the influence of magnetohydrodynamics nanofluid flow and thermal radiation through between two horizontal plates. Haq et al. [49] consider the heat impact of slip effects and thermal

radiation through a stretching surface on magnetohydrodynamics (MHD) stagnation point flow. Nadeem et al. [50] calculated the Casson nanofluid flow of magnetohydrodynamics with a convective boundary condition across a stretch surface. Su et al. [51] using the permeable wall to find the approximate solution of magnetohydrodynamics (MHD) Falkner–Skan flow. Yousif et al. [52] investigate the MHD Carreau nanofluid flow past an exponentially stretched plate in the existence of thermal radiation and heat source/sink.

It is known that during every thermal process, the entropy age estimates the amount of irreversibility. Cooling and heating are an important event in many industrial sectors and in the engineering process, especially in energy and electronic devices. Therefore, to avoid any irreversibility losses that may influence system efficiency, it is essential to minimize entropy production. To control entropy optimization, Bejan [53, 54] first concluded an excellent number as the proportion between thermal irreversibility and total heat loss because of liquid frictional factors, that is called Bejan number (Be). Bhatti et al. [55] analyzed the entropy age (or generation) on the interaction of nanoparticle over a stretching sheet saturated in porous medium. Successive linearization technique and Chebyshev spectral collocation scheme are employed to describe the numerical solution for Bejan number and entropy profile. Feroz et al. [56] demonstrate the magnetohydrodynamics (MHD) nanofluid flow of CNTs along with two parallel rotating plates under the impact of ion-slip effect and Hall current. Shahsavar et al. [57] numerically investigate the entropy generation characteristic of $Fe_3O_4/CNT - water$ hybrid nanofluid flow inside a concentric horizontal annulus. The rapid development of using $MWCNT/GNPs$ hybrid nanofluids in the area of heat transfer addressed by Hussien et al. [58] has been driven by huge changes in nanofluid thermo - physical properties over traditional fluids. Ellahi et al. [59] analyzed the performance of hydro-magnetic (MHD) heat transfer flow together under impact of entropy production as a

result of slip past a moving flat plate. Lu et al. [60] examine the entropy optimization and thermal radiation in the flow of hybrid nanoliquid over a curved sheet. The MATLAB function bvp4c is utilized to resolve the numerical solution.

Introduced by Markin [61] that the distribution of temperature is indicated by four heat transfer methods, i.e., (1) prescribed or constant heat, (2) prescribed or constant surface temperature, (3) combination of boundary conditions, and (4) Newtonian heat, where the rate of heat transfer from the finite heat capacity surface is proportionate to the temperature of the local surface and is commonly referred to as the conjugate convective flow. Due to their vast practical implementation including in convection flows, where heat is consumed by surfaces via radiation, conjugate heat transfer around fins, and to design heat exchanger, several scholars have recently used the influence of Newtonian heating. Lesnic et al. [62, 63] and Pop et al. [64] observed Newtonian heating on a horizontal and vertical sheet inserted in a porous medium with free-convection boundary layer. Nadeem et al. [65] analyzed the characteristic of heat transfer in viscoelastic fluid through an exponential stretching sheet with Newtonian heating. Suleman et al. [66] explored the role of Newtonian heating, with homogeneous heterogeneous reaction, of thermal radiation in the water-silver nanoliquid flow.

Keeping the above importance factors in mind, the current thesis contains of seven chapters in which **chapter 1** is dedicated to the introductory part, while others are listed below:

Chapter 2 is analyzed to "**Mathematical analysis of Falkner – Skan problem with double stratification**". In this chapter deliberates the importance of single wall carbon nanotube (SWCNTs) and multiple walls carbon nanotube (MWCNTs) over a static wedge with magnetohydrodynamics (MHD). The impact of thermal radiation, activation energy, heat generation and double stratification are also added. The set of differential equations is numerically evaluated using the bp4c tool in MATLAB. The

upshot of sundry variable on velocity, temperature, and concentration field are deliberated and calculated graphically. The chapter's content is published in " **Physica A: Statistical Mechanics and its Applications 547 (2020): 124054**".

Chapter 3 is studied to **"Heat transfer analysis and entropy generation in the SWCNT-MWCNT hybrid nanofluid flow"**. In this chapter the analysis of the transfer of heat of SWCNT – MWCNT/Water hybrid nanofluid with temperature dependent viscosity above a moving wedge are discussed. The Darcy-Forchheimer relationship specifies the nature of the flow in the porous medium. The second law of thermodynamics is utilized to measure the irreversibility factor. The numerical technique bvp4c are integrated to solve the highly nonlinear differential equation. For axial velocity, temperature profile, and entropy generation, a comparison was made between simple nanofluid and hybrid nanofluid. The chapter's content is available in " **Applied Nanoscience 10 (12): 5107-5119**".

Chapter 4 is considered to **"Impact of slip effects on the stagnation point nanofluid flow via Cattaneo – Christov heat flux"**. The main focus of this chapter is Cattaneo-Christov theory with temperature dependent thermal relaxation time and entropy production. The micropolar fluid with absorption of heat in the existence of mixed convection and partial slip are scrutinized. Two distinct nanoparticles (SWCNT, MWCNT) is immerged in micropolar fluid to interrogate the feature of mass and heat transfer. The non-dimensional similarity transformation is employed to transform the differential equations to nonlinear ordinary differential equations (ODEs) and associated coupled equations resolved numerically consuming bvp4c from Matlab. The chapter's content is published in " **Journal of Thermal Analysis and Calorimetry (2020): 1-13.**".

Chapter 5 is scrutinized to "**Analysis of two phase fluid flow in presence of Thomson and Troian slip condition**". In this chapter entropy generation in stagnation point flow

of a hybrid nanofluid past a nonlinear permeable stretching sheet with Thompson and Troian boundary condition are considered. We considered SWCNT and MWCNT with water as a regular liquid to discuss the hybrid nanofluid. The numerical method, i.e., bvp4c from Matlab, is operating to answer the converted ordinary differential equations (ODEs). The difference between a simple nanofluid and a hybrid nanoliquid is graphically illustrated. The properties of the involved parameter on different profiles are examined graphically and in tables. The chapter's content is published in "**Applied Nanoscience (2020) 10:4673-4687**".

Chapter 6 is considered to **"Impact of Newtonian heating on the micropolar CNT based hybrid nanofluid flow"**. This study addresses the impact of ion and Hall slip in micropolar nanoliquid flow in the occurrence of Newtonian heating. Further the influence of thermal radiation, Darcy – Forchheimer, viscous dissipation, and variable viscosity are discussed. Total entropy generation rate is calculated. Two distinct nanoparticles such as (SWCNT, MWCNT) used as a hybrid nanofluid. Built-in function bvp4c integrates the solution of simulated hydrodynamic boundary value problems. The effects on axial velocity, angular velocity, temperature field, concentration field, Bejan number, and entropy optimization of different flow field variables are displayed graphically. The chapter's content is published in "**Applied Nanoscience (2020): 1-13**".

Chapter 7 is considered to **"Heat transfer enhancement in a micropolar hybridized nanofluid flow in the presence of stratification"**. In this chapter the steady bio-convective micropolar hybrid nanofluid flow with the stratification conditions above a vertical exponentially stretching surface is examined. In the present chapter, SWCNT and MWCNT are combined in a water-based fluid to generate hybrid nanoparticles. To inspect the mass and heat transfer rate, the Cattaneo-Christov heat flux and rate of chemical reaction are factored into the equation. To answer the coupled equations, the Bvp4c Matlab approach is being used. The interpretation of numerous parameters is

scrutinized graphically. The microorganism field decays for rises the Peclet number, and bio - convection Schmidt number. The chapter's content accepts in "**proceedings of the institution of mechanical engineers part c journal of mechanical engineering sciences**".

2 Chapter 2

Mathematical analysis of Falkner – Skan problem with double stratification

2.1 Introduction

This chapter discusses the importance of single wall carbon nanotube (SWCNTs) and multiple walls carbon nanotube (MWCNTs) over a static wedge with magnetohydrodynamics (MHD). The impact of activation energy, thermal radiation, heat generation and double stratification are also taken into consideration. Employing the bvp4c package in Matlab, the system of differential equations is explained numerically. The results of a variety of parameters on the axial velocity, temperature, and concentration field are studied graphically. The temperature and concentration distribution diminish respectively with thermal and concentration stratified parameter. Furthermore, for both carbon nanotubes, solid volume fraction improves velocity and temperature profile.

2.2 Mathematical Formulation

Consider the two-dimensional steady flow with two different nanoparticles containing SWCNTs and MWCNTs with engine oil as a base fluid over a Falkner-Skan problem is demonstrated. The flow chart of the problem is given in *Fig. 2.1*. Moreover, it is presumed that the ambient velocity and moving wedge velocity is correspondingly taken as $u_e(x) = U_\infty x^n$ and $u_w(x) = U_w x^n$, where U_∞, U_w and n are constant. In Cartesian coordinate x-axis taking along the flow surface and y-axis along normal to x-axis or

perpendicular to fluid flow surface. With non-uniform strength $B(x) = B_0 x^{(n-1)/2}$, the magnetic field is applied across the y-axis.
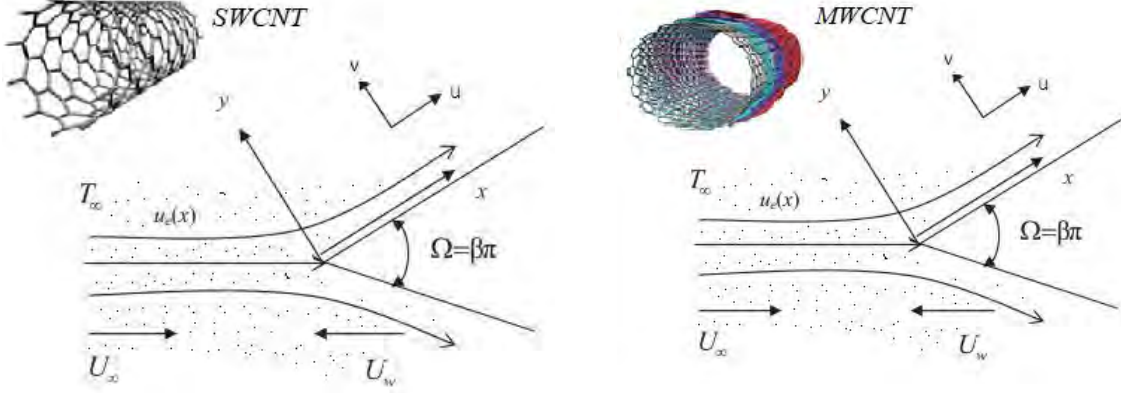
Fig. 2.1: Flow chart of the problem.

After applying the boundary layer approximation $(u = O(1) = x, v = O(\delta) = y)$, the continuity, momentum, energy and concentration equations become:

$$\frac{\partial v}{\partial y} + \frac{\partial u}{\partial x} = 0,\tag{2.1}$$

$$u\frac{\partial u}{\partial x} + v\frac{\partial u}{\partial y} + \frac{\sigma_{nf} B(x)^2}{\rho_{nf}}(u - u_e) = -u_e\frac{du_e}{dx} + \frac{\mu_{nf}}{\rho_{nf}}\frac{\partial^2 u}{\partial y^2},\tag{2.2}$$

$$v\frac{\partial T}{\partial y} + u\frac{\partial T}{\partial x} - \frac{(T - T_\infty)Q(x)}{(\rho C_p)_{nf}} = \alpha_{nf}\frac{\partial^2 T}{\partial y^2} + \frac{16\sigma^*}{3k^*}\frac{\partial}{\partial y}\left(T^3\frac{\partial T}{\partial y}\right).\tag{2.3}$$

$$v\frac{\partial C}{\partial y} + u\frac{\partial C}{\partial x} + k_r^2\left(\frac{T}{T_\infty}\right)^m \exp\left(\frac{-E_a}{kT}\right)(C - C_\infty) = (D_B)_{nf}\frac{\partial^2 C}{\partial y^2},\tag{2.4}$$

The suitable boundary conditions are given by:

$$u = 0,\ T = T_w(x) = T_0 + b_1 x,\ v = 0, C = C_w = C_0 + dx \ \text{at}\ \ y = 0,$$
$$u \to u_e(x) = U_\infty x^n,\quad T \to T_\infty = T_0 + b_2 x,\ C \to C_\infty = C_0 + ex \ \text{as}\ \ y = \infty.\tag{2.5}$$

19

In above equation (u,v) respectively determine the velocity along (x,y)-axis, $(D_B)_{nf}$ indicate the diffusion coefficient of nanofluid, k_r^2 symbolized the reaction rate, m demonstrate the fitted rate constant which normally lies in the range $-1 < m < 1$ and b,c,d,e all are constant. The thermophysical properties of the regular fluids i.e. engine oil, water and for nanoparticles such as SWCNTs and MWCNTs are specified below in *Table 2.1*.

Table 2.1. Thermophysical properties of the regular fluids and CNTs.

Thermophysical properties	Base fluids		Nanoparticles	
	Engine oil	Water	MWCNTs	SWCNTs
$C_p\ (J/kgK)$	1910.0	4179.0	796.0	425.0
$\rho\ (kg/m^3)$	884.0	997.1	1600.0	2600.0
$k\ (W/mK)$	0.144	0.613	3000.0	6600.0
$\sigma\ (S/m)$	1.07×10^{-6}	5.5×10^{-6}	1.9×10^{-4}	1.26×10^{6}
$\beta \times 10^{-5}\ (1/K)$	57	21	0.21	0.19

The proposed relation predicted by Xue [67] is characterized as follow

Table 2.2. Effective thermophysical quantities of nanofluids.

Nanofluid dynamic viscosity	$\mu_{nf} = (1-\phi)^{-2.5}\mu_f,$
Nanofluid density	$\rho_{nf} = \rho_f(1-\phi) + \phi\rho_{CNT},$
Nanofluid electric conductivity	$\dfrac{\sigma_{nf}}{\sigma_f} = 1 - \dfrac{3\phi[1 - \frac{\sigma_{CNT}}{\sigma_f}]}{[2 + \frac{\sigma_{CNT}}{\sigma_f}] + \phi[1 - \frac{\sigma_{CNT}}{\sigma_f}]},$
Nanofluid thermal expansion coefficient	$\dfrac{(\beta\rho)_{nf}}{(\beta\rho)_f} = 1 - \phi + \phi\dfrac{(\beta\rho)_{CNT}}{(\beta\rho)_f}$
heat capacity of nanofluid	$(\rho C_p)_{nf} = (\rho C_p)_{SWCNT}\phi + (\rho C_p)_f(1-\phi),$
thermal conductivity of nanofluid	$\dfrac{k_{nf}}{k_f} = \dfrac{2\phi\frac{k_{CNT}}{k_{CNT}-k_f}\ln(\frac{k_f+k_{CNT}}{2k_f}) + 1 - \phi}{2\phi\frac{k_f}{k_{CNT}-k_f}\ln(\frac{k_f+k_{CNT}}{2k_f}) + 1 - \phi},$

Nanofluid thermal diffusivity	$$\alpha_{nf} = \frac{k_{nf}}{(\rho C_p)_{nf}}.$$

Table 2.3. Effective thermophysical quantities of hybrid nanofluids.

Hybrid nanofluid dynamic viscosity	$$\mu_{hnf} = \frac{\mu_f (1-\phi_1)^{-2.5}}{(1-\phi_2)^{2.5}},$$
Hybrid nanofluid density	$$\frac{\rho_{hnf}}{\rho_f} = (1-\phi_2)\left\{1-\phi_1+\phi_1\frac{\rho_{MWCNT}}{\rho_f}\right\}+\phi_2\frac{\rho_{SWCNT}}{\rho_f}$$
Hybrid nanofluid electric conductivity	$$\frac{\sigma_{hnf}}{\sigma_{bf}} = \frac{\sigma_{SWCNT}+2\sigma_{bf}+2\phi_2[\sigma_{SWCNT}-\sigma_f]}{\sigma_{SWCNT}+2\sigma_{bf}-\phi_2[\sigma_{SWCNT}-\sigma_f]},$$ $$\frac{\sigma_{bf}}{\sigma_f} = \frac{\sigma_{MWCNT}+2\sigma_f+2\phi_1[\sigma_{MWCNT}-\sigma_f]}{\sigma_{MWCNT}+2\sigma_f-\phi_1[\sigma_{MWCNT}-\sigma_f]},$$
Hybrid nanofluid heat capacity	$$(\rho C_p)_{hnf} = (1-\phi_2)\left\{(\rho C_p)_f(1-\phi_1)+\phi_1(\rho C_p)_{MWCNT}\right\}+\phi_2(\rho C_p)_{SWCNT},$$,
Hybrid nanofluid thermal conductivity	$$\frac{k_{hnf}}{k_{bf}} = \frac{(1-\phi_2)+2\phi_2(\frac{k_{SWCNT}}{k_{SWCNT}-k_{bf}})\ln(\frac{k_{SWCNT}+k_{bf}}{k_{bf}})}{(1-\phi_2)+2\phi_2(\frac{k_{bf}}{k_{SWCNT}-k_{bf}})\ln(\frac{k_{SWCNT}+k_{bf}}{k_{bf}})},$$ $$\frac{k_{bf}}{k_f} = \frac{(1-\phi_1)+2\phi_1(\frac{k_{MWCNT}}{k_{MWCNT}-k_f})\ln(\frac{k_{MWCNT}+k_f}{k_f})}{(1-\phi_1)+2\phi_1(\frac{k_f}{k_{MWCNT}-k_f})\ln(\frac{k_{MWCNT}+k_f}{k_f})},$$
Hybrid nanofluid thermal diffusivity	$$\alpha_{hnf} = \frac{k_{hnf}}{(\rho C_p)_{hnf}}.$$

the non-dimensional variables mentioned below

$$\psi = \sqrt{\frac{2\nu_f\, xu_e(x)}{n+1}}f(\eta),\ \ \eta = \sqrt{\frac{(n+1)u_e(x)}{2\nu_f\, x}}y,\ u = U_\infty x^n f'(\eta),$$

$$v = -\sqrt{\frac{(n+1)x^{n-1}\nu_f U_\infty}{2}}\left\{f(\eta)-(\frac{1-n}{n+1})\eta f'(\eta)\right\},$$

$$\theta(\eta) = \frac{T-T_\infty}{T_w-T_0},\ \ \ \ g(\eta) = \frac{C-C_\infty}{C_w-C_0}.$$

(2.7)

Eq. (2.1) is fulfilled and Eqs. (2.2) to (2.4) yield the form

$$\frac{1}{(1-\phi)^{2.50}(1-\phi+\phi\frac{\rho_{CNT}}{\rho_f})}f''' + ff'' + \beta(1-f'^2) - M\frac{\left(\sigma_{nf}/\sigma_f\right)}{\left(\rho_{nf}/\rho_f\right)}(f'-1) = 0, \tag{2.8}$$

$$\left[\left(\frac{k_{nf}}{k_f} + R_d\left(1+(T_r-1)\theta\right)^3\right)\theta'\right]' + \Pr\left[1-\phi+\phi\frac{(\rho C_p)_s}{(\rho C_p)_f}\right]\left\{f\theta' - \left(\frac{2}{n+1}\right)S_1 f' - \left(\frac{2}{n+1}\right)\theta f'\right\}$$
$$+\left(\frac{2}{n+1}\right)D_c\theta = 0, \tag{2.9}$$

$$\frac{(1-\phi)^{2.5}}{S_c}g'' + g'f - \left(\frac{2S_2}{n+1}\right)f' - \left(\frac{2}{n+1}\right)f'g - \left(\frac{2R_c}{n+1}\right)(1+\delta\theta)^m\exp(-\frac{E}{1+\delta\theta}) = 0, \tag{2.10}$$

While the boundary conditions (2.5) take the resulting form

$$f'(\eta) = 0, \ \theta(\eta) = 1 - S_1, f(\eta) = 0, \ g(\eta) = 1 - S_2, \ at \ \eta = 0,$$

$$f'(\eta) = 1, \ \theta(\eta) = 0, \ g(\eta) = 0, \ \eta \to \infty. \tag{2.11}$$

Where $\quad M = \frac{2\sigma_f B_0^2}{(1+n)U_\infty \rho_f}, \quad R_d = \frac{16\sigma^* T_\infty^3}{3kk^*}, \quad D_c = \frac{Q_0}{(\rho C_p)_f U_\infty}, \quad \Pr = \frac{\nu_f}{\alpha_f}, \quad T_r = \frac{T_w}{T_\infty} \quad,$

$S_1 = \frac{b_2}{b_1}, \ S_2 = \frac{e}{d}$. Also, considered the Hartree pressure gradient parameter $\beta = \frac{2n}{n+1}$ this

relates to $\beta = \Omega/\pi$ for a wedge complete angle Ω. The positive β value denotes the negative or favorable pressure gradient while a negative β estimation symbolizes an unfavorable pressure gradient. Additional the boundary layer horizontal flat plate flow represents by $\beta = 0$ ($\Omega = 0°$) and $\beta = 1$ ($\Omega = 180°$) show the boundary later flow past a vertical flat plate near the stagnation point.

The physical measured variables are the friction drag, heat transfer rate, and the local Sherwood number

$$C_f = \frac{\mu_{nf}\left[\frac{\partial u}{\partial y}\right]_{y=0}}{\rho_f u_e^2}, \ Nu_x = \frac{x\left\{-k_{nf}\left[\frac{\partial T}{\partial y}\right]_{y=0} + [q_r]_w\right\}}{k_f(T_w - T_0)}, Sh_x = \frac{x\left\{-(D_B)_{nf}\left[\frac{\partial C}{\partial y}\right]_{y=0}\right\}}{D_B(C_w - C_0)}, \tag{2.12}$$

Using the similarity variable in above equation it become

$$[2\,\mathrm{Re}_x/(m+1)]^{1/2}\,C_f = \frac{1}{(1-\phi)^{2.5}}\,f''(0),$$

$$[(m+1)\,\mathrm{Re}_x/\,2]^{-1/2}\,Nu_x = -\left[\frac{k_{nf}}{k_f} + R_d(1+(T_r-1)\theta(0))^3\right]\theta'(0), \qquad (2.13)$$

$$[(m+1)\,\mathrm{Re}_x/\,2]^{-1/2}\,Sh_x = -(1-\phi)^{2.5}\,g'(0).$$

2.3 Solution Procedure

The Bvp4c method in MATLAB is being utilized to integrate the coupled equations (2.8 – 2.10) with boundary condition (2.11) numerically. The BVP-4c function of MATLAB only resolves the first order ordinary differential equation. For this reason, the first order differential equations are used instead of the third and second order differential equations and selected the sensible value of η_∞, and 10^{-6} were reserved the absolute convergence criteria, we set the resulting first order classifications,

$$A = (1-\phi)^{2.5}(1-\phi+\phi\frac{\rho_{CNT}}{\rho_f}),\, B = (1-\phi+\phi\frac{\rho_{CNT}}{\rho_f}),\, C = \mathrm{Pr}\left[1-\phi+\phi\frac{(\rho C_p)_s}{(\rho C_p)_f}\right],$$

$$D = \frac{k_{nf}}{k_f}, \qquad (2.14)$$

$$f'' = y(3),\, f' = y(2),\, f = y(1), \qquad (2.15)$$

$$yy1 = f''' = -A\left\{y(3)y(1)+\beta(1-y(2)y(2))-M\,\frac{\sigma_{nf}/\sigma_f}{B}(y(2)-1)\right\}, \qquad (2.16)$$

$$\theta = y(4),\, \theta' = y(5), \qquad (2.17)$$

$$yy2 = \theta'' = \frac{1}{\left(D + R_d\left(1+(T_r-1)\theta\right)^3\right)}\{-3\left(R_d\left(1+(T_r-1)\theta\right)^2\right)(T_r-1)\theta'^2$$

$$-C\left\{\begin{array}{c} y(5)y(1) - \left(\dfrac{2}{n+1}\right)S_1 y(2) \\ -\left(\dfrac{2}{n+1}\right)y(2)y(4) \end{array}\right\} - \Pr\left(\dfrac{2}{n+1}\right)D_c y(4)\}, \tag{2.18}$$

$$g = y(6), g' = (7), \tag{2.19}$$

$$yy3 = g'' = \frac{1}{(1-\phi)^{2.5}}\left\{\begin{array}{c} -S_c y(1)y(7) + \left(\dfrac{2}{n+1}\right)S_2 y(2) + \left(\dfrac{2}{n+1}\right)y(2)y(6) \\ + \left(\dfrac{2}{n+1}\right)R_c(1+\delta y(4))^m y(6)\exp(-\dfrac{E}{1+\delta y(4)}) \end{array}\right\}, \tag{2.20}$$

with the conditions,

$$y_0(1) = 0, \ y_0(2) = 0, \ y_0(4) = 1 - S_1, \ y_0(6) = 1 - S_2,$$

$$y_{\inf}(2) = 1, \ y_{\inf}(4) = 0, \ y_{\inf}(6) = 0. \tag{2.21}$$

For the present work, the conclusion of $\eta_\infty = 4$, to approach the asymptotic values specified in boundary condition (2.21). Since the relationship specifies a good knowledge and understanding for each assessed value, we are confident that the current outcome is correct and precise.

2.4 Results and Discussion

In order to explore the physical explanation of the present issue, the numerical estimation of axial velocity, temperature profile, and concentration profile have been calculated for resultant emergent parameter as the solid volume fraction (ϕ), magnetic parameter (M), thermal stratification parameter (S_1), radiation parameter (R_d), concentration stratification parameter (S_2), heat generation/absorption parameter (D_c), Schmidt number (S_c), activation energy (E) for both SWCNTs and MWCNTs respectively. *Table 2.4* shows the calculation of drag friction $f''(0)$ for several

estimations of *m* when in the nonappearance of magnetic field and nanoparticle have been compared with previous work of Yacob [68] and Nadeem et al. [69]. The numerical value of friction drag, heat transfer rate, and local Sherwood number are displayed in *Table (2.5-2.7)* respectively. *Table 2.5* demonstrates the numerical value of the friction drag. It is concluded that the numerical value of drag friction rises for solid volume fraction, magnetic parameter, and power index law, while for wedge parameter the skin factor diminishes for both cases SWCNTs and MWCNTs. In *Table 2.6,* we have displayed the numerical value of the rate of heat transfer for both CNTs. The numerical value of local Nusselt number declines for greater estimation of M, while it enhances for growing the values of ϕ, wedge parameter, index number, and radiation parameter for both cases SWCNTs and MWCNTs. *Table 2.7* displays the effect of numerous parameters on Sherwood number for both cases SWCNTs and MWCNTs. It is concluded that the Sherwood number enhances for enhancing the estimation of Schmidt number, dimensionless reaction rate, and power index law, while it is decrease for larger value of activation energy parameter. *Fig. 2.2 ((a) and (b))* illuminates the influence of ϕ on axial velocity and temperature distribution for SWCNTs and MWCNTs. With increasing the estimation of ϕ, the temperature and velocity curves for both cases decrease. Moreover, it is presumed that as the value of ϕ expands, the momentum boundary layer thickness declines while the thermal boundary layer thickness escalations. The fluid velocity is an enhancing function of magnetic parameter for both CNTs, as revealed in *Fig. 2.3 (a)*. *Fig. 2.3 (b)* displays the effect of magnetic parameter on fluid temperature for both cases. The temperature distribution diminishes for enhancing the estimation of M for both SWCNTs and MWCNTs. It is often demonstrated as M increases, the thermal boundary layer of MWCNTs decreases faster than that of SWCNTs. *Fig. 2.4 (a)* determines the result of power index parameter n on velocity distribution. Through expanding n the velocity profile boosts for both

CNTs. The temperature distribution enhances for boosting value of heat generation coefficient D_c for both cases SWCNTs and MWCNTs. This is verifying in *Fig. 2.4 (b)*. This is because, by raising the estimation of the heat generation coefficient, the internal energy of fluid particles increases. Thus, the temperature field enhances regularly. *Fig. 2.5 ((a) and (b))* determines the influence of S_1 and S_2 on temperature and concentration distribution respectively. For both the SWCNTs and MWCNTs the temperature and concentration field decreases. The impression of radiation parameter R_d on temperature profile for both CNTs is revealed in *Fig. 2.6 (a)*. Growing the temperature distribution for larger the value of radiation parameter R_d for both SWCNTs and MWCNTs. Physically radiation parameter R_d characterizes the proportional involvement of the transfer of heat from thermal radiation to thermal conduction heat transfer. Afterward thermal radiation enhances the nanofluid thermal diffusivity, for growing values of radiation parameter R_d heat should be transferred to the regime and temperatures will be improved. *Fig. 2.6 (b)* illustrates that the concentration is a reducing function of Schmidt number S_c. *Fig. 2.7 (a)* scrutinized the upshot of non-dimensional activation energy E for both CNTs. Through activation energy E, concentration in the nanofluid (i.e. SWCNTs and MWCNTs) expressively enhances. *Fig. 2.7 (b)* examines the effect of reaction rate R_c for SWCNTs and MWCNTs on concentration field. The concentration distribution diminishes for both cases with growing the estimation of R_c.

Table 2.4. Evaluation of $f''(0)$ for several values of n when $M = 0 = \phi$.

n	Yacob [68]	Nadeem et al. [69]	Present Results

0	0.4696	0.469600	0.46960
1/11	0.6550	0.654994	0.65499
0.2	0.8021	0.802125	0.80212
1/3	0.9277	0.927680	0.92768
0.4	-	0.976824	0.976824
0.5	1.0389	1.038900	1.03890
1	1.2326	1.232587	1.23258

Table 2.5. Numerical value of coefficient of skin friction with fixed value of $S_c = 1.0$, $S_1 = 0.5 = S_2$, and $\lambda = 0.1$.

ϕ	M	β	n	$[2\,\mathrm{Re}_x/(m+1)]^{1/2}C_f$	
				SWCNTs	MWCNTs
0.01	0.1	0.2	1.0	1.11306	1.11306
0.03				1.41201	1.40241
0.05				1.62113	1.61013
0.01	0.1	1.0	0.5	1.50130	1.49131
	0.5			1.64970	1.63472
	1.0			1.81860	1.80761
0.01	0.2	0.1	0.5	1.67811	1.66513
		0.3		1.65794	1.64714
		0.5		1.65699	1.64359
0.01	0.1	1.0	0.1	1.25201	1.24231
			0.5	1.45201	1.46251
			1.0	1.58920	1.57321

Table 2.6. Numerical value of local Nusselt number with fixed value of $S_c = 1.0$, $T_r = 0.5$, and $Pr = 4.0$.

ϕ	M	β	n	R_d	$[(m+1)\,\mathrm{Re}_x/2]^{-1/2}\,Nu_x$	
					SWCNTs	MWCNTs
0.01	0.1	0.2	1.0	0.5	0.78692	0.77692
0.03					1.02009	1.01009
0.05					1.24426	1.23426
0.01	0.1	1.0	0.5	0.5	1.35735	1.34735
	0.5				1.35176	1.34176
	1.0				1.34590	1.33590
0.01	0.2	0.1	0.5	0.5	1.34426	1.33426
		0.3			1.60844	1.59844
		0.5			1.66734	1.65734
0.01	0.1	1.0	0.1	0.5	1.41235	1.40235
			0.5		1.41408	1.40408
			1.0		1.41435	1.40435
0.01	0.1	0.1	0.5	0.1	1.41420	1.40420
				0.3	1.74050	1.73050
				0.5	2.12240	2.0224

Table 2.7. Numerical value of local Sherwood number with fixed value of
$M = \delta = 1, D_c = 0.1 = T_r$.

Sc	E	R_c	n	$[(m+1)\,\mathrm{Re}_x/2]^{-1/2}\,Sh_x$	
				SWCNTs	MWCNTs
0.1	1.0	1.0	0.5	0.26810	0.26610
0.5				0.67370	0.67000
1.0				1.00700	1.00300
1.0	1.0	1.0	0.5	1.00700	1.00300

	2.0			0.80690	0.80310
	5.0			0.54520	0.54810
1.0	1.0	2.0	0.5	1.35000	1.34400
		3.0		1.62600	1.61900
		5.0		2.07400	2.06600
0.1	1.0	1.0	-0.5	0.83780	0.83950
			0.0	0.91250	0.91170
			1.0	1.12600	1.11800
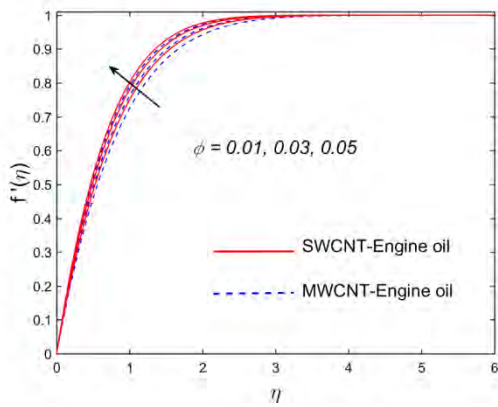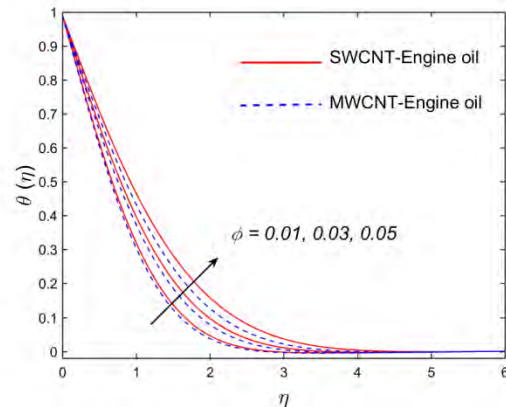
(a) *(b)*

Fig. 2.2: Velocity and temperature variation with volume fraction of SWCNT and MWCNT.
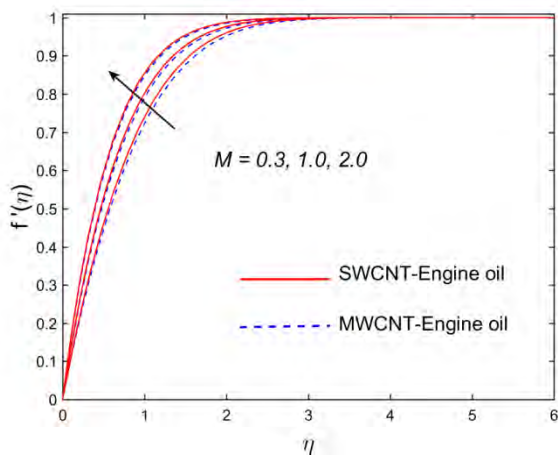
<div style="text-align:center">(a)</div>
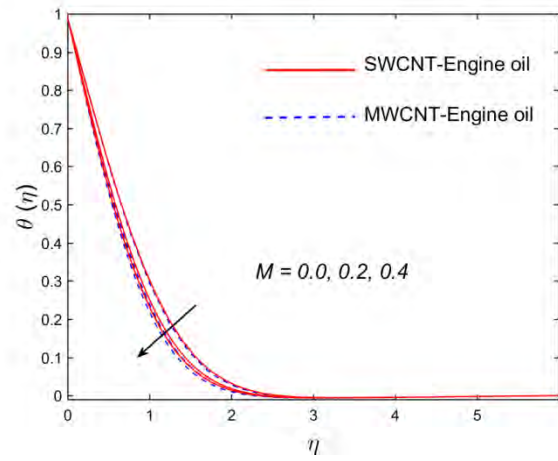
<div style="text-align:center">(b)</div>

Fig. 2.3: Velocity and temperature variation with magnetic parameter.
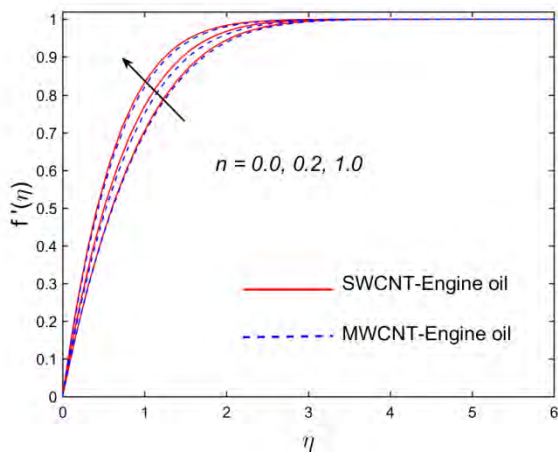
<div style="text-align:center">(a)</div>
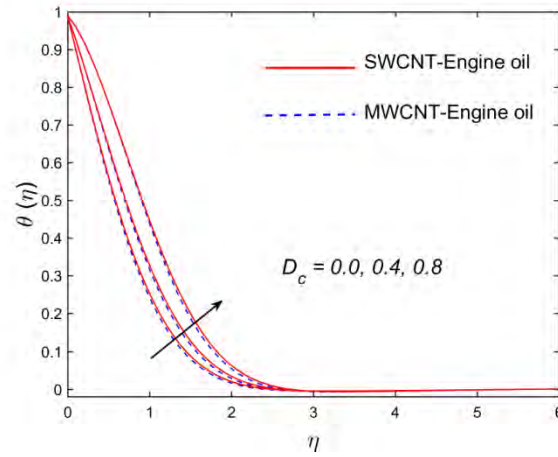
<div style="text-align:center">(b)</div>

Fig. 2.4: Velocity and temperature variation (a) with n and (b) with D_c.
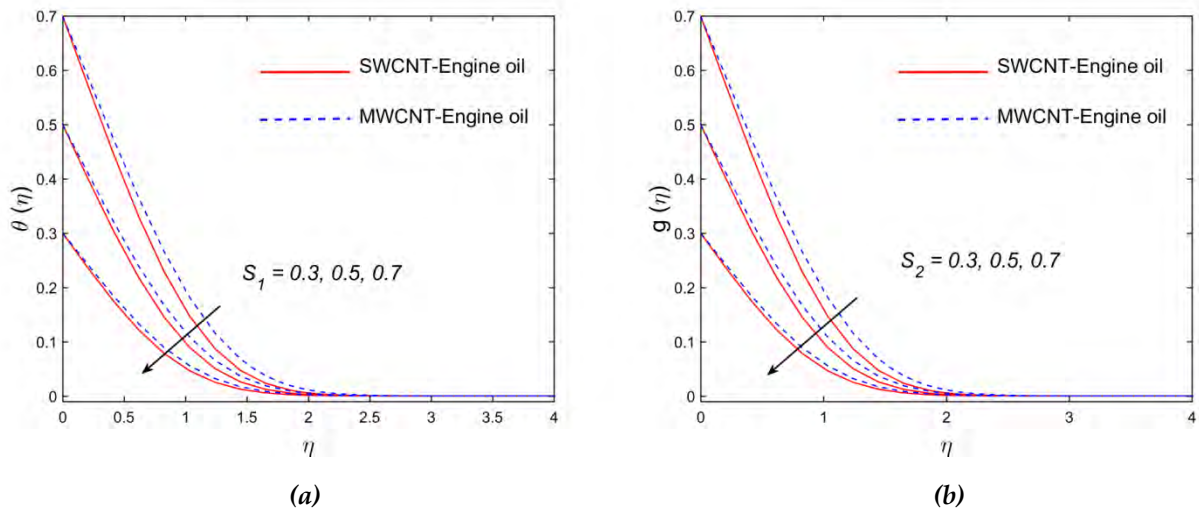
Fig. 2.5: Temperature and concentration variation (a) with S_1 and (b) with S_2.
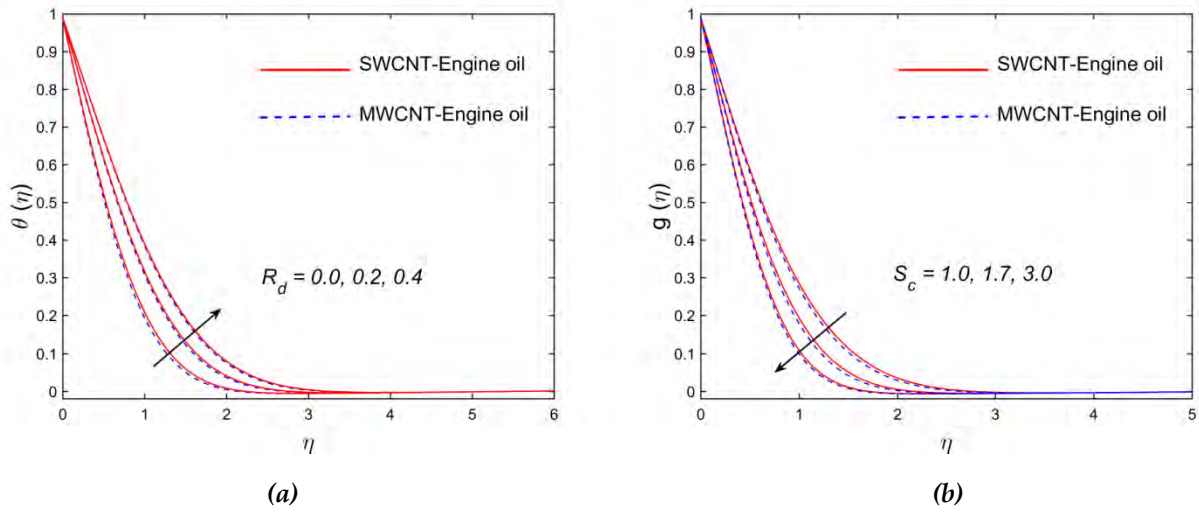
Fig. 2.6: Temperature and concentration variation (a) with R_d and (b) with S_c.

(a)   *(b)*
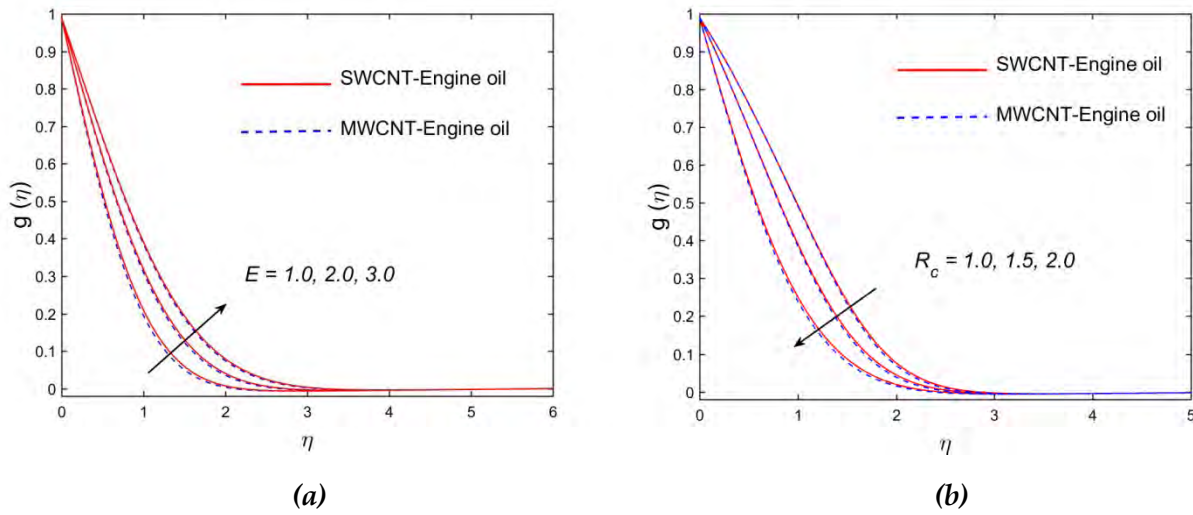
Fig. 2.7: Concentration variation (a) with E and (b) with R_c.

2.5 Concluding Remarks

In the existence of SWCNTs and MWCNTs the boundary layer flow is discussed past a Falkner-Skan problem with magnetic field. The mass and heat transfer feature is performed when thermal radiation, activation energy, and double stratification, are present. The finite-difference-based numerical technique, specifically, bvp4c from MATLAB are used to resolve the coupled ordinary differential equation.

The important findings of present study are detailed below:

➢ The axial velocity and temperature profile designate increment in nature for enhancing value of nanoparticle solid volume fraction.

➢ Magnetic parameter enhances the skin friction while diminishes Nusselt number.

➢ Temperature is an enhancing function of radiation, heat generation, and temperature ratio parameter.

➢ For maximum value of Schmidt number, solutal stratification parameter, and reaction rate variable, the concentration field exhibits diminishing behavior.

➢ The thickness of the concentration boundary layer improves in order to maximize the value of activation energy.

3 Chapter 3

Heat transfer analysis and entropy generation in the SWCNT-MWCNT hybrid nanofluid flow

3.1 Introduction

The current chapter particularly concerns the analysis of the flow and transfer of heat of CNTs based hybrid nanofluid with temperature dependent viscosity over a moving wedge. The Darcy-Forchheimer relationship specifies the nature of the flow in the porous medium. Further, the impacts of heat generation, activation energy, velocity and thermal slip, thermal radiation are added. The second law of thermodynamics is utilized to measure the irreversibility factor. The numerical technique bvp4c are integrated to solve the highly nonlinear differential equation. For axial velocity, temperature profile, and entropy generation, a comparison was made between nanofluid and hybrid nanofluid. The variable viscosity parameter improves the axial velocity and diminishes the temperature distribution for both simple nanofluid and hybrid nanofluid.

3.2 Mathematical Description

Fig. 2.1 demonstrates the geometric configuration and the considered problem's schematic physical model. In the present chapter we accept the steady, incompressible two-dimensional SWCNT-MWCNT/Water hybrid nanoliquid flow in the occurrence of thermal slip and activation energy past a permeable wedge. We find a Cartesian coordinate scheme (x, y), where y and x are the co-ordinates measured normal and along to the permeable wedge. The free stream velocity (inviscid flow) is also thought to be $u_\infty(x)$ and the velocity of the moving wedge is $u_w(x)$. Liquid and ambient fluid

temperature is T_w and T_∞, where $T_w > T_\infty$ is applied for wedge heating (assisting flow) and $T_w < T_\infty$ is used for wedge cooling (opposite flow).

The hybrid nanofluid is developed by combining SWCNT into MWCNT / Water. First, MWCNT (ϕ_1) nanoparticles are inserted in water to create a MWCNT-Water nanofluid and then SWCNT nanomaterial of different fractions (ϕ_2) are inserted to the nanofluid blend to obtain the homogenous solution of hybrid nanofluid SWCNT-MWCNT/ Water.

Imposing the approximation of the boundary layer and assuming that we have a system of equations,

$$\frac{\partial v}{\partial y} + \frac{\partial u}{\partial x} = 0, \tag{3.1}$$

$$u\frac{\partial u}{\partial x} + v\frac{\partial u}{\partial y} - u_\infty \frac{du_\infty}{dx} = \frac{1}{\rho_{hnf}} \frac{\partial}{\partial y}\left(\mu_{hnf}(T)\frac{\partial u}{\partial y}\right) + \frac{1}{\rho_{hnf}} \frac{\mu_{hnf}(T)}{K^{**}}(u_\infty - u) + F^{**}(u^2_\infty - u^2), \tag{3.2}$$

$$v\frac{\partial T}{\partial y} + u\frac{\partial T}{\partial x} + \frac{Q(x)}{(\rho C_p)_{hnf}}(T_\infty - T) = \frac{\mu_{hnf}(T)}{(\rho C_p)_{hnf}}\left(\frac{\partial u}{\partial y}\right)^2 + \alpha_{hnf}\frac{\partial^2 T}{\partial y^2} + \frac{16 T_\infty^3 \sigma^*}{3(\rho C_p)_{hnf} k^*}\frac{\partial^2 T}{\partial y^2}, \tag{3.3}$$

$$u\frac{\partial C}{\partial x} + v\frac{\partial C}{\partial y} = (D_B)_{hnf}\frac{\partial^2 C}{\partial y^2} + k_r^2\left(\frac{T}{T_\infty}\right)^m \exp\left(\frac{-E_a}{kT}\right)(C_\infty - C), \tag{3.4}$$

The interrelated conditions are,

$$v = 0, u = u_w(x) + N_1(x)\upsilon_f \frac{\partial u}{\partial y},\ C = C_w,\ T = T_w + D_1(x)\frac{\partial T}{\partial y},\ \text{at } y \to 0,$$
$$T \to T_\infty, u \to u_\infty(x), C \to C_\infty,\ \text{as } y \to \infty. \tag{3.5}$$

The variable viscosity which is vary inversely to temperature is defined as [8]

$$\mu_f(T) = \frac{1}{a(T - T_r)},$$ (3.6)

Where $a = \frac{\delta^*}{\mu_{f\infty}}$ and $T_r = T_\infty - \frac{1}{\delta^*}$, δ, and a are constant. To achieve true similarity solution, we defined variable velocity and thermal slip as,

$$u_\infty(x) = cx^n, \ T_w = T_\infty + bx^{\frac{5n-1}{2}},$$
$$D_1(x) = D_1^* x^{\frac{1-n}{2}}, N_1(x) = N_1^* x^{\frac{1-n}{2}}.$$ (3.7)

Where b and c are the constants and $n = \beta/(2-\beta)$ with β is Hartree parameter of pressure gradient.

The similarity variables are accepted by,

$$u = cx^n f'(\eta), \ v = -\frac{1}{2}\sqrt{cv_f} \ x^{\frac{n-1}{2}} \left[\eta f'(\eta)(n-1) + f(\eta)(n+1)\right],$$
$$\eta = \sqrt{\left(\frac{c}{v_f}\right)} yx^{\frac{n-1}{2}}, \ \theta(\eta) = \frac{T - T_\infty}{T_w - T_\infty}, g(\eta) = \frac{C - C_\infty}{C_w - C_\infty}.$$ (3.8)

Using similarity transformation, the above equations (3.1 – 3.4) give,

$$\frac{1}{1-\%_{\theta_r}} f''' + \frac{\left((1-\phi_2)\left\{(1-\phi_1) + \phi_1 \frac{\rho_{MWCNT}}{\rho_f}\right\} + \phi_2 \frac{\rho_{SWCNT}}{\rho_f}\right)}{(1-\phi_1)^{-25/10}(1-\phi_2)^{-25/10}} \left(\frac{n+1}{2} f''f + n - nf'^2 + F_r(1 - f'^2)\right)$$
$$+ \frac{f''\theta'}{\theta_r\left(1-\%_{\theta_r}\right)^2} + \frac{P_m(1 - f')}{1-\%_{\theta_r}},$$ (3.9)

$$\left(\frac{k_{hnf}}{k_f} + R_d\right)\theta'' + \Pr\left(D_c\theta + \frac{E_c}{(1-\%_{\theta_r})(1-\phi_1)^{25/10}(1-\phi_2)^{25/10}} f''^2\right) +$$
$$\frac{n+1}{2}\Pr\left((1-\phi_2)\left\{(1-\phi_1) + \phi_1\frac{(\rho C_p)_{MWCNT}}{(\rho C_p)_f}\right\} + \phi_2\frac{(\rho C_p)_{SWCNT}}{(\rho C_p)_f}\right)f\theta' = 0,$$ (3.10)

$$\left(\frac{(1-\phi_1)^{25/10}(1-\phi_2)^{25/10}}{S_c}\right)g'' + \left(\frac{n+1}{2}\right)fg' - R_c(1 + \delta\theta)^m g \exp(\frac{-E}{1+\delta\theta}) = 0,$$ (3.11)

The appropriate conditions are,

$$f'(\eta) = \lambda + Af''(\eta), \, f(\eta) = 0, \, \theta(\eta) = 1 + B\theta'(\eta), \, g(\eta) = 1, \text{ when } \eta \to 0,$$

$$f'(\eta) = 1, \, g(\eta) = 0, \, \theta(\eta) = 0, \text{ when } \eta \to \infty. \tag{3.12}$$

Here differentiation with respect to η is denoted by prime and λ is the parameter of the continuous moving wedge with $\lambda > 0$ and $\lambda < 0$, the moving wedge refers to the free stream in the same and opposite directions, whereas $\lambda = 0$ communicates to the static wedge and the other involved parameters are defines as below:

$$\Pr = (C_p \rho_f) / k_f, B = D_1^* \sqrt{\tfrac{(n+1)c}{2\nu_f}}, A = N_1^* \nu_f \sqrt{\tfrac{(n+1)c}{2\nu_f}}, F_r = \frac{C_b}{\sqrt{K^{**}} \rho_f}, P_m = \frac{\nu_f}{cK^{**}},$$

$$E_c = \frac{u_\infty^2}{\Delta T C_{pf}}, D_c = \frac{Q_0}{c(\rho C_p)_f}, \theta_r = \frac{1}{\delta(T_w - T_\infty)}, R_d = \frac{16\sigma^* T_\infty^3}{3k_f k^*}, R_c = \frac{k_r^2}{c}, E = \frac{E_a}{kT_\infty},$$

3.3 Entropy Generation Analysis

In the domain of a few engineering and industrial procedures, entropy generation (or production) reduces the available energy. It is thus essential to determine the rate of entropy generation in a system.

The volumetric rate of local entropy production of viscous fluid is given as:

$$S_G = \frac{k_f}{T_\infty^2} \left[\frac{k_{hnf}}{k_f} + \frac{16\sigma^* T_\infty^3}{3k^* k_f} \right] \left(\frac{\partial T}{\partial y} \right)^2 + \left(\frac{\mu_{hnf}(T)}{T_\infty} \right) \left(\frac{\partial u}{\partial y} \right) \left(\frac{\partial u}{\partial y} \right) + \frac{DR}{C_\infty} \left(\frac{\partial C}{\partial y} \right) \left(\frac{\partial C}{\partial y} \right)$$

$$+ \frac{DR}{T_\infty} \left(\frac{\partial T}{\partial y} \right) \left(\frac{\partial C}{\partial y} \right) + \frac{u^2}{T_\infty} \left(\frac{\mu_{hnf}(T)}{K^{**}} + F^{**} |u| \right), \tag{3.13}$$

The associated information will assist model the dimensionless entropy production

$$N_s = \frac{(y/\eta)^2 T_\infty}{k_f (T_w - T_\infty)} S_G, \tag{3.14}$$

After exploiting the similarity transformation (3.8) the dimensionless form of entropy generation develops:

$$N_s(\eta) = \left(\frac{k_{hnf}}{k_f} + R_d\right)\delta\theta'^2 + \frac{Br\left(1 - \%_{\theta_r}\right)^{-1}}{(1-\phi_1)^{2.5}(1-\phi_2)^{2.5}} f''^2 + \frac{BrP_m\left(1 - \%_{\theta_r}\right)^{-1}}{(1-\phi_1)^{2.5}(1-\phi_2)^{2.5}} f'^2$$

$$+ F_r Brf'^3 + L\frac{\alpha_2}{\delta} g'^2 + Lg'\theta',$$

(3.15)

Variable used in above equation are identified as,

$$\delta = \frac{\Delta T}{T_\infty}, \alpha_2 = \frac{\Delta C}{C_\infty}, Br = \frac{\mu_f u_\infty^2}{k_f \Delta T}, L = \frac{RD(C_w - C_\infty)}{k_f}.$$

(3.16)

Bejan number is describe as

$$Be = \frac{\text{entropy production due to thermal irreversibility}}{\text{total entropy generation}},$$

(3.17)

In mathematical form it expresses as,

$$Be = \frac{\left(\frac{k_{hnf}}{k_f} + R_d\right)\delta\theta'^2}{\left(\frac{k_{hnf}}{k_f} + R_d\right)\delta\theta'^2 + \frac{Br\left(1 - \%_{\theta_r}\right)^{-1}}{(1-\phi_1)^{2.5}(1-\phi_2)^{2.5}} f''^2 + \frac{BrP_m\left(1 - \%_{\theta_r}\right)^{-1}}{(1-\phi_1)^{2.5}(1-\phi_2)^{2.5}} f'^2 + F_r Brf'^3 + L\frac{\alpha_2}{\delta} g'^2 + Lg'\theta'}.$$

Bejan number requirement lie among $0 < Be < 1$. $Be = 0$ means that there is no entropy generation because of heat transfer. Similarly, the entropy minimization is less due to heat transfer than fluid friction when $Be < 0.5$.

3.4 Results and Discussion

The numerical solution is accomplished by means of finite difference method bvp4c from MATLAB. For manipulating this technique first, we transform the given nonlinear third order differential equation to first order ODEs by presented substitution. The convergence criteria were allotted as 10^{-5}. The accuracy of our problem, the present result in the absence of slip condition, hybrid nanofluid, and porosity parameter has been related with the earlier available result of Zaib and Haq. [70] and Yih [71] (see in *Table 3.1*). This result show good agreement with the above published articles.

The influences of inertia coefficient $0.1 \leq F_r \leq 1.0$, porous parameter $0.1 \leq P_m \leq 0.5$, variable viscosity parameter $0.4 \leq \theta_r \leq 1.0$, wedge parameter $0.1 \leq \lambda \leq 0.3$, and velocity slip $0.1 \leq A \leq 0.7$ and thermal slip $0.1 \leq B \leq 0.7$ on velocity field, temperature field, concentration profile, entropy minimization, and Bejan number are graphically studied. The upshot of inertia coefficient F_r and porous parameter P_m on axial velocity are discussed in *Fig. 3.1 ((a) and (b))*. The velocity distribution enhances with boosting the F_r and P_m. Further the momentum boundary layer thickness declines with larger the F_r and P_m. *Fig. 3.2 ((a) and (b))* highlights the upshot of θ_r on velocity and temperature distribution. Velocity filed upgrade while temperature diminishes with larger variable viscosity. Physically by increasing the parameter of variable viscosity, momentum transfer dominates due to low fluid viscosity, which improves the distribution of velocity (see in *Fig. 3.2 (a)*). The conclusion of velocity and thermal slip is carried out for velocity and temperature field separately in *Fig. 3.3 ((a) and (b))*. The velocity profile improves for improving the velocity slip parameter, while their consistent momentum boundary layer thickness reduces which is proven in *Fig. 3.3 (a)*. In the incidence of thermal slip, a smaller amount of heat transfer from the surface to liquid, as a result distribution of temperature diminishes which is illuminate in *Fig. 3.3 (b)*. *Fig. 3.4 ((a) and (b))* disclosed the influence of velocity through moving wedge parameter λ and Eckert number E_c. Here velocity is an enhancing function of λ for both simple nanofluid and hybrid nanofluid (see in *Fig. 3.4 (a)*). In *Fig. 3.4 (b)* temperature profile is display to measure the effect of Eckert number. Mechanical energy converted to thermal energy due to higher Eckert number which produced friction inside the fluid as a result temperature field enhances. *Figs. (3.5 ((a) and (b)) – 3.6 ((a) and (b)))* manifest the conclusion of Brinkman number, radiation parameter, temperature difference and concentration difference on entropy production and Bejan number. Entropy minimization enhances with upgrade the Brinkman number while it reduces with

39

radiation parameter for both cases. This is validating in Figs. 3.5 ((a) and (b)). Further the Bejan number increases for increasing the temperature difference and concentration difference (see in *Fig. 3.6 ((a) and (b))*. The numerical values of drag friction, heat transfer rate, and local Sherwood number are reviewed in *Table 3.2 - 3.4*.
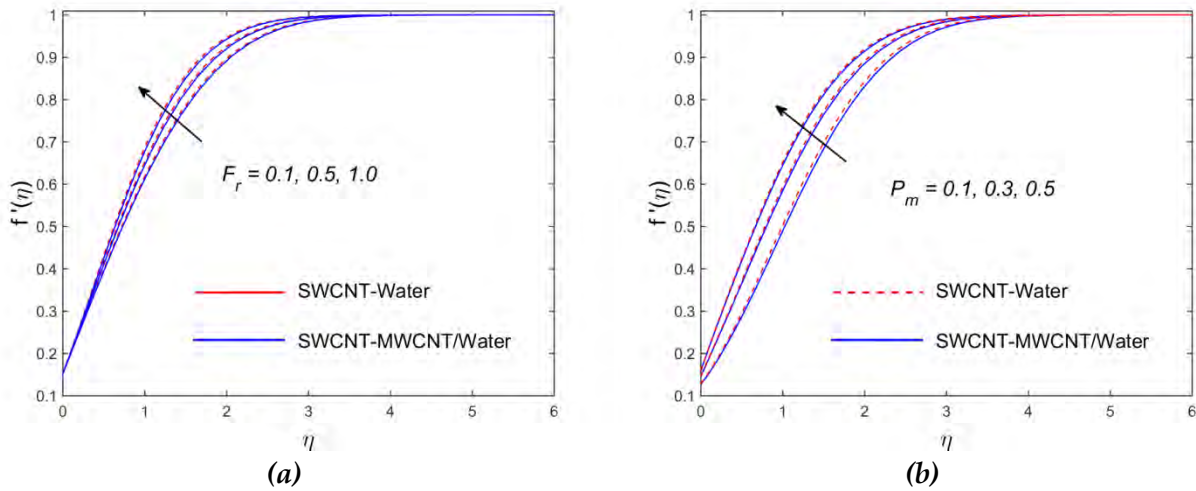
Fig. 3.1: Velocity variation (a) with F_r and (b) with P_m.
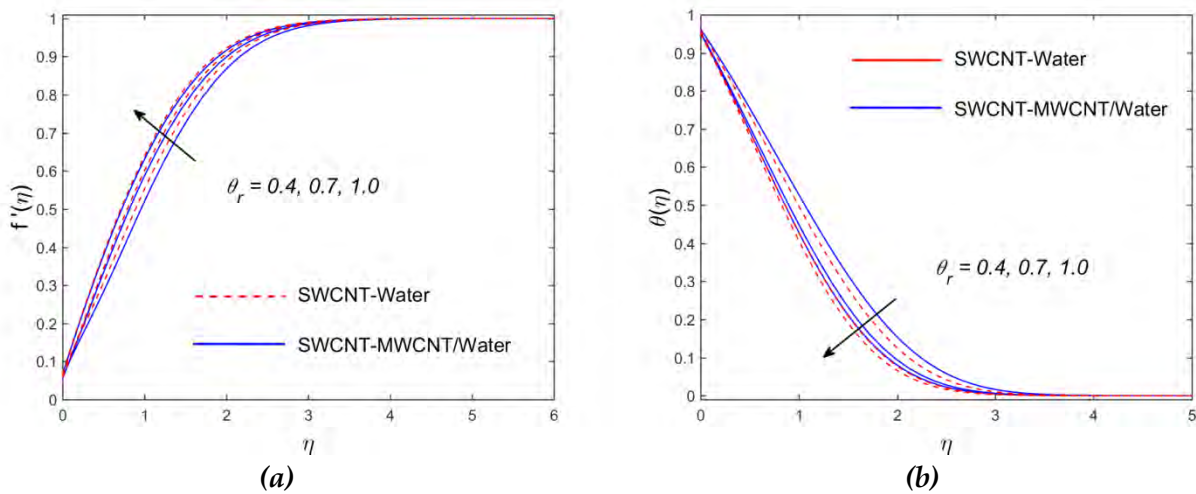
Fig. 3.2: Velocity and temperature variation with θ_r.
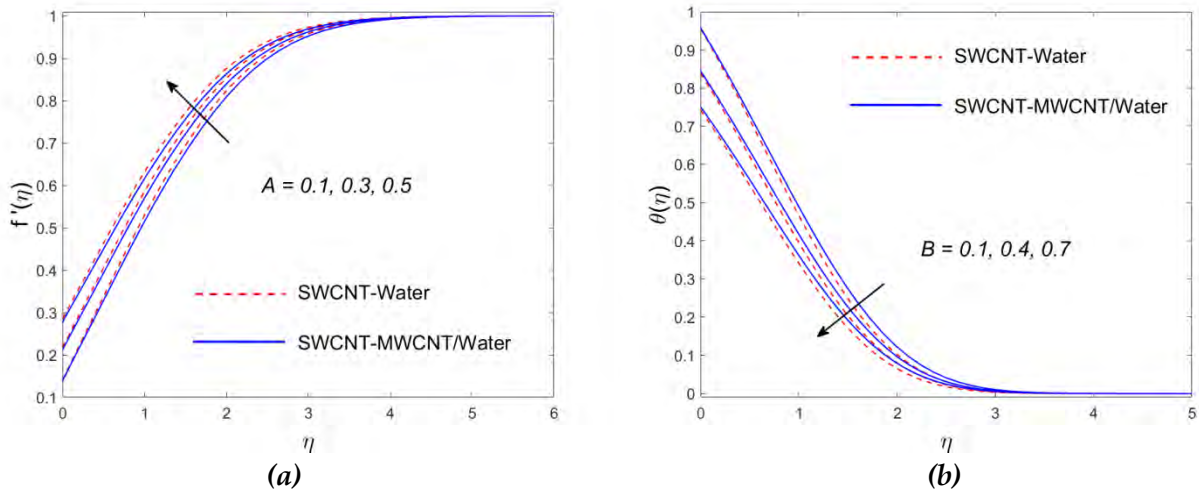
Fig. 3.3: Velocity and temperature variation (a) with A and (b) with B.
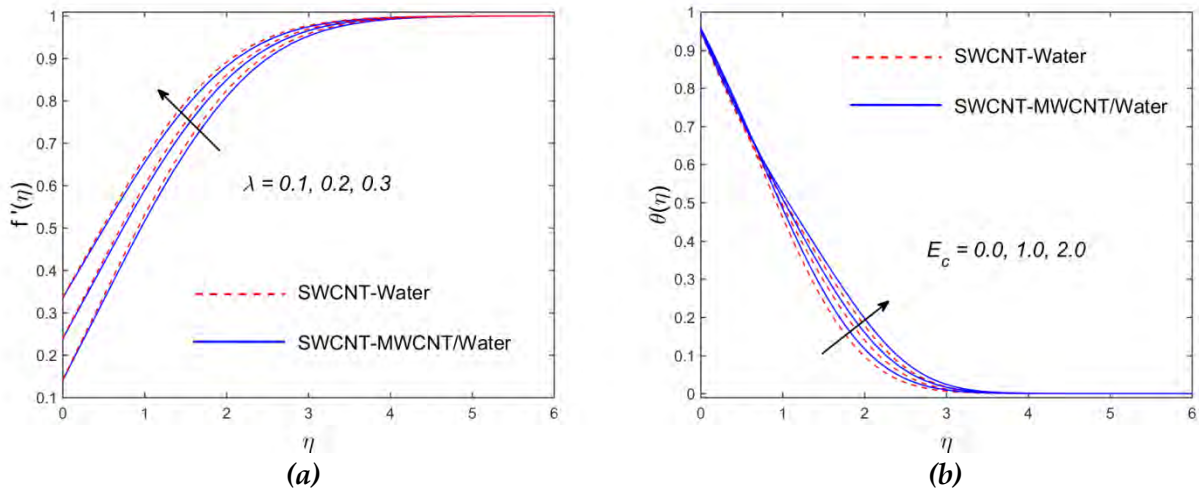
Fig. 3.4: Velocity and temperature variation (a) with λ (b) with E_c.

(a)   *(b)*
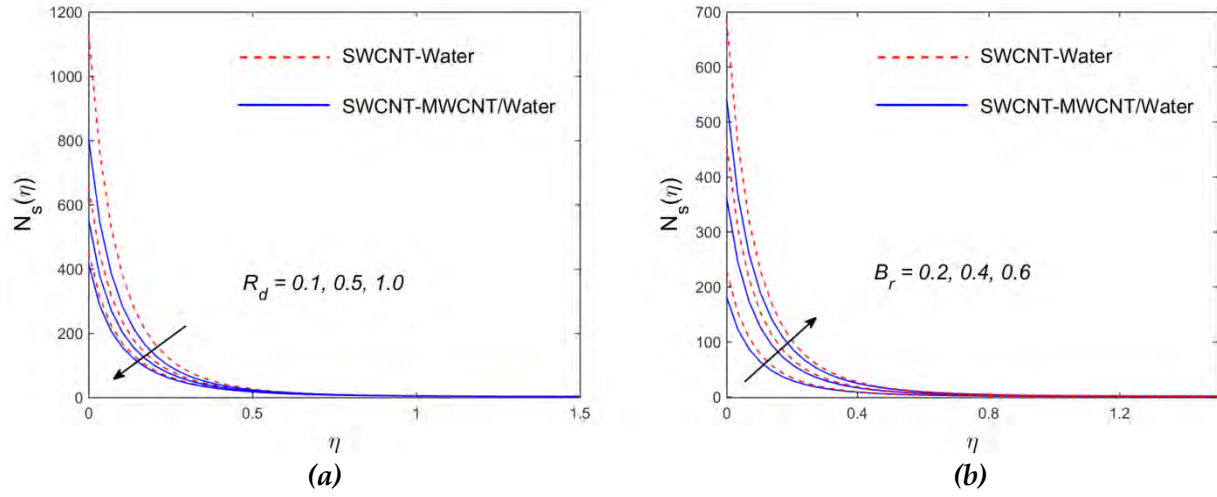
Fig. 3.5: Entropy generation variation (a) with R_d and (b) with B_r.

(a)   *(b)*
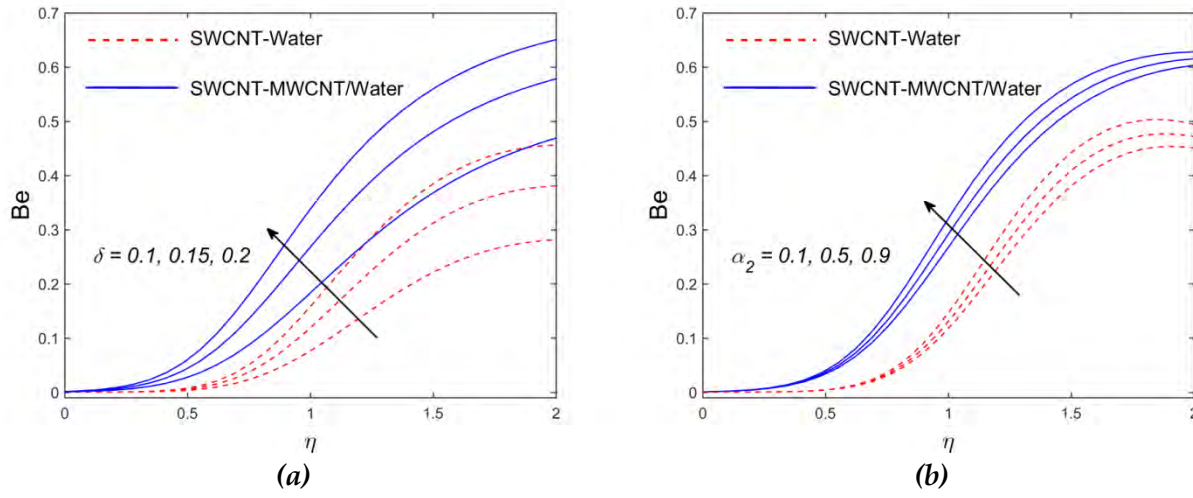
Fig. 3.6: Bejan number variation (a) with δ and (b) with α_2.

Table 3.1. *Evaluation of* $f''(0)$ *with earlier published results when* $P_m = F_r = 0 = \phi = \lambda = A$.

n	Yih [71]	Zaib and Haq [70]	Present results $f''(0)$
-0.05	0.213484	0.2138	0.21380
0.0	0.332057	0.3326	0.33260
1/3	0.757448	0.7574	0.75745
1.0	1.232588	1.2326	1.23259

Table 3.2. *Numerical value of skin friction when* $\Pr = 6.2, n = 0.5, \phi_1 = 0.03$ *and* $A = 0.1$.

ϕ_2	θ_r	P_m	F_r	λ	$\mathrm{Re}_x^{1/2} C_{fx}$	
					Simple nanofluid	Hybrid nanofluid
0.01	0.5	0.1	0.1	0.1	-0.34308	-0.35512
0.03					-0.35750	-0.36454
0.05					-0.37228	-0.37397
0.01	0.5				-0.34308	-0.35512
	0.6				-0.25194	-0.26628
	0.7				-0.17329	-0.18572
	0.5	0.2			-0.40618	-0.43043
		0.4			-0.50762	-0.54990
		0.6			-0.58846	-0.64420
		0.1	0.3		-0.31722	-0.32050
			0.5		-0.28825	-0.28215
			1.0		-0.20312	-0.17002
			0.1	0.2	-0.31982	-0.33083
				0.4	-0.26008	-0.26909
				0.6	-0.18478	-0.19149

Table 3.3. Numerical values of Nusselt number when $\Pr = 6.2, n = 0.5,$ and $\phi_1 = 0.03$.

ϕ_2	R_d	E_c	γ	B	$\mathrm{Re}_x^{-1/2} Nu_x$	
					Simple nanofluid	Hybrid nanofluid
0.01	1.0	1.0	0.1	0.1	0.69751	0.91291
0.03					0.83837	1.09210
0.05					0.97165	1.25890
0.01	0.5				0.77509	0.99614
	1.0				0.69751	0.91291
	1.5				0.63918	0.84711
	1.0	0.1			0.61119	0.79307
		0.3			0.63050	0.82031
		0.5			0.64981	0.84723
		1.0	0.1		0.69751	0.91291
			0.2		0.47528	0.61992
			0 .3		0.10081	0.11261
			0.1	0.2	0.64550	0.85288
				0.3	0.60030	0.79958
				0.4	0.56025	0.75151

Table 3.4. Numerical value of Sherwood number when $\Pr = 6.2, n = 0.5, E = 1.0,$ and $\phi_1 = 0.03$.

ϕ_2	S_c	R_c	δ	$\mathrm{Re}_x^{-1/2} Sh_x$	
				SWCNT\Water	SWCNT-MWCNT\Water
0.01	1.0	1.0	1.0	1.0145	1.0632
0.03				1.0469	1.0978
0.05				1.0803	1.1334

0.01	0.5			0.7080	0.7425
	1.0			1.0145	1.0632
	1.5			1.2508	1.3102
	1.0	1.0		1.0145	1.0632
		2.0		1.3994	1.4697
		3.0		1.7123	1.7982
		1.0	0.0	0.7478	0.7709
			0.5	0.8805	0.9170
			1.0	1.0145	1.0632

3.5 Concluding Remarks

In current chapter two dimensional, steady, incompressible hybrid nanofluid embedded in porous medium are scrutinized. Entropy generation is found using second law of thermodynamics. By means of transformation, the governing non-linear partial differential equations (PDEs) are changed into ordinary differential equations (ODEs) and tackled these equations numerically by applying the finite difference technique bvp4c. The main perceiving points of existing analysis are itemized below:

➤ Higher inertia coefficient F_r, porous P_m and variable viscosity parameter θ_r reduces the momentum boundary layer thickness.

➤ Thermal field show boosting impact via larger E_c and B for both simple nanofluid and hybrid nanofluid.

➤ The friction drag, heat transfer rate, and local Sherwood number boosts with higher the estimation of solid volume fraction.

➤ Nusselt number reduces for enlarge the value of thermal slip and radiation parameter.

➤ Entropy generation is an enhancing function of Brinkman number.

4 Chapter 4

Impact of slip effects on the stagnation point nanofluid flow via Cattaneo – Christov heat flux

4.1 Introduction

Cattaneo-Christov with temperature dependent thermal relaxation time and entropy minimization is the main concern of this chapter. The micropolar fluid with absorption of heat in the existence of mixed convection and partial slip are scrutinized. Two distinct nanoparticles (SWCNT, MWCNT) are immerged in micropolar fluid to interrogate the feature mass and heat transfer. The non-dimensional similarity transformation is consumed to translate the partial differential equations to nonlinear ordinary differential equations (ODEs) and resulting equations explained numerically consuming bvp4c from Matlab. The present results show the fabulous agreement with previous published results. The temperature distribution diminishes with larger the thermal relaxation time parameter. Furthermore, increasing the solid volume fraction reduces the velocity field while increasing thermal performance and entropy production.

4.2 Mathematical Formulation

The steady two-dimensional viscous incompressible flow is demonstrated. The flow is micropolar with thermal stratification. *Fig. 4.1* shows the problem model, as well as the flow construction and coordinate system. The time independent micropolar fluid of a stagnation point flow through a moving wedge with heat absorption is analyzed. Moreover, in the direction of flow a magnetic field is used which is normal to the

surface of wedge. The governing equations of mass, linear and angular momentum, and energy using above supposition are follow as,

Fig. 4.1: Physical representation of flow chart.

The governing equations of mass, linear and angular momentum, and energy using above supposition are follow as,

$$\frac{\partial v}{\partial y} + \frac{\partial u}{\partial x} = 0, \tag{4.1}$$

$$v\frac{\partial u}{\partial y} + u\frac{\partial u}{\partial x} = \left(\frac{(\kappa + \mu_{nf})}{\rho_{nf}}\right)\frac{\partial^2 u}{\partial y^2} - u_\infty \frac{du_\infty}{dx} + \frac{\kappa}{\rho_{nf}}\frac{\partial N}{\partial y} - \frac{\sigma_{nf}B(x)^2}{\rho_{nf}}(u - u_e)$$
$$+ \frac{g^*(\rho\beta)_{nf}}{\rho_{nf}}(T - T_\infty)\sin(\frac{\Omega^*}{2}), \tag{4.2}$$

$$v\frac{\partial N}{\partial y} + u\frac{\partial N}{\partial x} = \frac{\gamma_{nf}}{j\rho_{nf}}\frac{\partial^2 N}{\partial y^2} - \frac{\kappa}{j\rho_{nf}}\left(2N + \frac{\partial u}{\partial y}\right), \tag{4.3}$$

$$v\frac{\partial T}{\partial y} + u\frac{\partial T}{\partial x} - \frac{\tau_T}{1 + \varepsilon(T - T_\infty)}\left(u^2\frac{\partial^2 T}{\partial x^2} + u\frac{\partial v}{\partial x}\frac{\partial T}{\partial y} + u\frac{\partial T}{\partial x}\frac{\partial u}{\partial x} + v\frac{\partial u}{\partial y}\frac{\partial T}{\partial x} + v^2\frac{\partial^2 T}{\partial y^2} + v\frac{\partial u}{\partial y}\frac{\partial T}{\partial y} + 2uv\frac{\partial^2 T}{\partial x\partial y}\right)$$
$$+ \frac{\tau_T\varepsilon}{(1 - \varepsilon(T_\infty - T))^2}\left(\begin{array}{c}u^2\frac{\partial T}{\partial x}\frac{\partial(T - T_\infty)}{\partial x} \\ -v^2\frac{\partial T}{\partial y}\frac{\partial(T_\infty - T)}{\partial y}\end{array}\right) = \alpha_{nf}\frac{\partial^2 T}{\partial y^2}. \tag{4.4}$$

47

The related conditions are,

$$u = u_w(x) + N_1(x)\left[(\kappa + \mu_{nf})\frac{\partial u}{\partial y} + \kappa N\right], v = 0, N = -n^*\frac{\partial u}{\partial y},$$

$$T = D_1(x)\frac{\partial T}{\partial y} + T_w \quad \left\} \quad \text{at } y \to 0, \right.$$

$$N \to 0, \quad T \to T_\infty, u \to u_\infty(x), \text{ as } y \to \infty.$$

(4.5)

Here u and v are the component of velocity in the direction of x and y respectively.

The similarity variables are assumed by,

$$u = cx^n f'(\eta), \quad v = -\frac{1}{2}\sqrt{cv_f}\, x^{\frac{n-1}{2}}\left[(n-1)\eta f'(\eta) + (n+1)f(\eta)\right],$$

$$\eta = \sqrt{(\frac{c}{v_f})}\, y x^{\frac{n-1}{2}}, \quad N(\eta) = \sqrt{\frac{cx^{n-1}}{v_f}}cx^n h(\eta), \quad \theta(\eta) = \frac{T-T_\infty}{T_m-T_\infty},$$

$$\gamma_{nf} = (\mu_{nf} + \frac{\kappa}{2})j(x), \quad j(x) = \frac{v_f}{c}x^{1-n}.$$

(4.6)

Using similarity variables, the above equations (4.1 – 4.5) give,

$$\left(\frac{1}{(1-\phi)^{2.5}} + K\right)f''' - \left((1-\phi) + \phi\frac{\rho_{CNT}}{\rho_f}\right)\left(\frac{n+1}{2}ff'' - n(f'^2 - 1)\right) - M\left(1 + \frac{3\phi(\frac{\sigma_{CNT}}{\sigma_f}-1)}{(\frac{\sigma_{CNT}}{\sigma_f}+2)-(\frac{\sigma_{CNT}}{\sigma_f}-1)\phi}\right)(f'-1)$$

$$+ Kh' + \lambda_m\left((1-\phi) + \phi\frac{(\rho\beta)_{CNT}}{(\rho\beta)_f}\right)\theta\sin(\frac{\Omega^*}{2}) = 0,$$

(4.7)

$$\left(\frac{1}{(1-\phi)^{2.5}} + \frac{K}{2}\right)h'' + \left((1-\phi) + \phi\frac{\rho_{CNT}}{\rho_f}\right)\left(\frac{n+1}{2}fh' - \frac{3n-1}{2}fh\right) - K(f'' + 2h) = 0,$$

(4.8)

$$\frac{k_{nf}}{k_f}\theta'' + \Pr\left((1-\phi) + \phi\frac{(\rho C_p)_{CNT}}{(\rho C_p)_f}\right)$$

$$\left[\frac{n+1}{2}f\theta' + \frac{\gamma_c}{1+\theta_T\theta}\left(\frac{(n+1)^2}{2n-2}\theta''f^2 - \frac{1}{(n-1)}ff'\theta' + \frac{n-1}{2}ff\theta'\right)\right.$$

$$\left.- \frac{\gamma_c\theta_T}{(1+\theta\theta_T)^2}\left(\frac{(n-1)^2}{2}\eta^2 f'^2\theta'^2 + \eta^2 f'^2\theta'^2 + (\frac{n^2-1}{4})(\frac{n+1}{2})f^2\theta'^2 + (n+1)(\frac{n-1}{2})^2\eta ff'\theta'^2\right)\right] = 0.$$

(4.9)

The suitable conditions are,

$$h(\eta) = -n^* f''(\eta),\; f'(\eta) = \lambda + A(\frac{1}{(1-\phi)^{2.5}} + K)f''(\eta),\; f(\eta) = 0,$$
$$\theta(\eta) = 1 + B\theta'(\eta),$$
$$\left.\right\} \text{ at } \eta = 0,$$
$$f'(\eta) = 1,\; g(\eta) = 0,\; \theta(\eta) = 0,\; \text{as } \eta \to \infty. \tag{4.10}$$

The involved parameters are defined as:

$$K = \kappa / \mu_f,\; \lambda_m = \frac{Gr_x}{\operatorname{Re}_x^{5/2}} = g\beta_f \nu^{\frac{1}{2}} / c^{\frac{5}{2}},\; B = D_1^* \sqrt{\frac{(n+1)c}{2\nu_f}},\; A = N_1^* \upsilon_f \sqrt{\frac{(n+1)c}{2\nu_f}}$$

Skin friction C_f is given as,

$$C_f = \frac{\tau_w}{\rho_f u_\infty^2},$$
$$\tau_w = \left[(\mu_{nf} + \kappa)\frac{\partial u}{\partial y} + \kappa N\right]_{y=0}. \tag{4.11}$$

Using equation (4.6) in equation (4.11) we get,

$$\operatorname{Re}_x^{1/2} C_{fx} = \left(\frac{1}{(1-\phi)^{2.5}} + K(1-n^*)\right)f''(0). \tag{4.12}$$

Here local Reynolds number is $\operatorname{Re}_x = \frac{xu_\infty}{\nu_f}$.

4.3 Entropy Generation Analysis

The volumetric rate of local entropy production of viscous fluid is given as:

$$E_G = \underbrace{\frac{k_{nf}}{T_\infty^2}\left(\frac{\partial T}{\partial y}\right)^2}_{heat\ transfer\ irreversibility} + \underbrace{\left(\frac{\mu_{nf} + \kappa}{T_\infty}\right)\left(\frac{\partial u}{\partial y}\right)^2 + \frac{\sigma_{nf}}{T_\infty}B(x)^2 u^2}_{fluid\ friction\ irreversibility}. \tag{4.13}$$

The dimensionless entropy age can be molded by the accompanying relation

$$N_s = \frac{T_\infty^2 (y/\eta)^2}{k_{nf}(T_w - T_\infty)}E_G. \tag{4.14}$$

Exploiting the similarity transformation (4.6) the entropy generation (or production) converted:

$$N_s(\eta) = \frac{k_{nf}}{k_f} \operatorname{Re}_x \theta'^2 + \left(K + (1-\phi)^{-25/10}\right) \frac{\operatorname{Re}_x Br}{\delta} f''^2 + \frac{\operatorname{Re}_x BrM^2}{\delta} \frac{\sigma_{nf}}{\sigma_f} f'^2, \qquad (4.15)$$

The involved parameters are delineate as,

$$\delta = \frac{\Delta T}{T_\infty}, Br = \frac{\mu_f u_w^2}{k_f \Delta T}, \operatorname{Re}_x = \frac{xu_w}{\upsilon_f}.$$

In mathematical form the Bejan number is expresses as,

$$Be = \frac{\dfrac{k_{nf}}{k_f} \operatorname{Re}_x \theta'^2}{\dfrac{k_{nf}}{k_f} \operatorname{Re}_x \theta'^2 + \left(K + (1-\phi)^{-2.5}\right)\dfrac{\operatorname{Re}_x Br}{\Omega} f''^2 + \dfrac{\operatorname{Re}_x BrM^2}{\Omega} \dfrac{\sigma_{nf}}{\sigma_f} f'^2}.$$

Bejan number requirement lie among $0 < Be < 1$. Consequently, $Be = 0$ explain that the irreversibility due to viscous dissipation dominates, while $Be = 1$ means that heat transfer irreversibility dominates. Clearly the $Be = 0.5$ is the situation wherein the irreversibility because of heat transfer is equal to viscous dissipation in the entropy generation.

4.4 Results and Discussion

The systems of equations (4.7) - (4.9) with boundary condition (4.10) are explained numerically by means of bvp4c function form MATLAB. While using this method, the third and second order ODEs are transformed into the system of first order ODEs. The convergence requirements are allotted as 10^{-5}. To warranty of every numerical solution approach asymptotic value accurately we take $\eta_\infty = 5$. The evaluation amongst existing outcomes of the skin friction with previously available information is recorded in *Table 3.1*. *Table 4.1* tabulated the numerical values of friction drag for dissimilar variables. It is found that the drag force improves with larger the values of solid volume fraction and diminishes with magnetic parameters, material parameter, and moving wedge parameter. The influences of different parameter on velocity profile, micro-rotation field, temperature distribution, entropy minimization, and Bejan number are studied

graphically. *Fig. 4.2 ((a) and (b))* examined the upshot of solid volume fraction on microrotation profile and entropy generation profile. With enhancement in solid volume fraction the entropy profile shows increasing behavior while the microrotation profile shows dual behavior. It is seen that near the surface the microrotation profile enhances and far the boundary it diminishes (see in *Fig. 4.2 (b)*). *Fig. 4.3 (a – d)* dissected the influence of material parameter on linear and angular velocity field, temperature distribution, and entropy production. The material parameter diminishes the axial velocity. This is demonstrated in *Fig. 4.3 (a)*. The microrotation, temperature, and entropy generation distribution improve with developing the assessment of material parameter for both cases which is illustrate in *Fig. 4.3 (c – d)*. The improved K increases the fluid's associated viscosity and, due to higher viscous forces, induces more heat. Therefore, as shown in *Fig. 4.3 (c)*, the temperature and also thermal boundary layer thickness improved with an escalation value K. In *Fig. 4.4 (a)* the temperature profile diminishes with larger the value of thermal relaxation time. It is due because that for huge γ_c the particles of material need greater opportunity to move heat to its neighboring particles. It is concluded that for $\gamma_c = 0$ the heat moves speedily all over the objects. As such temperature distribution is larger for $\gamma_c = 0$. The temperature difference parameter reduces the temperature distribution, which is delineating in *Fig. 4.4 (b)*. *Fig. 4.5 ((a) and (b))* manifests the upshot of Brinkman number on Bejan number and Reynolds number Re_x on entropy generation respectively. The Bejan number decline with enlarger the value of Brinkman number and entropy generation enhance for Reynolds number.

(a)   *(b)*
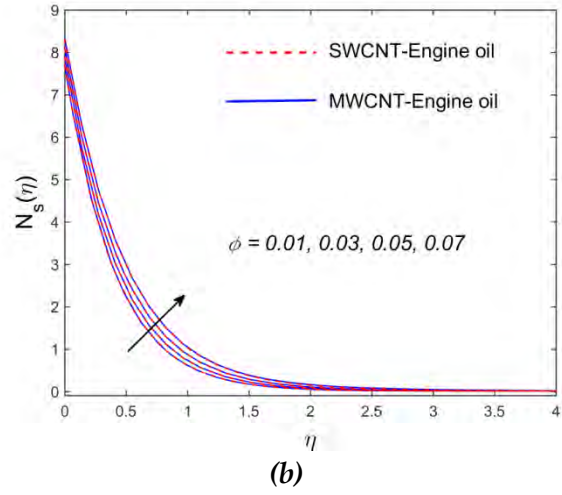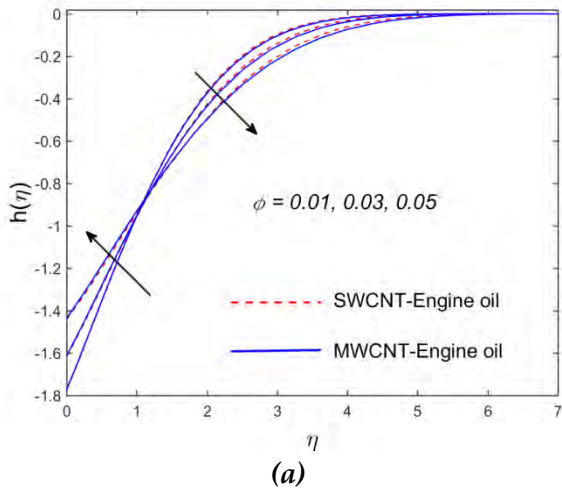
Fig. 4.2: Angular velocity and entropy generation variation with solid volume fraction.

(a)   *(b)*

(c)   *(d)*

Fig. 4.3: Linear and angular velocity, temperature, and entropy generation variation with micropolar parameter.

(a)   *(b)*

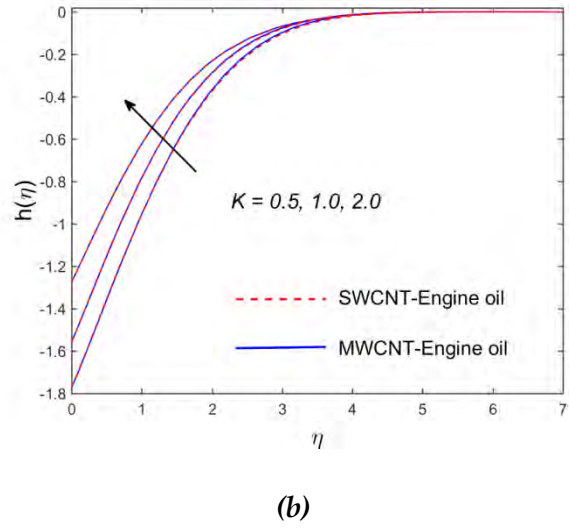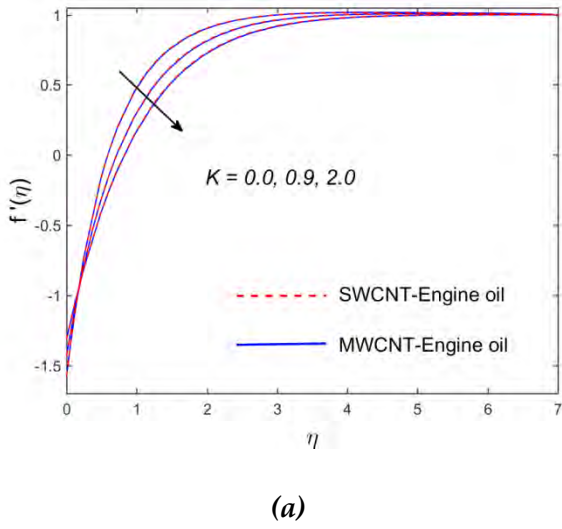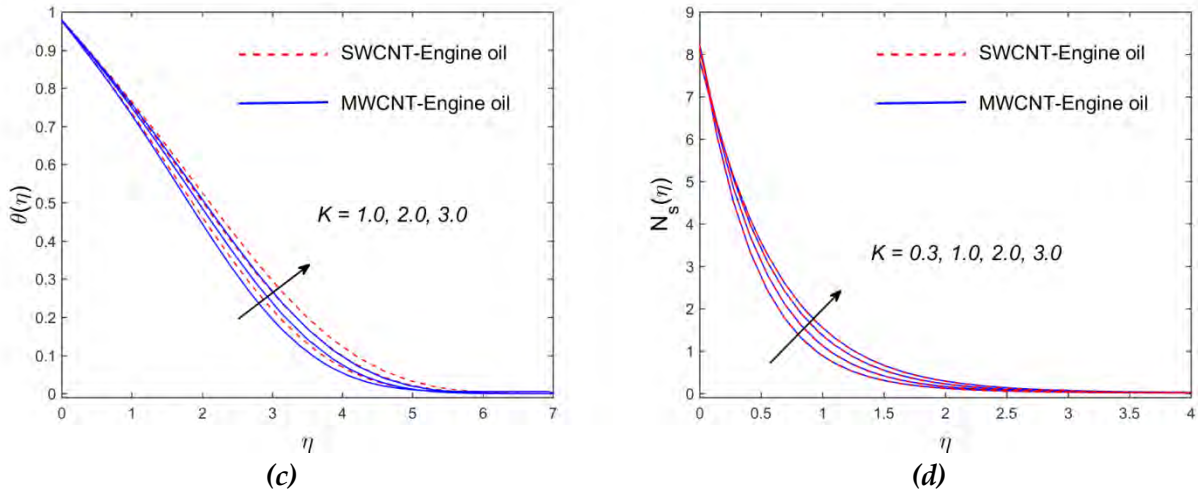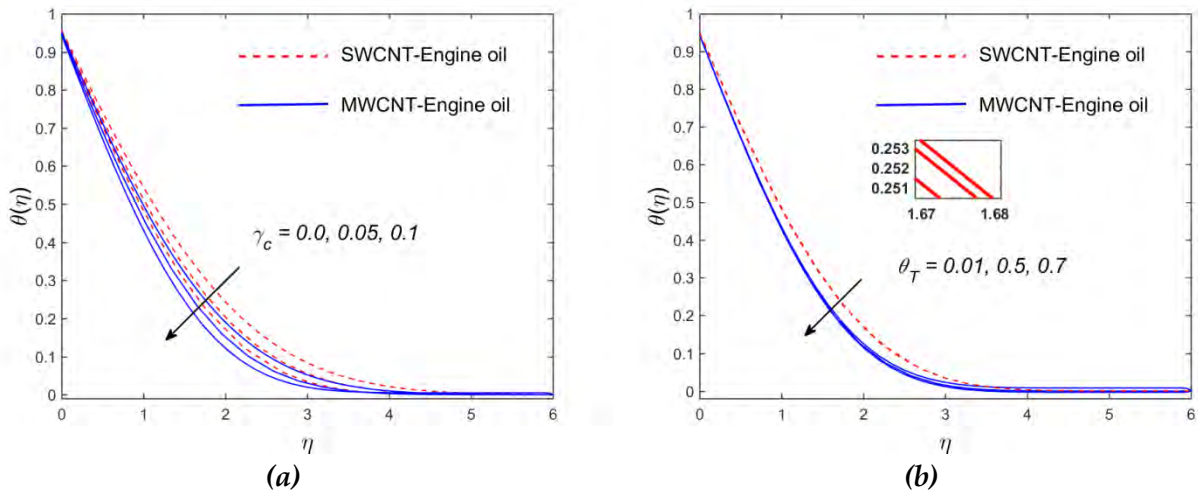***Fig. 4.4: Temperature variation (a) with γ_c and (b) with θ_T.***
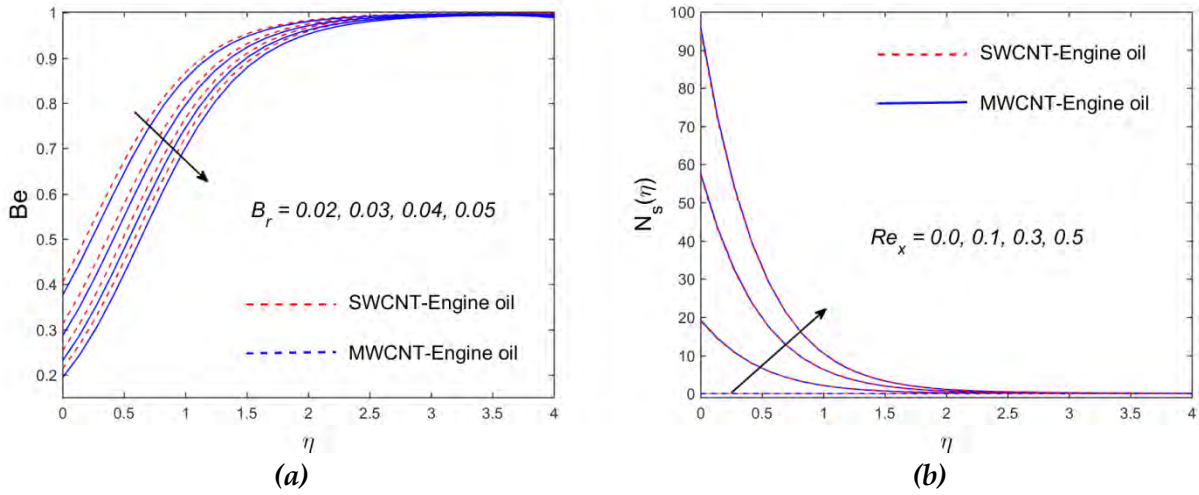
Fig. 4.5: Bejan number and entropy generation variation (a) with B_r and (b) with Re_x.

Table 4.1. Numerical value of local skin friction for dissimilar parameters when
$n^* = 0.5, A = 0.1, \ \lambda_m = 0.5, \ and \ n = 0.1.$

ϕ	M	λ	K	$\mathrm{Re}_x^{1/2} C_{fx}$	
				SWCNTs	MWCNTs
0.01	0.1	1.0	0.1	0.69843	0.68727
0.03				0.72241	0.74196
0.05				0.79800	0.82660
0.01	0.3	1.0	0.1	0.55296	0.60168
	0.5			0.54671	0.54937
	1.0			0.46210	0.46505
0.01	0.1	0.5	0.1	0.79351	0.80000
		1.0		0.69843	0.68727
		1.5		0.54293	0.55451
0.01	0.1	1.0	0.1	0.69843	0.68727
			0.2	0.58965	0.68648
			0.3	0.50755	0.59570

4.5 Concluding Remarks

In present chapter, the two dimensional, steady, and incompressible micropolar fluids past a moving wedge are examined. The energy equation is supported in the existence of thermal slip and temperature dependent thermal relaxation time. The numerical clarification is gained by applying the technique bvp4c. The main observing points of present analysis are specified beneath:

- ➢ Entropy generation enhances for enhancing estimation of Reynolds number and material parameter (K), and Bejan number is reduced with Brinkman number.
- ➢ Thermal relaxation parameter reduces the temperature and their related thermal boundary layer thickness.
- ➢ Angular velocity and entropy generation, rises while axial velocity reduces with rising the solid volume fraction ϕ.
- ➢ Local skin friction declines with magnetic parameter, stretching parameter, and material parameter however for solid volume fraction it's upgraded.

5 Chapter 5

Analysis of two phase fluid flow in presence of Thomson and Troian slip condition

5.1 Introduction

This chapter considers entropy minimization in stagnation point flow of a hybrid nanofluid over a nonlinear permeable stretching surface with Thomson and Troian boundary condition. Due to porous medium the Darcy-Forchheimer relation is added. The energy equation is deliberated under the effect of heat generation, viscous dissipation, and Cattaneo-Christov theory. Further the influence of variable viscosity, activation energy and variable mass diffusivity are taken into account. For first time, hybrid nanofluid involving of carbon nanotubes with Thomson and Troian boundary conditions and induced MHD has been implemented and has not yet been studied. The bvp4c function from Matlab is utilized to solve the transformed ordinary differential equation (ODEs). This method has good certainty to solve this problem, compared to previous works. It is noticed that the solid volume fraction declines the velocity profile and enhance the temperature distribution. Further, compared to simple nanofluid, hybrid nanofluid has greater thermal conductivity and better heat transfer performance.

5.2 Mathematical Description

In current chapter, we examined the two-dimensional incompressible hybrid nanoliquid stagnation point flow over a nonlinear stretching surface along Thomson and Troian boundary condition. The flow analysis is studied through the application of Darcy-Forchheimer law. The total entropy minimization rate is found by implement the second law of thermodynamics. Physical description of the present flow is given in *Fig.*

5.1. It is accept that the flat surface moving in the x-direction along velocity $u_w(x) = ax^n$, and free stream (inviscid flow) velocity is thought to be $u_e(x)$. Induced magnetic field H is assumed. Moreover H_1 and H_2 are parallel and normal components of H.
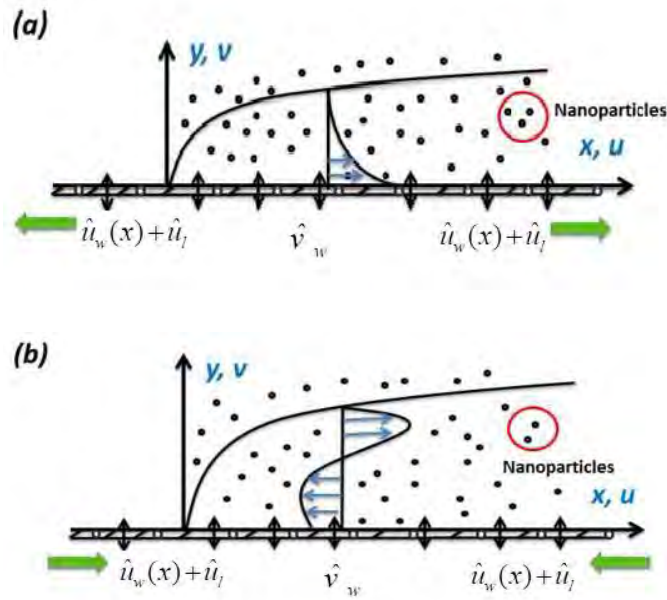
Fig. 5.1: Physical description of problem for (a) stretching sheet $\lambda > 0$ and (b) shrinking sheet $\lambda < 0$.

Variable viscosity, and mass diffusivity is mathematically described by [18]

$$\mu_f(T) = \frac{\mu_\infty}{1 + \varepsilon(T - T_\infty)}, \tag{5.1}$$

$$D(C) = D_f(1 + \varepsilon_1 g). \tag{5.2}$$

Imposing the approximation of the boundary layer and assuming that we have a system of equations:

$$\frac{\partial H_2}{\partial y} + \frac{\partial H_1}{\partial x} = 0, \quad \frac{\partial v}{\partial y} + \frac{\partial u}{\partial x} = 0, \tag{5.3}$$

$$v\frac{\partial u}{\partial y}+u\frac{\partial u}{\partial x}+\frac{\mu_0 H_e}{4\pi\rho_{hnf}}\frac{\partial H_e}{\partial x}-u_e\frac{du_e}{dx}=\frac{1}{\rho_{hnf}}\frac{\partial}{\partial y}\left(\mu_{hnf}(T)\frac{\partial u}{\partial y}\right)+\frac{\mu_0}{4\pi\rho_{hnf}}\left(H_1\frac{\partial H_1}{\partial x}+H_2\frac{\partial H_1}{\partial y}\right)$$

$$-\frac{1}{\rho_{hnf}}\frac{\mu_{hnf}(T)}{K^{**}}(u-u_e)-F^{**}(u^2-u_e^2),\tag{5.4}$$

$$v\frac{\partial H_1}{\partial y}+u\frac{\partial H_1}{\partial x}=\mu_e\frac{\partial^2 H_1}{\partial y^2}-\left(\frac{\partial u}{\partial x}H_1+\frac{\partial u}{\partial y}H_2\right),\tag{5.5}$$

$$u\frac{\partial T}{\partial x}+v\frac{\partial T}{\partial y}+\tau_T\left(\begin{array}{l}u^2\frac{\partial^2 T}{\partial x^2}+2uv\frac{\partial^2 T}{\partial x\partial y}+v^2\frac{\partial^2 T}{\partial y^2}+u\frac{\partial v}{\partial x}\frac{\partial T}{\partial y}\\+v\frac{\partial u}{\partial y}\frac{\partial T}{\partial x}+v\frac{\partial v}{\partial y}\frac{\partial T}{\partial y}+u\frac{\partial u}{\partial x}\frac{\partial T}{\partial x}+2\mu_{hnf}(T)(u\frac{\partial^2\hat{v}}{\partial x^2}+v\frac{\partial^2 u}{\partial y^2})\end{array}\right)=\frac{\partial}{\partial y}\left(\left(\alpha_{hnf}+\frac{16\sigma^* T^3}{3k^*(\rho C_p)_{hnf}}\right)\frac{\partial T}{\partial y}\right)$$

$$-\tau_T\left[\frac{Q(x)}{(\rho C_p)_{hnf}}\left(u\frac{\partial(T-T_\infty)}{\partial x}+v\frac{\partial(T-T_\infty)}{\partial y}\right)\right]+\frac{2\mu_{hnf}(T)}{(\rho C_p)_{hnf}}\left(\frac{\partial u}{\partial y}\right)^2+\frac{Q(x)}{(\rho C_p)_{hnf}}(T-T_\infty),\tag{5.6}$$

$$u\frac{\partial C}{\partial x}+v\frac{\partial C}{\partial y}-\frac{D_f(1+\varepsilon_1 g)}{(1-\phi_1)^{-2.5}(1-\phi_2)^{-2.5}}\frac{\partial^2 C}{\partial y^2}=\frac{D_f\varepsilon_1}{(1-\phi_1)^{-2.5}(1-\phi_2)^{-2.5}}\frac{\partial g}{\partial y}\frac{\partial C}{\partial y}$$

$$-k_r^2\left(\frac{T}{T_\infty}\right)^m\exp\left(\frac{-E_a}{kT}\right)(C-C_\infty).\tag{5.7}$$

The connected boundary conditions are [72],

$$u\big|_{y=0}=u_w(x)+u_l=ax^n+\gamma^*(1-\xi^*\frac{\partial u}{\partial y}\big|_{y=0})^{-1/2}\frac{\partial u}{\partial y}\big|_{y=0},\quad v\big|_{y=0}=0,\quad T\big|_{y=0}=T_w,\tag{5.8}$$

$$C\big|_{y=0}=C_w,\quad \frac{\partial H_1}{\partial y}\big|_{y=0}=0,\ H_2\big|_{y=0}=0,$$

$$u\big|_{y\to\infty}\to u_e(x),\ v\big|_{y\to\infty}\to 0, H_1\big|_{y\to\infty}\to H_e=H_0 x^n, T\big|_{y\to\infty}\to T_\infty,\ C\big|_{y\to\infty}\to C_\infty.\tag{5.9}$$

The suitable variables are recognized by,

$$\psi=\sqrt{\frac{2cv_f x^{n+1}}{1+n}}f(\eta),\eta=\sqrt{\frac{c(n+1)x^{n-1}}{2v_f}}y,\ \theta(\eta)=\frac{T_\infty-T}{T_\infty-T_w},g(\eta)=\frac{C-C_\infty}{C_w-C_\infty},$$

$$u=cx^n f'(\eta),v=-\sqrt{\frac{(1+n)cv_f x^{n-1}}{2}}[f(\eta)+\frac{n-1}{1+n}\eta f'(\eta)],\tag{5.10}$$

$$H_2=-H_0\sqrt{\frac{2v_f x^{n-1}}{U_\infty(1+n)}}[nq(\eta)+\frac{n-1}{2}\eta q'(\eta)], H_1=H_0 x^n q'(\eta).$$

Using similarity transformation, the above equations (5.3 – 5.9) give,

$$D_1 = \left((1-\phi_2)\left\{(1-\phi_1)+\phi_1 \tfrac{\rho_{MWCNT}}{\rho_f}\right\}+\phi_2 \tfrac{\rho_{SWCNT}}{\rho_f}\right), D_2 = (1-\phi_1)^{2.5}(1-\phi_2)^{2.5},$$

$$D_3 = \left((1-\phi_2)\left\{(1-\phi_1)+\phi_1 \tfrac{(\rho C_p)_{MWCNT}}{(\rho C_p)_f}\right\}+\phi_2 \tfrac{(\rho C_p)_{SWCNT}}{(\rho C_p)_f}\right),$$

$$\frac{f'''}{1+\theta_r\theta}+D_1D_2\left(ff''+\left(\frac{2n}{n+1}\right)(1-f'^2)-\frac{2F_r}{n+1}(f'^2-1)\right)+\frac{2M}{n+1}D_2(nq'^2-nqq''-n)$$
$$-\frac{\theta_r\theta'f''}{(1+\theta_r\theta)^2}-\frac{2P_m}{(n+1)(1+\theta_r\theta)}(f'-1), \tag{5.11}$$

$$M_1q'''-\frac{2n}{n+1}qf''+fq''=0 \tag{5.12}$$

$$\left(\frac{k_{hnf}}{k_f}+R_d\left(1+(T_r-1)\theta\right)^3\right)\theta''+3R_d\left(1+(T_r-1)\theta\right)^2(T_r-1)\theta'^2+\Pr\left(D_c\theta+\frac{E_c f''^2}{(1+\theta_r\theta)D_2}\right)$$
$$+\Pr D_3\left[f\theta'-\gamma_c\left\{\begin{array}{l}(6-2n)ff'\theta'+\frac{(n-1)^2\eta^2}{2n+2}f'^2\theta''+\frac{n+1}{2}f^2\theta''\\[2mm]+\eta(n-1)ff'^2\theta''-2(n-1)\eta ff'\theta''+\frac{\gamma_c D_c}{D_3}(f\theta'-f'\theta)\\[2mm]+\frac{2E_c}{(1+\theta_r\theta)D_2}(f'f''^2-ff''f''')\end{array}\right\}\right]=0, \tag{5.13}$$

$$\left(\frac{D_2}{S_c(1+\varepsilon_1h)^{-1}}\right)g''+\varepsilon_1 g'^2+fg'-\frac{2}{n+1}R_c(1+\delta\theta)^m h\exp(\frac{-E}{1+\delta\theta})=0. \tag{5.14}$$

The appropriate conditions are,

$$f(0)=0, q(0)=0, f'(0)=\lambda+Af''(0)\left[1-\xi f''(0)\right]^{-1/2}, q''(0)=0, \theta(0)=1=g(0), \tag{5.15}$$

$$f'(\eta)=q'(0)=1, \quad \theta(\eta)=0=g(\eta)=0, \text{ at } \eta\to\infty. \tag{5.16}$$

In Eq. (5.15), A is slip velocity parameter and ξ is critical shear rate which are defined as

$$A=\sqrt{\frac{(n+1)c}{2\upsilon_f}}x^{\frac{n-1}{2}}\gamma^*(x), \quad \xi=c\sqrt{\frac{cn+c}{2\upsilon_f}}\xi^*(x)x^{\frac{3n-1}{2}}. \tag{5.17}$$

For similarity solution of Eqs. (5.11) to (5.16) A and ξ suggested to be constant instead of function of variable x. This can be accomplished, if we accept $\xi^*(x)$ relative to $x^{\frac{1-3n}{2}}$ and $\gamma^*(x)$ proportional to $x^{\frac{1-n}{2}}$, so we define

$$\gamma^*(x) = a^{**} x^{\frac{1-n}{2}}, \quad \xi^*(x) = b^{**} x^{\frac{1-3n}{2}}, \tag{5.18}$$

Consuming Eq. (5.18) in Eq. (5.17), we find

$$A = a^{**}\sqrt{\frac{cn+c}{2\upsilon_f}}, \quad \xi = c\sqrt{\frac{cn+c}{2\upsilon_f}} b^{**}, \tag{5.19}$$

The dimensionless parameter involved in Eqs. (5.11) to (5.16) are mathematically concluded as:

$$\Pr = \frac{\nu_f}{\alpha_f}, \lambda = \frac{a}{c}, F_r = \frac{C_b}{\sqrt{K^{**}}\rho_f}, P_m = \frac{\upsilon_f}{cK^{**}}, M_1 = \frac{\mu_e}{\upsilon_f}, M = \frac{\mu_0}{4\pi\rho_f}\left(\frac{H_0}{c}\right)^2,$$

$$E_c = \frac{u_e^2}{\Delta T C_{pf}}, D_c = \frac{Q_0}{c(\rho C_p)_f}, \gamma_c = c\lambda_1, \theta_r = \varepsilon(T_w - T_\infty), R_d = \frac{16\sigma^* T_\infty^3}{3k_f k^*},$$

$$\alpha_1 = \frac{T_w - T_\infty}{T_\infty}, S_c = \frac{\upsilon_f}{D_f}, R_c = \frac{k_r^2}{c}, E = \frac{E_a}{kT_\infty},$$

5.3 Entropy Generation Analysis

The volumetric rate of local entropy production of viscous fluid is given as:

$$
\begin{aligned}
S_G = \frac{k_f}{T_\infty^2}\left[\frac{k_{hnf}}{k_f} + \frac{16\sigma^* T_\infty^3}{3k^* k_f}\right]\left(\frac{\partial T}{\partial y}\right)^2 + \left(\frac{\mu_{hnf}(T)}{T_\infty}\right)\left(\frac{\partial u}{\partial y}\right)^2 + \frac{u^2}{T_\infty}\left(\frac{\mu_{hnf}(T)}{K^{**}} + F^{**}|u|\right) \\
+ \frac{DR}{T_\infty}\left(\frac{\partial C}{\partial y}\frac{\partial T}{\partial y}\right) + \frac{DR}{C_\infty}\left(\frac{\partial C}{\partial y}\right)^2,
\end{aligned}
\tag{5.20}
$$

The dimensionless form of entropy minimization is required using below relation

$$N_s = \frac{(y/\eta)^2 T_\infty}{k_f(T_w - T_\infty)} S_G, \tag{5.21}$$

After exploiting the similarity transformation (5.10), Eq. (5.21) becomes:

$$N_s(\eta) = \left(\frac{k_{hnf}}{k_f} + R_d \left(1 + (T_r - 1)\theta \right)^3 \right) \left(\frac{n+1}{2} \right) \delta \theta'^2 + \frac{Br(1 + \theta_r\theta)^{-1}}{D_2} \left(\frac{n+1}{2} \right) f''^2$$

$$+ \frac{BrPm(1 + \theta_r\theta)^{-1}}{D_2} f'^2 + F_r Brf'^3 + L\frac{\alpha_2}{\delta} g'^2 + Lg'\theta'. \tag{5.22}$$

Variable used during above equation are describes as,

$$\delta = \frac{\Delta T}{T_\infty}, \alpha_2 = \frac{\Delta C}{C_\infty}, Br = \frac{\mu_f u_e^2}{k_f \Delta T}, L = \frac{RD(C_w - C_\infty)}{k_f}. \tag{5.23}$$

5.4 Results and Discussion

The finite difference technique bvp4-c function from MATLAB is integrate to solve the influence of solid volume fraction (ϕ_2), velocity slip parameter (γ_1), magnetic parameter (M), reciprocal magnetic Prandtl number (M_1), Eckert number (E_c), concentration difference on velocity distribution, induced magnetic profile, temperature field, concentration profile, and entropy generation. *Fig. 5.2 ((a) – (b))* scrutinized the effect of ϕ_2 on velocity profile, induced magnetic field, temperature profile, and concentration profile. Velocity and induced magnetic field reduced with larger the value of ϕ_2. Physically, enhanced ϕ_2 the thermal conductivity of nanofluid increases which slow the fluid motion and boost the heat transfer rate as a consequence temperature improves (see in *Fig. 5.2 (c)*). Concentration profile diminishes for both cases with enhances solid volume fraction ϕ_2. It is given in *Fig. 5.2 (d)*. *Fig. 5.3 (a)* shows decreasing behavior of the velocity field through a magnetic parameter. This is based on the fact that Lorentz force determines the existence of the transverse magnetic field, which occurs in retarding force on the velocity field. Thus, the retarding force and therefore the velocity reduces as the estimation of M improve. *Fig. 5.3 (b)* depicts the impact of reciprocal Prandtl number on $q'(\eta)$. Physically Lorentz forces boosts with higher the assessment

of M_1 which decrease the $q'(\eta)$. **Fig. 5.4 (a)** determines the result of velocity slip parameter on velocity field. It is perceived that an enlargement in γ_1 produce a stronger $f'(\eta)$. **Fig. 5.4 (b)** characterizes the temperature distribution against Eckert number E_c for both cases. Here temperature sketch $\theta(\eta)$ increases through larger values of E_c for both nanofluid and hybrid nanofluid. Further it is seen that the thermal boundary layer thickness is higher for hybrid nanofluid than nanofluid. **Fig. 5.5 ((a) and (b))** describes entropy generation number $N_s(\eta)$ to the α_2 and L. It is found that enhancing α_2 and L leads to a substantial increment in entropy generation $N_s(\eta)$, in the near of the sheet. **Fig. 5.6 (a)** illustrated the influence of critical shear rate ξ verses SWCNT solid volume fraction ϕ_2 on skin friction coefficient. It is seen that $f''(0)$ sketch diminishes by enhancing the estimation of ξ while it is enhances with ϕ_2. The Sherwood number is graphically demonstrated in **Fig. 5.6 (b)** against temperature difference δ verses ϕ_2. It is found that the Sherwood number boosts with boosting the estimation of δ and ϕ_2. **Table 5.1** demonstrates the comparison table with previous published result. **Table 5.2 and 5.3** show the numerical values of friction drag and local Sherwood number for distinct parameters. It is realized that the friction drag enhances for larger values of ϕ_2 variable viscosity θ_r, porosity parameter P_m and F_r, while it is reduce for M and ξ. Similarly, for increasing the estimation of ϕ_2, S_c, R_c, α_2 Sherwood number enhances.
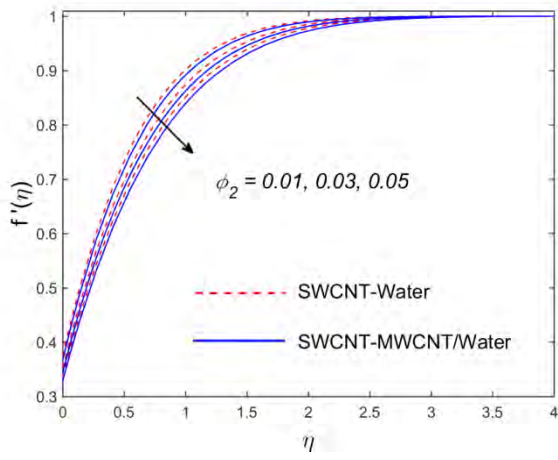
(a)
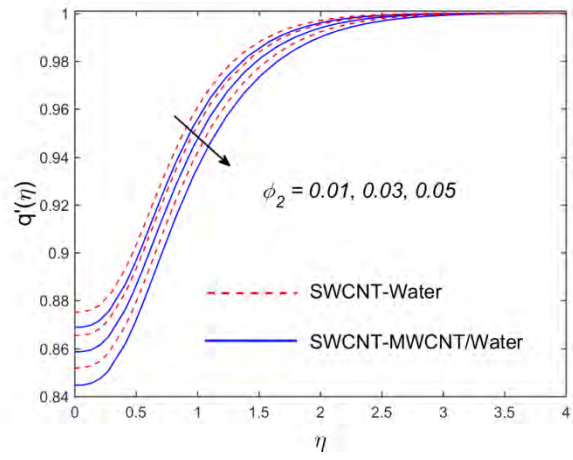
(b)
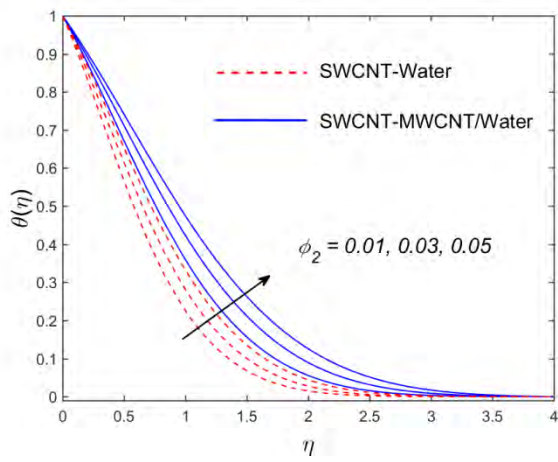
(c)
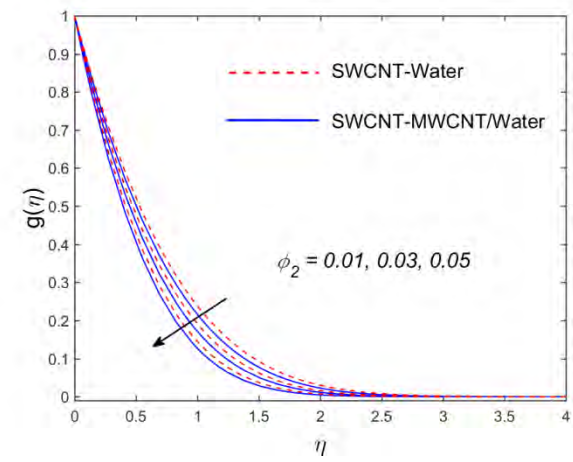
(d)

Fig. 5.2: Velocity, induced magnetic field, temperature, and concentration variation with solid volume fraction.
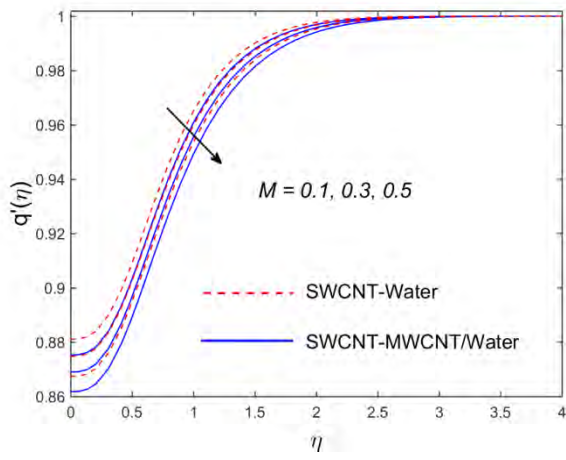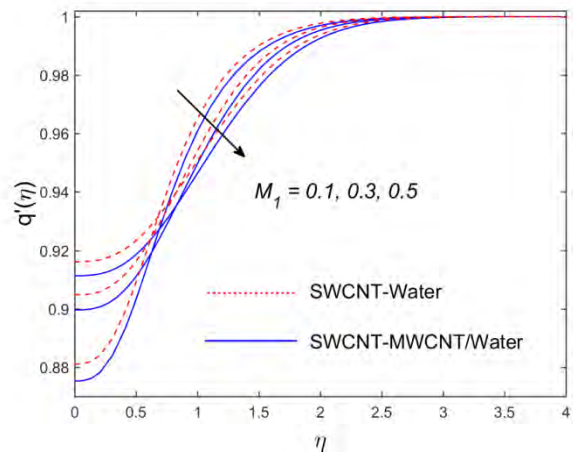
(a)   *(b)*

Fig. 5.3: Induced magnetic field variation (a) with M (b) with M_1.
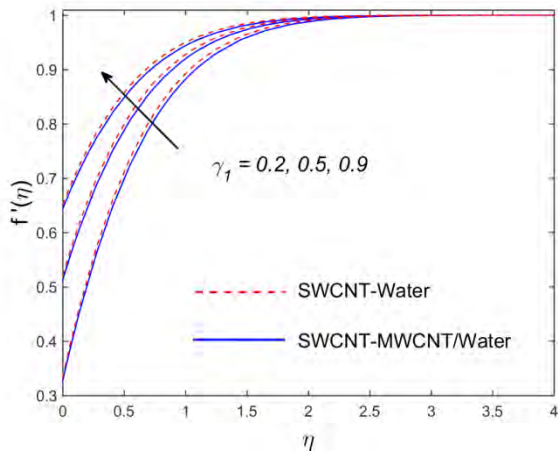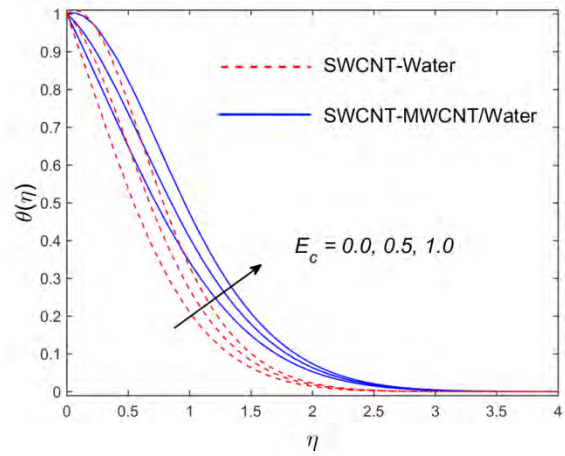
(a)   *(b)*

Fig. 5.4: Velocity and temperature variation (a) with γ_1 (b) with E_c.
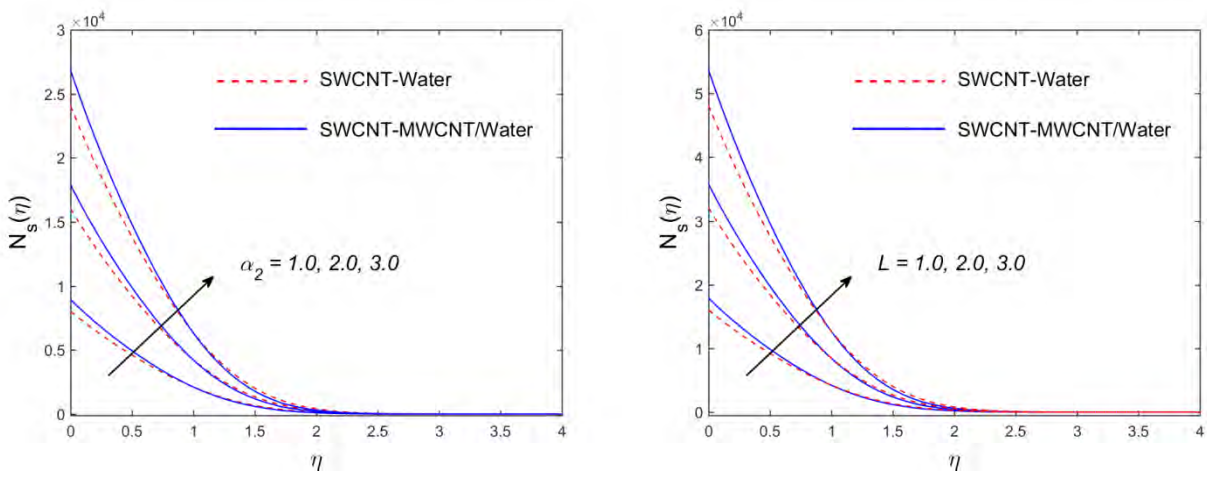
Fig. 5.5: Entropy generation variation (a) with α_2 (b) with L.
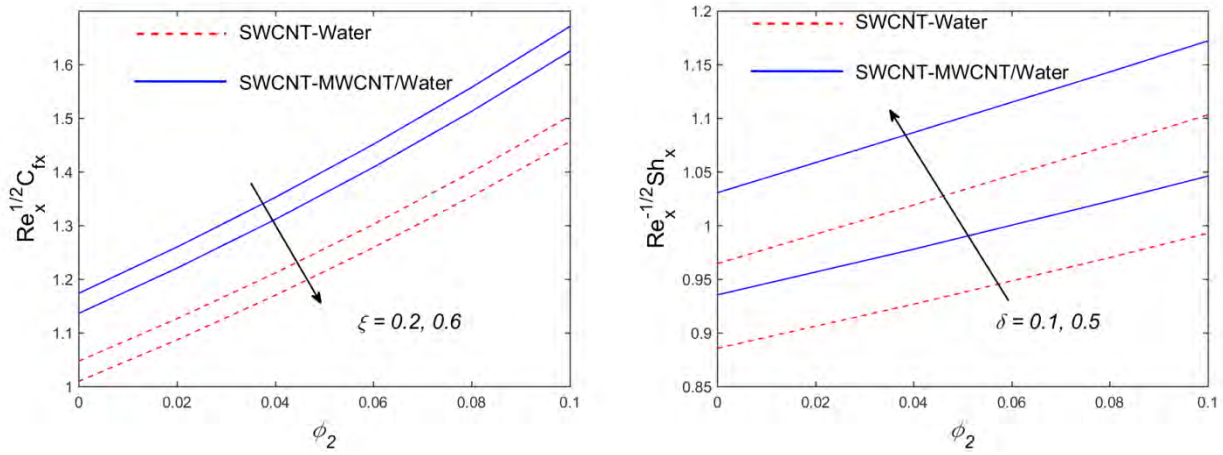
Fig. 5.6: Skin friction and Sherwood number variation (a) with ξ (b) with δ versus ϕ_2.

Table 5.1. Comparison of $f''(0)$ with previous published results when $P_m = F_r = M_1 = 0 = \xi = \theta_r = \phi_i$.

λ	Wang [36]	Khan et al. [35]	Present result $f''(0)$
5.0	−10.26475	−10.2647	−10.265
3.0		−4.27654	−4.2765
2.0	−1.88731	−1.8873	−1.8873
1.0	0.0000	0.0000	0.0000
0.5	0.7133	0.71329	0.7132
0.0	1.232588	1.23259	1.2325

Table 5.2. Numerical value of skin friction when $\Pr = 6.2, n = 0.5, \phi_1 = 0.05$, **and** $\lambda = 0.1$.

| ϕ_2	θ_r	P_m	F_r	M	ξ	$Re_x^{1/2} C_{fx}$	
						Simple nanofluid	Hybrid nanofluid
0.01	0.5	0.1	0.1	0.2	0.2	1.1227	1.2612
0.03						1.2034	1.3495
0.05						1.2913	1.4464
0.01	0.3					0.9175	1.0358
	0.4					1.0188	1.1472
	0.5					1.1227	1.2612
		0.2				1.1512	1.2976
		0.4				1.2017	1.3615
		0.6				1.2452	1.4162
			0.3			1.1829	1.3311
			0.5			1.2752	1.4392
			1.0			1.3443	1.5210
				0.1		1.1246	1.2633

				0.3		1.1208	1.2590
				0.5		1.1169	1.2545
					0.2	1.1227	1.2612
					0.4	1.0846	1.2222
					0.6	1.0420	1.1785

Table 5.3. Numerical value of local Sherwood number when $\Pr = 6.2, n = 0.5, \phi_1 = 0.05.$

ϕ_2	S_c	R_c	δ	$\mathrm{Re}_x^{-1/2}\, Sh_x$	
				Simple nanofluid	Hybrid nanofluid
0.01	1.0	0.3	0.1	0.63298	0.64893
0.03				0.6399	0.65523
0.05				0.64675	0.66142
	0.5			0.52656	0.54365
	1.0			0.63298	0.64893
	1.5			0.68709	0.69775
		1.0		0.52199	0.52994
		2.0		0.63298	0.64893
		3.0		0.73110	0.75334
			0.0	0.73878	0.76252
			0.5	0.75331	0.77979
			1.0	0.76688	0.79582

5.5 Concluding Remarks

In present chapter two dimensional, incompressible, steady SWCNT-MWCNT/water hybrid nanofluid past a nonlinear stretching sheet are considered. Cattaneo-Christov

model of heat flux is used instead of Fourier Law to evaluate the energy equation. By means of transformation, the governing PDEs are changed into ODEs and tackled these equations numerically by applying the finite difference technique bvp4c. The main finding of this problem is given below:

➢ Axial velocity $f'(\eta)$ enhances with enhancing the parameter γ_1.

➢ Induced magnetic field $g'(\eta)$ diminishes for greater value of M, ϕ_2 and M_1.

➢ Skin friction $\mathrm{Re}_x^{1/2} C_{fx}$ reduces for enlarge ξ and boosts for ϕ_2.

➢ The Sherwood number enhances with the SWCNT volume fraction.

➢ Improvement in entropy production rate is observed for higher α_2 and L.

6 Chapter 6

Impact of Newtonian heating on the micropolar CNT based hybrid nanofluid flow

6.1 Introduction

This chapter discusses the impact of ion and Hall slip in micropolar hybrid nanoliquid with Newtonian heating. Further the impact of thermal radiation, Darcy – Forchheimer, viscous dissipation, and variable viscosity are discussed. Total entropy generation rate is calculated. Two distinct nanoparticles such as (SWCNT, MWCNT) used as a hybrid nanofluid. Built-in function bvp4c integrates the solution of simulated hydrodynamic boundary value problems. The effects on axial velocity, angular velocity, temperature field, concentration field, Bejan number, and entropy optimization of different flow field variables are displayed graphically. The nanoparticle fraction increases the temperature, Bejan number, and entropy generation, while the linear and angular velocity diminishes. Further the entropy generation enhances with higher the Brinkman number and variable viscosity parameter.

6.2 Mathematical Description

We considered SWCNT and (SWCNT, MWCNT) to be hybrid nano solid structures in water (base liquid) above the horizontal surface moving with velocity $\mathbf{V}_w = \left[(x+y)^n a, (x+y)^n d \right]$ and combined with non-uniform magnetic field $B_0 (x+y)^{(n-1)/2}$. Further the variable viscosity with ion and Hall slip effects are considered. *Fig. 6.1* is the graphical representation of flow field.
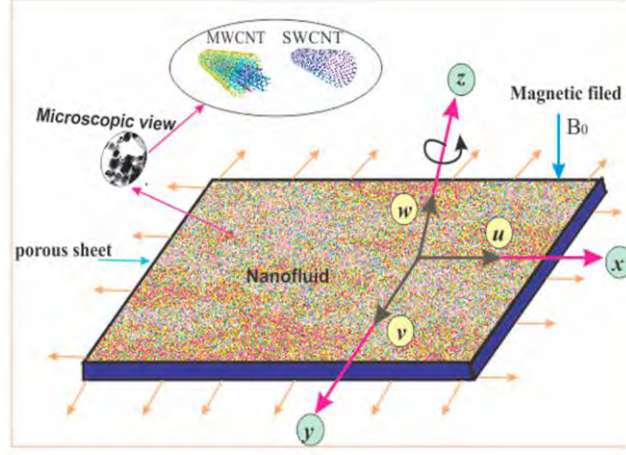
Fig. 6.1: Physical representation of flow field.

The boundary layer equations for micropolar nanofluid with non-uniform MHD and Darcy Forchheimer terms are directly defined as

$$\frac{\partial w}{\partial z} + \frac{\partial v}{\partial y} + \frac{\partial u}{\partial x} = 0,$$ (6.1)

$$v\frac{\partial u}{\partial y} + u\frac{\partial u}{\partial x} + w\frac{\partial u}{\partial z} = \frac{1}{\rho_{hnf}}\frac{\partial}{\partial z}\left\{\frac{\partial u}{\partial z}\left(\mu_{hnf}(T)+\kappa\right)\right\} - \frac{\kappa}{\rho_{hnf}}\frac{\partial N_2}{\partial z} - \frac{\mu_{hnf}(T)}{\rho_{hnf}K^{**}}u - F^{**}u^2$$
$$- \frac{\sigma_{hnf}B_0^2(x+y)^{n-1}\left[(1+\beta_e\beta_i)u - \beta_e v\right]}{\rho_{hnf}\left[(1+\beta_e\beta_i)^2 + \beta_e^2\right]},$$ (6.2)

$$w\frac{\partial v}{\partial z} + v\frac{\partial v}{\partial y} + u\frac{\partial v}{\partial x} = \frac{1}{\rho_{hnf}}\frac{\partial}{\partial z}\left\{\frac{\partial v}{\partial z}\left(\mu_{hnf}(T)+\kappa\right)\right\} + \frac{\kappa}{\rho_{hnf}}\frac{\partial N_1}{\partial z} - \frac{\sigma_{hnf}B_0^2\left[(1+\beta_e\beta_i)v + \beta_e u\right]}{\rho_{hnf}\left[(1+\beta_e\beta_i)^2 + \beta_e^2\right]}$$
$$- F^{**}v^2 - \frac{\mu_{hnf}(T)}{\rho_{hnf}K^{**}}v,$$ (6.3)

$$v\frac{\partial N_1}{\partial y} + u\frac{\partial N_1}{\partial x} + w\frac{\partial N_1}{\partial z} = \frac{\gamma_{hnf}}{j\rho_{hnf}}\frac{\partial^2 N_1}{\partial z^2} - \kappa\left(2N_1 + \frac{\partial v}{\partial z}\right),$$ (6.4)

$$v\frac{\partial N_2}{\partial y} + u\frac{\partial N_2}{\partial x} + w\frac{\partial N_2}{\partial z} = \frac{\gamma_{hnf}}{j\rho_{hnf}}\frac{\partial^2 N_2}{\partial z^2} - \kappa\left(2N_2 - \frac{\partial u}{\partial z}\right),$$ (6.5)

70

$$v\frac{\partial T}{\partial y}+u\frac{\partial T}{\partial x}+w\frac{\partial T}{\partial z}=\frac{\partial}{\partial y}\left(\left(\alpha_{hnf}+\frac{16\sigma^{*}T^{3}}{3k^{*}(\rho C_{p})_{hnf}}\right)\frac{\partial T}{\partial z}\right)+\frac{\sigma_{hnf}B_{0}^{2}(u^{2}+v^{2})}{(\rho C_{p})_{hnf}\left[(1+\beta_{e}\beta_{i})^{2}+\beta_{e}^{2}\right]}$$
$$+\frac{(\mu_{hnf}(T)+\kappa)}{(\rho C_{p})_{hnf}}\left\{\left(\frac{\partial v}{\partial z}\right)^{2}+\left(\frac{\partial u}{\partial z}\right)^{2}\right\}. \tag{6.6}$$

The following boundary conditions were introduced in order to answer the above set of governing equations:

$$v\big|_{z=0}=V_{w}=(y+x)^{n}d,\ u\big|_{z=0}=U_{w}=(y+x)^{n}c,$$
$$\frac{\partial T}{\partial z}\bigg|_{z=0}=-hT\big|_{z=0},w\big|_{z=0}=0,N_{2}\big|_{z=0}=n\frac{\partial u}{\partial z}\bigg|_{z=0},N_{1}\bigg|_{z=0}=-n\frac{\partial v}{\partial z}\bigg|_{z=0}, \tag{6.7}$$

$$u\big|_{z\to\infty}\to0,\ N_{1}\big|_{z\to\infty}\to0,T\big|_{z\to\infty}\to T_{\infty},v\big|_{z\to\infty}\to0,N_{2}\big|_{z\to\infty}\to0. \tag{6.8}$$

To change the non-linear differential equations (6.1 – 6.6), i.e., using the suitable non-dimensional variables,

$$\eta=z\sqrt{\frac{1+n}{2}\frac{c(y+x)^{n-1}}{\upsilon_{f}}},N_{2}=\sqrt{\frac{1+n}{2}\frac{c^{3}(y+x)^{n-1}}{\upsilon_{f}}}(x+y)^{n}h_{2}(\eta),N_{1}=\sqrt{\frac{1+n}{2}\frac{c^{3}(y+x)^{n-1}}{\upsilon_{f}}}(y+x)^{n}h_{1}(\eta),$$
$$\theta(\eta)\left(T_{w}-T_{\infty}\right)=T-T_{\infty}, \tag{6.9}$$

$$u=(y+x)^{n}cf'(\eta),v=(y+x)^{n}cG'(\eta),$$
$$w=-\sqrt{\frac{n+1}{2}\upsilon_{f}c(y+x)^{n-1}}\left[(G+f)+\left(\frac{n-1}{n+1}\right)\eta(G'+f')\right]. \tag{6.10}$$

Continuity equation is automatically satisfied, and Eqs. (6.2) to (6.6) transform into,

$$D_{2}=\left((1-\phi_{2})\left\{(1-\phi_{1})+\phi_{1}\frac{\rho_{MWCNT}}{\rho_{f}}\right\}+\phi_{2}\frac{\rho_{SWCNT}}{\rho_{f}}\right),D_{1}=(1-\phi_{1})^{25/10}(1-\phi_{2})^{25/10},$$
$$D_{4}=\left((1-\phi_{2})\left\{(1-\phi_{1})+\phi_{1}\frac{(\rho C_{p})_{MWCNT}}{(\rho C_{p})_{f}}\right\}+\phi_{2}\frac{(\rho C_{p})_{SWCNT}}{(\rho C_{p})_{f}}\right),$$

$$\left(\frac{1}{D_{1}(1+\theta_{r}\theta)}+K\right)f'''-Kh_{2}'+D_{2}\left\{-\frac{2}{n+1}f'(G'+f')+f''(G+f)-\frac{2F_{r}}{n+1}f'^{2}\right\}$$
$$-\frac{\theta_{r}\theta'f''}{D_{1}(1+\theta_{r}\theta)^{2}}-\frac{2P_{m}f'}{(n+1)D_{1}(1+\theta_{r}\theta)}-\left(\frac{2}{n+1}\right)\left(\frac{\sigma_{hnf}}{\sigma_{f}}\right)\frac{M((1+\beta_{e}\beta_{i})f'-\beta_{e}G')}{\left[(1+\beta_{e}\beta_{i})^{2}+\beta_{e}^{2}\right]}=0, \tag{6.11}$$

$$\left(\frac{1}{D_1\left(1+\theta_r\theta\right)}+K\right)G'''+D_2\left\{(G+f)G''-\frac{2F_r}{n+1}G'^2-\frac{2n}{n+1}(G'+f')G'\right\}-\frac{\theta_r\theta'G''}{D_1\left(1+\theta_r\theta\right)^2}$$

$$+Kh_1'-\frac{2P_mG'}{(n+1)D_1(1+\theta_r\theta)}-\left(\frac{\sigma_{hnf}}{\sigma_f}\right)\frac{2M\left((1+\beta_e\beta_i)G'+\beta_ef'\right)}{(n+1)\left[(1+\beta_e\beta_i)^2+\beta_e^2\right]}=0, \quad (6.12)$$

$$\left(\frac{1}{D_1}+\frac{K}{2}\right)h_1''+D_2\left(\frac{n+1}{2}(fh_1'+Gh_1')-\frac{3n-1}{2}(f'h_1+G'h_1)\right)-K(2h_1+G'')=0, \quad (6.13)$$

$$\left(\frac{1}{D_1}+\frac{K}{2}\right)h_2''+D_2\left(\frac{n+1}{2}(G+f)h_2'-\frac{3n-1}{2}(G'+f')h_2\right)-K(2h_2-f'')=0, \quad (6.14)$$

$$\left(\frac{k_{hnf}}{k_f}+\left(1+\theta(T_r-1)\right)^3 R_d\right)\theta''+3R_d\left(1+\theta(T_r-1)\right)^2(T_r-1)\theta'^2+\left(\frac{\sigma_{hnf}}{\sigma_f}\right)\left(\frac{M\,\mathrm{Pr}\,E_c\left[f'^2+G'^2\right]}{\left[(1+\beta_e\beta_i)^2+\beta_e^2\right]}\right)$$

$$+\left(\frac{1}{D_1\left(1+\theta_r\theta\right)}+K\right)\mathrm{Pr}\,E_c\left[f''^2+G''^2\right]+\mathrm{Pr}\,D_4(f+G)\theta'=0, \quad (6.15)$$

and the boundary conditions (6.7 and 6.8) become

$$f'(0)=1, f(0)=0,\ \theta'(0)=-n_H\left[1+\theta(0)\right], G'(0)=\lambda, G(0)=0, h_1(0)=\tfrac{-1}{2}n^*G''(0),$$

$$h_2(0)=\tfrac{1}{2}n^*f''(0), \quad (6.16)$$

$$f'(\eta)=0,\ \theta(\eta)=0,\ h_1(\eta)=h_2(\eta)=0, G'(\eta)=0,\ \text{at}\ \ \eta\to\infty. \quad (6.17)$$

The expressions of the parameters involved is defined as

$$M=\frac{\sigma_fB_0^2}{c\rho_f},\ \ \mathrm{Pr}=\frac{v_f}{\alpha_f}, F_r=\frac{C_b}{\rho_f\sqrt{K^{**}}},\ P_m=\frac{v_f}{cK^{**}},\ \lambda=\frac{d}{c}, T_r=\frac{T_w}{T_\infty}, K=\kappa/\mu_f$$

$$\theta_r=\varepsilon(T_w-T_\infty), R_d=\frac{16\sigma^*T_\infty^3}{3k_fk^*}, n_H=h_s\sqrt{\frac{2v_f}{c(m+1)}}, \delta=\frac{T_w-T_\infty}{T_\infty}. \quad (6.18)$$

6.3 Entropy Generation Analysis

The local entropy generation defined in term of heat transfer irreversibility, thermal radiation, viscous dissipation, and magnetohydrodynamics with Hall and ion effects are

$$S_G = \frac{k_f}{T_\infty^2} \left[\frac{k_{hnf}}{k_f} + \frac{16T_\infty^3 \sigma^*}{3k_f k^*} \right] \left(\frac{\partial T}{\partial z} \right)^2 + \left(\frac{\mu_{hnf}(T) + \kappa}{T_\infty} \right) \left\{ \left(\frac{\partial v}{\partial z} \right)^2 + \left(\frac{\partial u}{\partial z} \right)^2 \right\}$$

$$+ \frac{\sigma_{hnf} B_0^2 (v^2 + u^2)}{T_\infty \left[(1 + \beta_e \beta_i)^2 + \beta_e^2 \right]}.$$

(6.19)

The dimensionless form of entropy production is attained by using the following relation

$$N_s = \frac{T_\infty (z/\eta)^2}{k_f (T_w - T_\infty)} S_G,$$

(6.20)

After manipulating the similarity transformation (6.9 and 6.10), the non-dimension form of entropy minimization develops:

$$N_s(\eta) = \left(\frac{k_{hnf}}{k_f} + R_d (1 + (T_r - 1)\theta)^3 \right) \left(\frac{n+1}{2} \right) \delta\theta'^2 + \left(\frac{\sigma_{hnf}}{\sigma_f} \right) \left(\frac{MBr\left[G'^2 + f'^2 \right]}{\left[(1 + \beta_e \beta_i)^2 + \beta_e^2 \right]} \right)$$

$$+ Br \left(\frac{1}{D_1 (1 + \theta_r \theta)} + K \right) \left(\frac{n+1}{2} \right) \left(G''^2 + f''^2 \right).$$

(6.21)

The Bejan number expression is define as,

$$Be = \frac{\left(\frac{k_{hnf}}{k_f} + R_d (1 + \theta(T_r - 1))^3 \right) \left(\frac{n+1}{2} \right) \delta\theta'^2}{\left\{ \left[\left(\frac{k_{hnf}}{k_f} + R_d (1 + \theta(T_r - 1))^3 \right) \left(\frac{n+1}{2} \right) \delta\theta'^2 + Br \left(\frac{1}{D_1 (1 + \theta_r \theta)} + K \right) \left(\frac{1+n}{2} \right) \left(G''^2 + f''^2 \right) \right] + \left(\frac{MBr\left[G'^2 + f'^2 \right]}{\left[(1 + \beta_e \beta_i)^2 + \beta_e^2 \right]} \right) \right\}}.$$

6.4 Solution Procedure:

The numerical solution of equations (6.11 – 6.15) equivalent to boundary condition (6.16 and 6.17) is clarified by means of bvp4c from MATLAB. For this reason, the transformed third order differential equations are changed to first order differential equation using new variables. In this method chose the appropriate initial guess to acquire the boundary layer asymptotically. A convergence criterion of 10^{-6} is set for the

acquired solution. We employed suitable finite values of $\eta \rightarrow \infty$, that is $\eta = \eta_\infty = 5$, depending on the values of the parameters involved. The relation is made between the published paper Khan et al. [32] and our current finding, which is depicted in *Table 6.1*, in the non-appearance of temperature dependent viscosity, hybrid nanofluid, and mixed convection.

6.5 Results and Discussion

The influence of SWCNT solid volume fraction (ϕ_2) on entropy generation ($N_s(\eta)$) and Bejan number (Be) are presented in *Fig. 6.2 ((a) and (b))*. Moreover an interesting result is observed for higher ϕ_2 from *Fig. 6.2 (a)*, that the entropy generation increases near the surface of wall while reduces far away for both simple nanofluid and hybrid nanofluid. The Bejan number show dual behavior for enhancing value of ϕ_2, near the surface it diminishes while far away the boundary it increases (see in *Fig. 6.2 (b)*). *Fig. 6.3 (a)* designate the impacts of inertia parameter on velocity distribution along x and y direction via simple nanofluid and hybrid nanofluid. It is examined that the velocity ($f'(\eta)$, $G'(\eta)$) reduces with increasing values of inertia parameter F_r. It is also detected that the velocity field more decay in hybrid nanofluid case than simple nanofluid. The same observation is seen for axial veocity when porosity parameter enhances (see in *Fig. 6.3 (b)*). *Fig. 6.4 (a)* looks at the declining trend of ($f'(\eta)$ and $G'(\eta)$) for larger M values. Because magnetic parameter is dependent on Lorentz force, the resistance between the liquid particles increases for larger magnetic parameter, which helps to diminish ($f'(\eta)$ and $G'(\eta)$) and increase the distribution of temperature (see in *Fig. 6.4 (b)*). *Fig. 6.5 ((a)– (d))* tells the performance of ($f'(\eta)$, $G'(\eta)$, $h_1(\eta)$, $h_2(\eta)$ and $\theta(\eta)$) for variation of micro-polar parameter K. It is perceived from *Fig. 6.5 (a)* that the fluid motion is more for enlarge estimation of K. *Fig. 6.5 ((a) and (b))* illustrate the similar outcomes as identified in *Fig. 6.5 (a)*. *Fig. 6.5 (d)* is calculated to examine the

temperature for larger micro-polar parameter (K). One can recognized that enhancing behavior occurs for K on temperature profile. ***Fig. 6.6 (a)*** demonstrated the result of Hall parameter on velocity distribution along x and y direction. It is seen that the x component of velocity ($f'(\eta)$) enhances with β_e boosts, while the y component of velocity ($G'(\eta)$) show opposite behavior. ***Fig. 6.6 (b)*** shows attempt to see the effect of β_e on $\theta(\eta)$. It is seen that the temperature and their related thermal boundary layer enhances with larger estimation of Hall parameter β_e. ***Fig. 6.7 ((a) and (b))*** depict the impacts of conjugate parameter (n_H) and temperature difference (T_r) on temperature distribution. It is found that the temperture distribution boosts for both larger values of conjugate parameter (n_H) and temperature difference (T_r). It is also seen that the hybrid nanofluid profile is larger than simple nanofluid. The result of Brinkman number on entropy generation is discussed in ***Fig. 6.8***. Entropy generation show increasing performance for boosting estimation of Br. In ***Table 6.1*** the numerical values of drag friction are given for distinct parameters. It is seen that for parameters ϕ_2, M and θ_r skin friction value enhances while for parameters K and β_i values of skin friction diminishes. ***Table 6.2*** calculate the numerical values of local Nusselt number for distinct parameters.
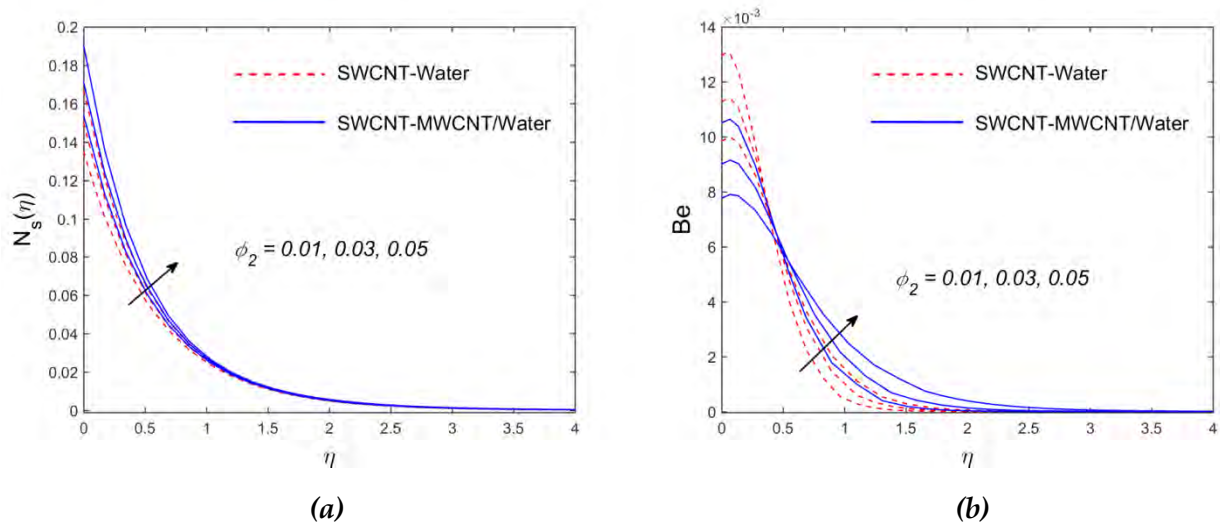
(a)   *(b)*

Fig.6.2: Entropy generation and Bejan number variation with solid volume fraction.

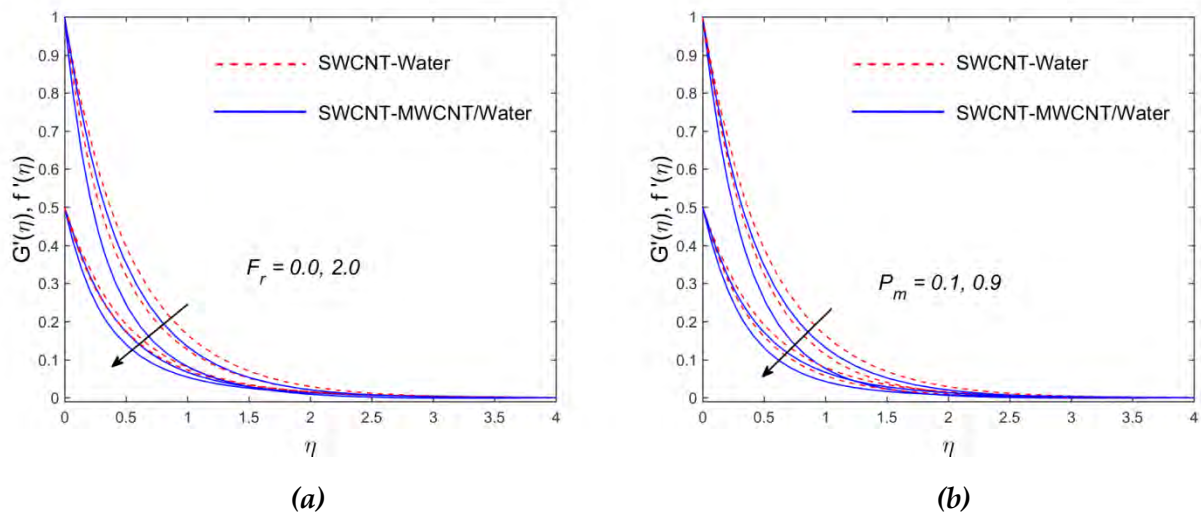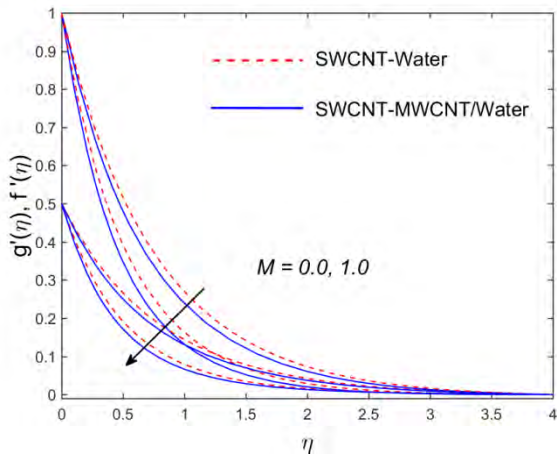*(a)*   *(b)*

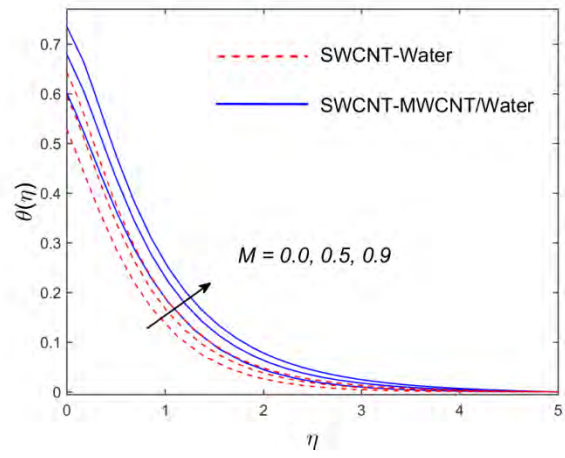*Fig. 6.3: Horizontal and vertical velocity variation (a) with F_r (b) with P_m.*

(a)   *(b)*

Fig. 6.4: Velocity and temperature variation with magnetic parameter.

(a)   *(b)*
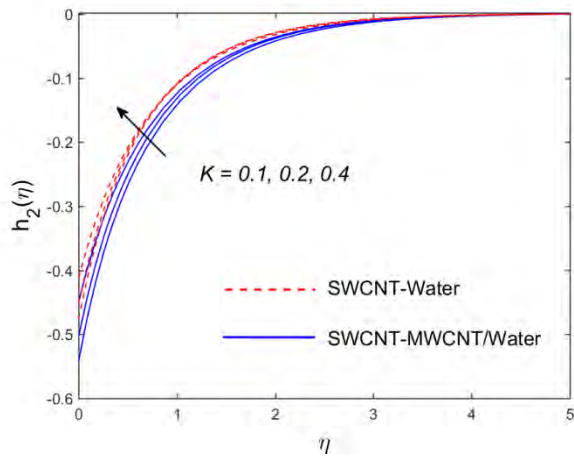
(c)

(d)

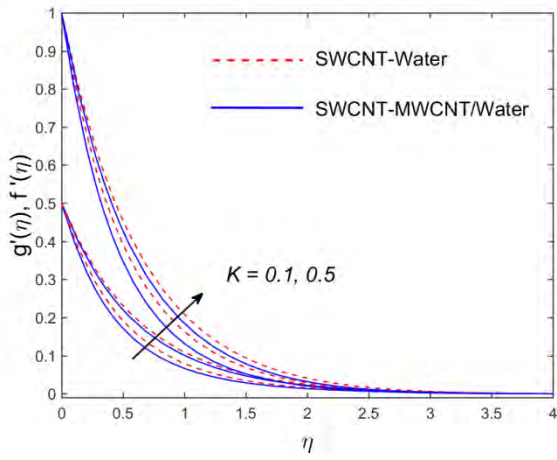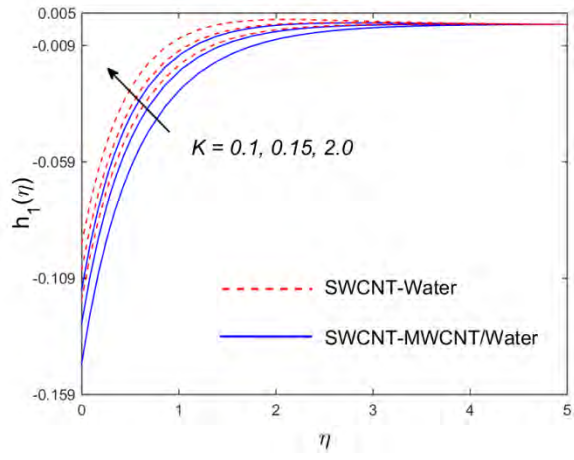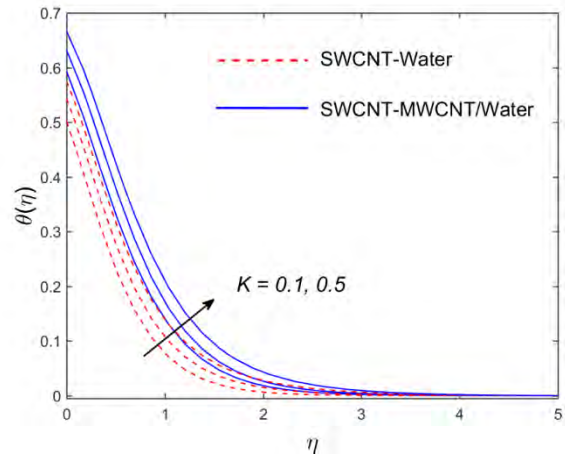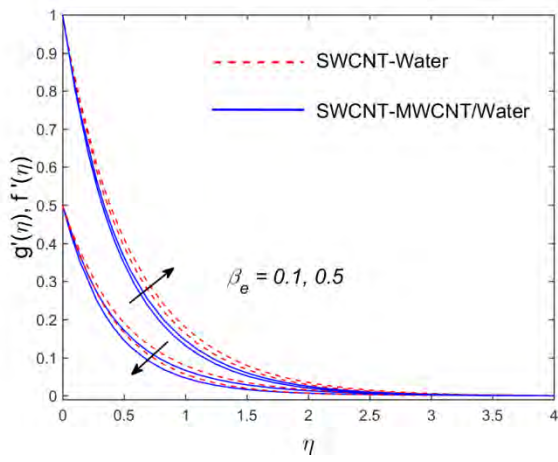*Fig. 6.5: Velocity and micropolar field along x and y-axis, and temperature variation with K .*

(a)
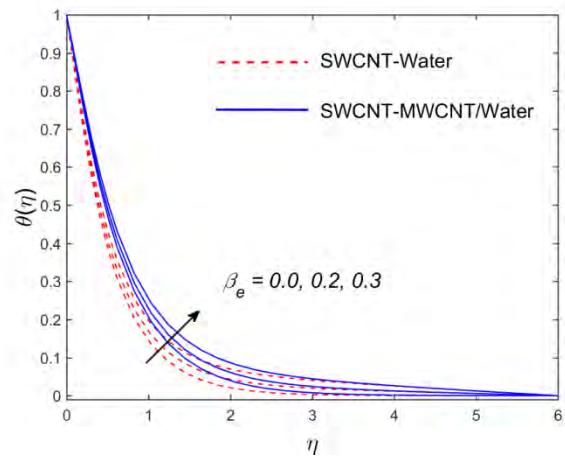
(b)

Fig. 6.6: Velocity and temperature variation with Hall parameter.
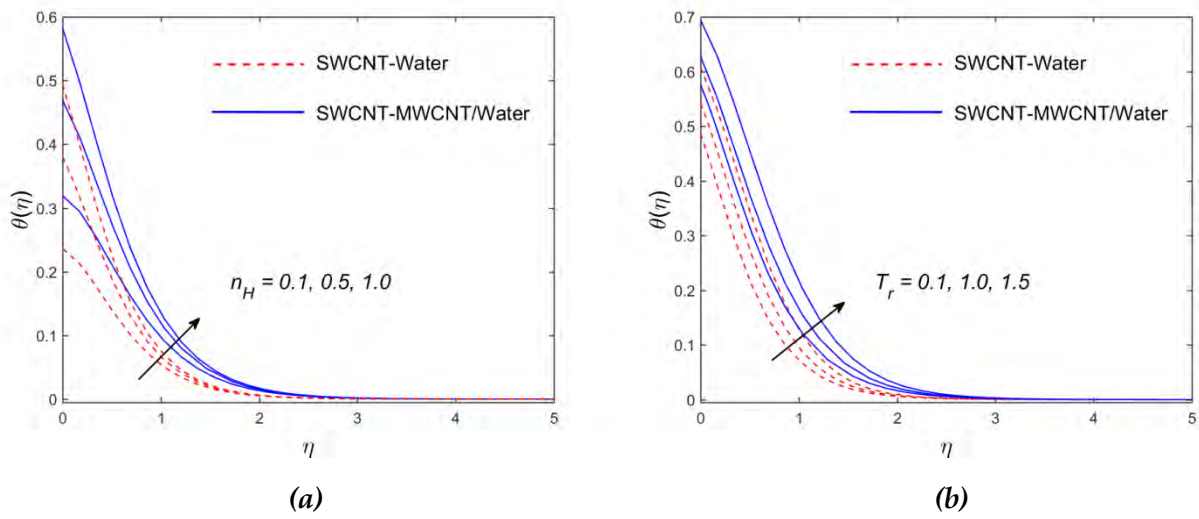
Fig. 6.7: Temperature variation with (a) with conjugate parameter (b) with temperature difference.
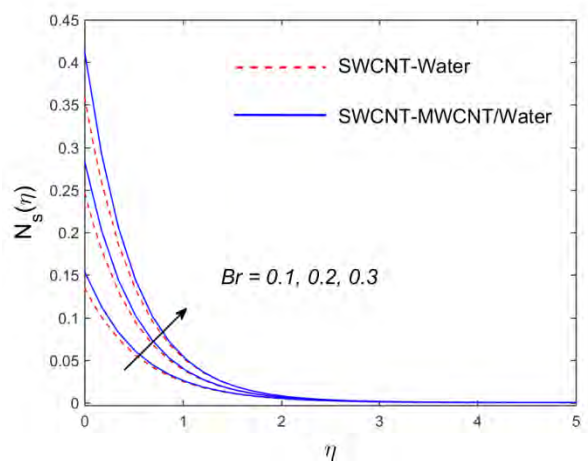
Fig. 6.8: Entropy generation variation with Brinkman number.

Table 6.1. Evaluation of $f''(0)$ and $G''(0)$ for different values of λ when $n^* = 1, M = F_r = \theta_r = 0$

λ	Nawaz et al. [17] $f''(0)$	Nawaz et al. [17] $G''(0)$	Present results $f''(0)$	Present results $G''(0)$
0.0	1.0001434	0	1.00042	0
0.5	1.224440	0.613220	1.22445	0.61332
1.0	1.4142725	1.4148725	1.41427	1.41497

Table 6.2. Numerical value of local skin friction for numerous variables when $\phi_1 = 0.03, P_m = 0.1 = F_r$.

K	β_i	ϕ_2	M	θ_r	$-\mathrm{Re}^{1/2} C_f$		$-\mathrm{Re}^{1/2} C_g$	
					Simple nanofluid	Hybrid nanofluid	Simple nanofluid	Hybrid nanofluid
0.1	0.1	0.01	1.0	0.5	1.7843	1.8424	0.62266	0.65354
0.3					1.7337	1.7939	0.46895	0.48295

0.5					1.6771	1.7398	0.23200	0.26050
	0.2				1.7975	1.8564	0.62690	0.64378
	0.3				1.7803	1.8489	0.61401	0.63053
	0.5				1.7761	1.8344	0.59123	0.60715
		0.02			1.8279	1.8872	0.64698	0.66453
		0.03			1.8520	1.9118	0.65339	0.67127
		0.05			1.9038	1.9648	0.66729	0.68593
			0.1		1.5289	1.5800	0.41551	0.42731
			0.5		1.6622	1.7157	0.53377	0.54737
			0.9		1.7784	1.8362	0.62183	0.63830
				0.2	1.6568	1.7179	0.61087	0.62957
				0.4	1.7589	1.8186	0.63183	0.64951
				0.6	1.8482	1.9067	0.64935	0.66626

Table 6.3. Numerical value of local Nusselt number for numerous parameters when $\phi_1 = 0.03, \text{Pr} = 6.2, \beta_e = 0.5.$

ϕ_2	M	θ_r	E_c	R_d	$[\text{Re}]^{-1/2} Nu_x$	
					Simple nanofluid	Hybrid nanofluid
0.02	1.0	0.5	0.1	1.1	1.0000	0.80061
0.03					0.8310	0.64240
0.05					0.7189	0.54930
	0.1				1.6080	1.25300

0.5				1.3310	1.03750
0.9				1.0520	0.82316
	0.2			1.2160	0.99775
	0.4			1.1930	0.97858
	0.6			1.1730	0.96156
		0.2		1.1304	0.93005
		0.4		0.8261	0.85044
		0.6		0.7220	0.77079
			0.3	1.1315	0.93468
			0.5	1.1446	0.94357
			0.7	1.1574	0.95239

6.6 Concluding Remarks

The principle contributions of the present flow problem are reported below:

➢ For both simple nanofluid and hybrid nanofluid, fluid velocities ($f'(\eta), G'(\eta)$) are reduced by larger (M, F_r, and P_m).

➢ An escalate of material parameter K improves ($f'(\eta), G'(\eta)$).

➢ The micro-rotation field enhances for larger estimation of micropolar parameter K.

➢ Thermal boundary layer boosts for higher Hall parameter (β_e) and conjugate parameter (n_H).

➢ Escalation the SWCNT volume fraction (ϕ_2) entropy and Bejan number increases.

➢ Temperature field is an increasing function of T_r, M, and K.

7 Chapter 7

Heat transfer enhancement in a micropolar hybridized nanofluid flow in the presence of stratification

7.1 Introduction

In the present chapter, it is scrutinized the steady bio-convective micropolar hybrid nanofluid flow with the stratification conditions above a vertical exponentially stretching surface. Both SWCNT and MWCNT are jointly used in a base fluid of water to formulate the Hybrid nanoparticles in the current chapter. The impact of activation energy and Cattaneo Christov theory is also examined. The bvp4c Matlab function is applied to solve the numerical solution of the nonlinear coupled equation. The influence of the involved parameter is discussed graphically. The physical numbers were observed via graphs, such as friction factor, local Sherwood number, and local microorganism number. It is worth observing that the drag friction, local Sherwood, and microorganism number enhanced with the increase of solid volume fraction of SWCNT and MWCNT. Further, the motile microorganism distribution is declining with improving values of microorganism stratification parameter, Peclet number, and bio - convection Schmidt number.

7.2 Mathematical Description

In the existing study, we perceived steady, two dimensional boundary layer flow past a verticle stretching sheet in the presence of mixed convection and velocity slip effect. The influence of triple stratification, rate of chemical reaction, and microorganism is carried out. The physical diagram of flow field is specified in *Fig. 7.1*. The fluid stretching

velocity is $u_w = aExp\left(\frac{x}{l}\right)$. The surface temperature is T_w, concentration is C_w, and microorganism density is n_{1w}, while the ambient temperature, concentration, and microorganism density is denoted by T_∞, C_∞, and $n_{1\infty}$ respectively.
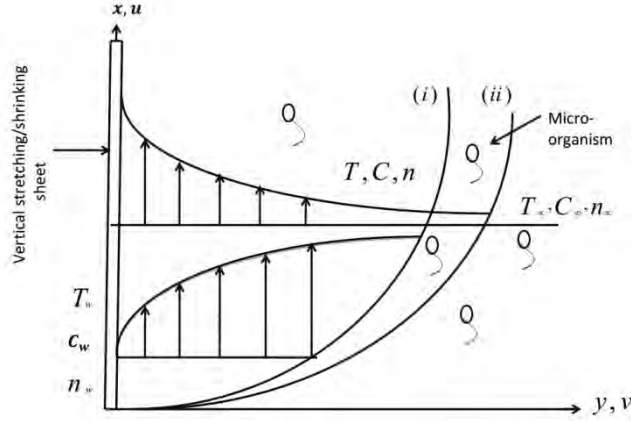

Fig. 7.1: Physical representation of flow field.

The flow model is described as follows, consuming the above said suppositions and boundary layer approximation:

$$\frac{\partial u}{\partial x} + \frac{\partial v}{\partial y} = 0 \tag{7.1}$$

$$
u\frac{\partial u}{\partial x} + v\frac{\partial u}{\partial y} = \left(\frac{\mu_{hnf}+\kappa}{\rho_{hnf}}\right)\frac{\partial^2 u}{\partial y^2} + \frac{\kappa}{\rho_{hnf}}\frac{\partial N}{\partial y} - \frac{\nu_{hnf}}{K^{**}}u
$$
$$
+\frac{g^*}{\rho_{hnf}}\left\{\begin{array}{c}\beta_T(1-C_\infty)\rho_{f\infty}(T-T_\infty) - (\rho_p - \rho_{f\infty})\beta_C(C-C_\infty) \\ -(\rho_m - \rho_{f\infty})\gamma_1{}^*(n_1 - n_{1\infty})\end{array}\right\}, \tag{7.2}
$$

$$u\frac{\partial N}{\partial x} + v\frac{\partial N}{\partial y} = \frac{\gamma_{hnf}}{\rho_{hnf}j}\frac{\partial^2 N}{\partial y^2} - \frac{\kappa}{\rho_{hnf}j}\left(2N + \frac{\partial u}{\partial y}\right), \tag{7.3}$$

$$u\frac{\partial T}{\partial x} + v\frac{\partial T}{\partial y} + \tau_T\left\{v\frac{\partial v}{\partial y}\frac{\partial T}{\partial y} + u^2\frac{\partial^2 T}{\partial x^2} + v^2\frac{\partial^2 T}{\partial y^2} + u\frac{\partial u}{\partial x}\frac{\partial T}{\partial x} + u\frac{\partial v}{\partial x}\frac{\partial T}{\partial y} + v\frac{\partial T}{\partial x}\frac{\partial u}{\partial y} + 2uv\frac{\partial^2 T}{\partial x\,\partial y}\right\} =$$
$$\alpha_{hnf}\frac{\partial^2 T}{\partial y^2}, \tag{7.4}$$

$$u\frac{\partial C}{\partial x} + v\frac{\partial C}{\partial y} = (D_B)_{hnf}\frac{\partial^2 C}{\partial y^2} - k_r^2(C - C_\infty)\left(\frac{T}{T_\infty}\right)^m Exp\left(\frac{E_a}{kT}\right), \tag{7.5}$$

$$u\frac{\partial n_1}{\partial x} + v\frac{\partial n_1}{\partial y} + \frac{b^*W_c}{C_w - C_\infty}\left[\frac{\partial}{\partial y}\left(n_1\frac{\partial C}{\partial y}\right)\right] = (D_m)_{hnf}\frac{\partial^2 n_1}{\partial y^2}. \tag{7.6}$$

The appropriate boundary conditions are specified by:

$$\left(\begin{array}{c} u = u_w + N_1(x)\left[(\mu_{hnf} + \kappa)\frac{\partial u}{\partial y} + \kappa N\right], v = 0, N = -n^*\frac{\partial u}{\partial y}, \\ T = T_w(x) = T_0 + b_1 x, \\ C = C_w(x) = C_0 + dx, \ n_1 = n_{1w}(x) = n_{10} + e_1 x. \end{array} \right), \qquad \text{as } y \to 0. \qquad (7.7)$$

$$u \to 0, N \to 0, T \to T_\infty = T_0 + b_2 x, C \to C_\infty = C_0 + ex, n_1 \to n_{1\infty} = n_{10} + e_2 x, \text{ as}$$

$$y \to \infty.$$

(7.8)

The suitable variables are specified as,

$$\begin{cases} \eta = y\sqrt{\dfrac{c}{2l\nu_f}}Exp\left(\dfrac{x}{2l}\right), \psi = f(\eta)\sqrt{2lc\nu_f}Exp\left(\dfrac{x}{2l}\right), \\[2mm] N = h(\eta)\sqrt{\dfrac{c^3}{2l\nu}}Exp\left(\dfrac{3x}{2l}\right), \ T = T_\infty + T_0 Exp\left(\dfrac{x}{2l}\right)\theta(\eta), \\[2mm] C = C_\infty + C_0 Exp\left(\dfrac{x}{2l}\right)g(\eta), n_1 = n_{1\infty} + n_{10}Exp\left(\dfrac{x}{2l}\right)\chi(\eta), \\[2mm] \theta = \dfrac{T - T_\infty}{T_w - T_0}, g = \dfrac{C - C_\infty}{C_w - C_0}, \chi = \dfrac{n_1 - n_{1\infty}}{n_{1w} - n_{10}}, \end{cases}$$

(7.9)

Using Eq. (7.9), in equation Eqs. (7.1 − 7.8) become,

$$D_2 = \left((1-\phi_2)\left\{(1-\phi_1) + \phi_1\frac{\rho_{s1}}{\rho_f}\right\} + \phi_2\frac{\rho_{s2}}{\rho_f}\right), D_1 = (1-\phi_1)^{2.5}(1-\phi_2)^{2.5},$$

$$D_4 = \left((1-\phi_2)\left\{(1-\phi_1) + \phi_1\frac{(\rho C_p)_{s1}}{(\rho C_p)_f}\right\} + \phi_2\frac{(\rho C_p)_{s2}}{(\rho C_p)_f}\right).$$

$$\left(\frac{1}{D_1} + K\right)f''' + D_2\{ff'' - 2f'^2\} + Kh' - \frac{P_m}{D_1}f' - \lambda_m(\theta - Nrg - Nc\chi) = 0, \qquad (7.10)$$

$$\left(\frac{1}{D_1} + \frac{K}{2}\right)h'' + D_2\{fh' - 3f'h\} - K(f'' + 2h) = 0, \qquad (7.11)$$

$$\left(\frac{k_{hnf/k_f}}{D_4} - Pr\gamma_c(f^2 - 2\eta f)\right)\theta'' - Pr\{f'\theta - f\theta'\} - Pr\gamma_c\{3\theta f'^2 - 3ff'\theta' - ff''\theta +$$

$$28\eta\theta'\} = 0, \qquad (7.12)$$

$$\frac{D_1}{Sc}g'' - f'g + fg' - R_c(1 + \delta\theta)^m Exp\left(\frac{-E}{1 + \delta\theta}\right)g = 0, \qquad (7.13)$$

$$\frac{D_1}{Sb}\chi'' - f'\chi + f\chi' - \frac{Pe}{Sb}((\chi + \Omega_1)g'' + \chi'g') = 0. \qquad (7.14)$$

The appropriate boundary conditions are,

$$
\left(
\begin{array}{l}
f(\eta) = 0, \ f'(\eta) = A\left(K + \frac{1}{D_1}\right)f''(\eta) + \lambda, \ h(\eta) = -n^* f''(\eta), \ \theta(\eta) = 1 - S_1, \\
g(\eta) = 1 - S_2, \ \chi(\eta) = 1 - S_3, \ \text{When } \eta \to 0, \\
\quad f'(\eta) = 0, \ h(\eta) = \theta(\eta) = 0 = g(\eta) = \chi(\eta) \ \text{When } \eta \to \infty.
\end{array}
\right) \tag{7.15}
$$

The containing parameters are mathematically expressed as:

$$
K = \frac{\kappa}{\mu_f}, \ \lambda_m = \frac{l^2 \beta g (1-C_\infty)(T-T_\infty)}{c^2 \rho_f}, \ P_m = \frac{l\nu_f}{cK^{**}}, \ N_r = \frac{(\rho_p - \rho_{f\infty})(C-C_\infty)}{\beta_T \rho_f (T-T_\infty)(1-C_\infty)}, \ S_b = \frac{\nu_f}{(D_m)_f},
$$

$$
P_e = \frac{b^* W_c (D_m)_f}{\nu_f^2}, \ S_c = \frac{\nu_f}{(D_B)_f}, \ \gamma_c = \frac{c}{l}\tau_T, \ \delta = \frac{\Delta T}{T_\infty}, \ A = N_1{}^* \mu_f \sqrt{\frac{c}{l\nu_f}}, \ \Pr = \frac{\nu_f}{\alpha_f}, \ \Omega_1 = \frac{\Delta n_1}{n_{1\infty}}, \tag{7.16}
$$

$$
S_3 = \frac{e_2}{e_1}, \ S_2 = \frac{e}{d}, \ S_1 = \frac{b_2}{b_1}, \ N_c = \frac{\gamma_1{}^*(\rho_m - \rho_{f\infty})(n_1 - n_{1\infty})}{\beta_C (T-T_\infty)(1-C_\infty)}, \ \lambda = \frac{a}{c}, \ R_c = \frac{k_r^2}{c}, \ E = \frac{E_a}{kT_\infty}.
$$

The physical variables such as drag force, local microorganism number, and local Sherwood number is define as,

$$
C_{fx} = \frac{\tau_w}{\rho_f u_w^2}, \quad Sh_x = \frac{x q_m}{(D_B)_f (C_w - C_\infty)}, \quad Q_{nx} = \frac{x j_w}{(D_m)_f n_{1w}},
$$

$$
\tau_w = 2\left[(\mu_{hnf} + \kappa)\frac{\partial u}{\partial y}\Big|_{y=0} + \kappa(N)_{y=0}\right], \tag{7.17}
$$

$$
q_m = -(D_B)_{hnf}\frac{\partial C}{\partial y}\Big|_{y=0}, \quad j_w = -(D_m)_{hnf}\frac{\partial n}{\partial y}\Big|_{y=0}.
$$

The dimensionless form of the above equation become,

$$
\begin{aligned}
Re_x^{1/2} C_{fx} &= 2\left(\frac{1}{D_1} + K\right)f''(0), \\
Re_x^{-1/2} Sh_x &= -D_1 g'(0), \\
Re_x^{-1/2} Q_{nx} &= -D_1 \chi'(0).
\end{aligned} \tag{7.18}
$$

Here $\mathrm{Re}_x = \frac{lu_w}{\nu}$ stands the local Reynolds number.

7.3 Results and Discussion

The nonlinear ODEs (7.10 – 7.14) including boundary condition (7.15) are numerically attempted by exploiting the bvp4c function in MATLAB. The influence of different

involved variables on the velocity field $f'(\eta)$, temperature $\theta(\eta)$, concentration $g(\eta)$, microorganism distribution $\chi(\eta)$, skin factor (C_f), mass transfer rate (Sh_x), and local microorganism number Nn_x are emphasized in **Figs. (7.2 – 7.7)**. The velocity ratio parameter A diminishes the velocity distribution, which is explained in **Fig. 7.2 (a)**. Physically, the slip boundary condition at the surface is applied when the viscosity influence of the liquid at the surface is low. More resistance is detected in the transfer of the stretching velocity to the fluid motion due to the weak bond among the fluid and the surface as a result of the partial slip. In a conclusion, as the slip parameter is increased, the fluid velocity decreases. In **Fig. 7.2 (b)**, the effect of the shrinking/stretching parameter λ on the $f'(\eta)$ can be seen. For the λ, it is noticed that $f'(\eta)$ grows. Because when the value of λ improves, the velocity near the surface enhances. The upshot of micropolar parameter is observed in **Fig. 7.3 (a)**. The velocity distribution is an enhancing function of the material parameter K. Because the dynamic viscosity is low for a higher value of material parameter K. Lower viscosity means that low resistance occurs in the fluid flow, which enhances the linear and angular velocity distribution (see in **Figs. 7.3 (b)**). On the other hand, the temperature field diminishes. This is clarified in **Fig 7.3 (c)**. From **Fig. 7.4 (a)** and **(b)**, we notice that as P_m and γ_c enhances, the velocity $f'(\eta)$ and temperature $\theta(\eta)$ decrease respectively. The behavior of thermal stratification (S_1), concentration stratification (S_2), and microorganism stratification (S_3) on temperature $\theta(\eta)$, concentration $g(\eta)$, and microorganism field $\chi(\eta)$ is observed in **Fig. 7.5((a) - (c))**. It is seen that the $(\theta(\eta), g(\eta), \chi(\eta))$ decreases with (S_1, S_2, S_3) respectively. **Fig. 7.6 (a)** depicts the influence of P_e on motile microorganisms $\chi(\eta)$. With greater P_e, the $\chi(\eta)$ is thought to be reduced. The result of S_b (bioconvection Schmidt number) on $\chi(\eta)$ is shown in **Fig. 7.6 (b)**. It is revealed that as S_b is estimated more, the $\chi(\eta)$ sketch decreases. Because the S_b has an inverse relationship with the diffusion coefficient of motile microorganisms, the $\chi(\eta)$ sketch

declines. ***Figs. 7.7 ((a) – (c))*** look at the effects of volume fraction (ϕ_1, ϕ_2) against stretching parameter on skin factor, local Sherwood number, and local microorganisms number. The skin friction, local Sherwood number, and local microorganisms number enhances with higher values of solid volume fraction and stretching parameter.
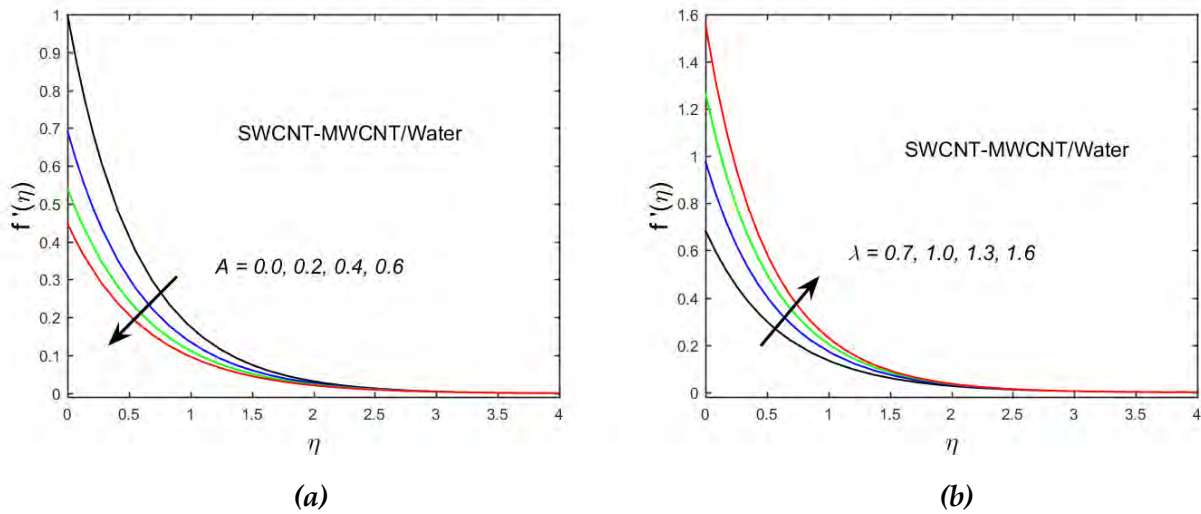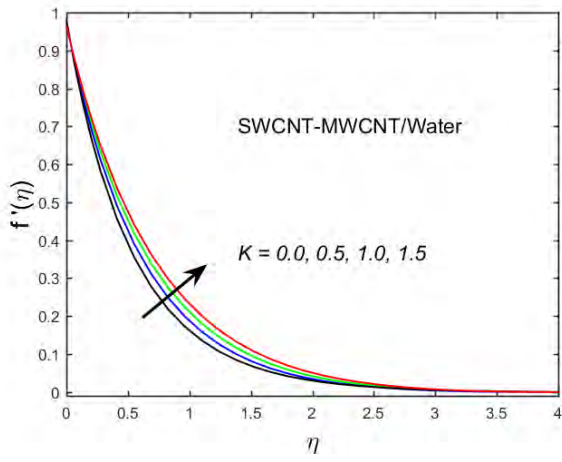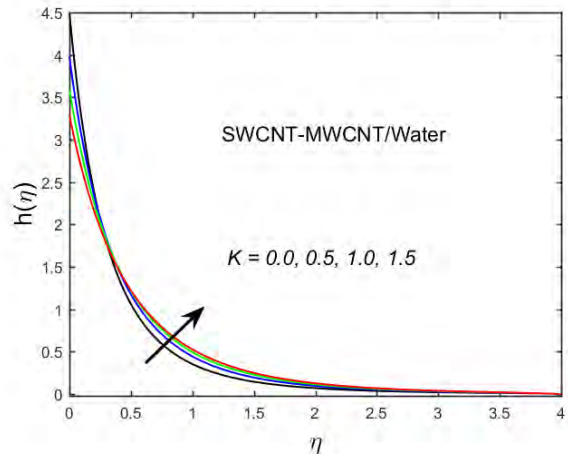

(a)   *(b)*

Fig. 7.2: Vertical velocity variation (a) with A (b) with λ .

(a)

(b)
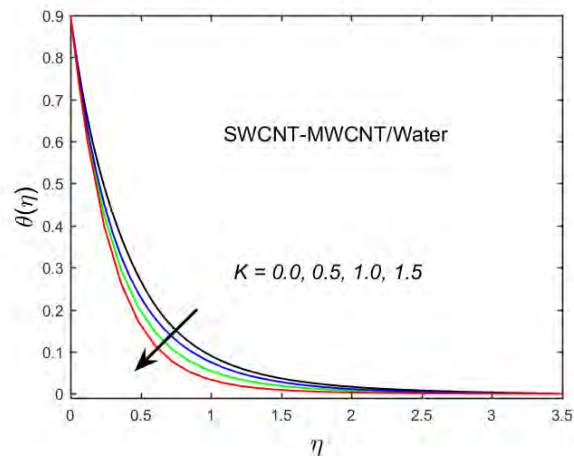
(c)

Fig. 7.3: Velocity, micro-rotation and temperature variation with K .

(a)
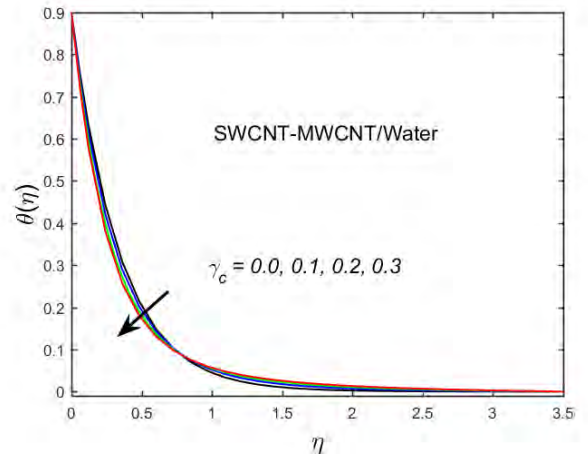
(b)

Fig. 7.4: Velocity and temperature variation (a) with P_m (b) with γ_c.

(a)

(b)

(c)
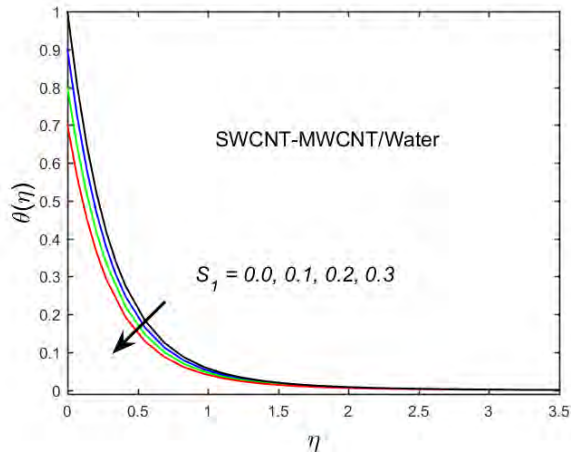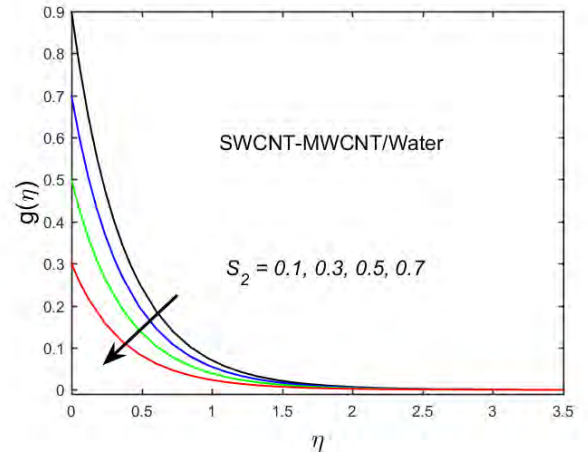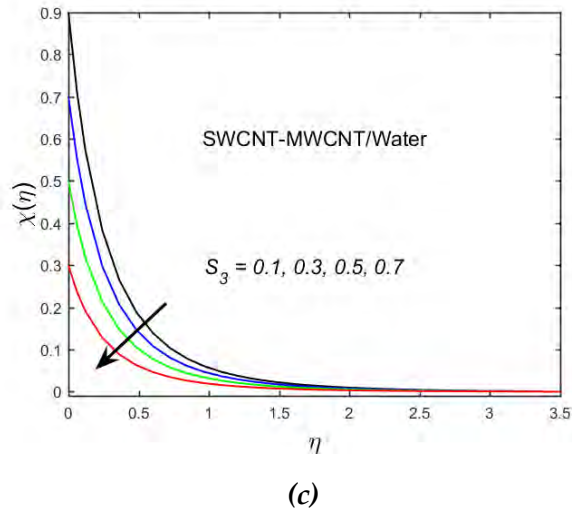
Fig. 7.5: Temperature, concentration, and microorganism variation (a) with S_1 (b) with S_2 (c) with S_3.

(a)

(b)
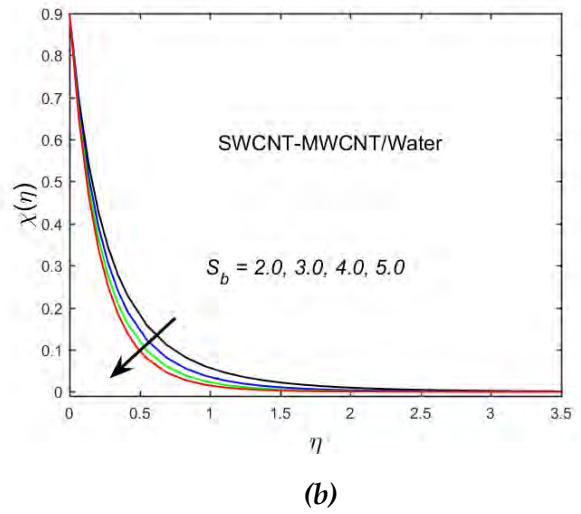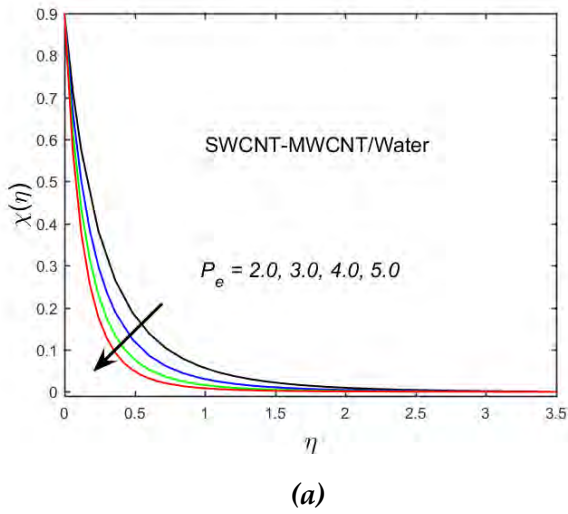
Fig. 7.6: Microorganism variation (a) with P_e (b) with S_b.

(a)

(b)

(c)
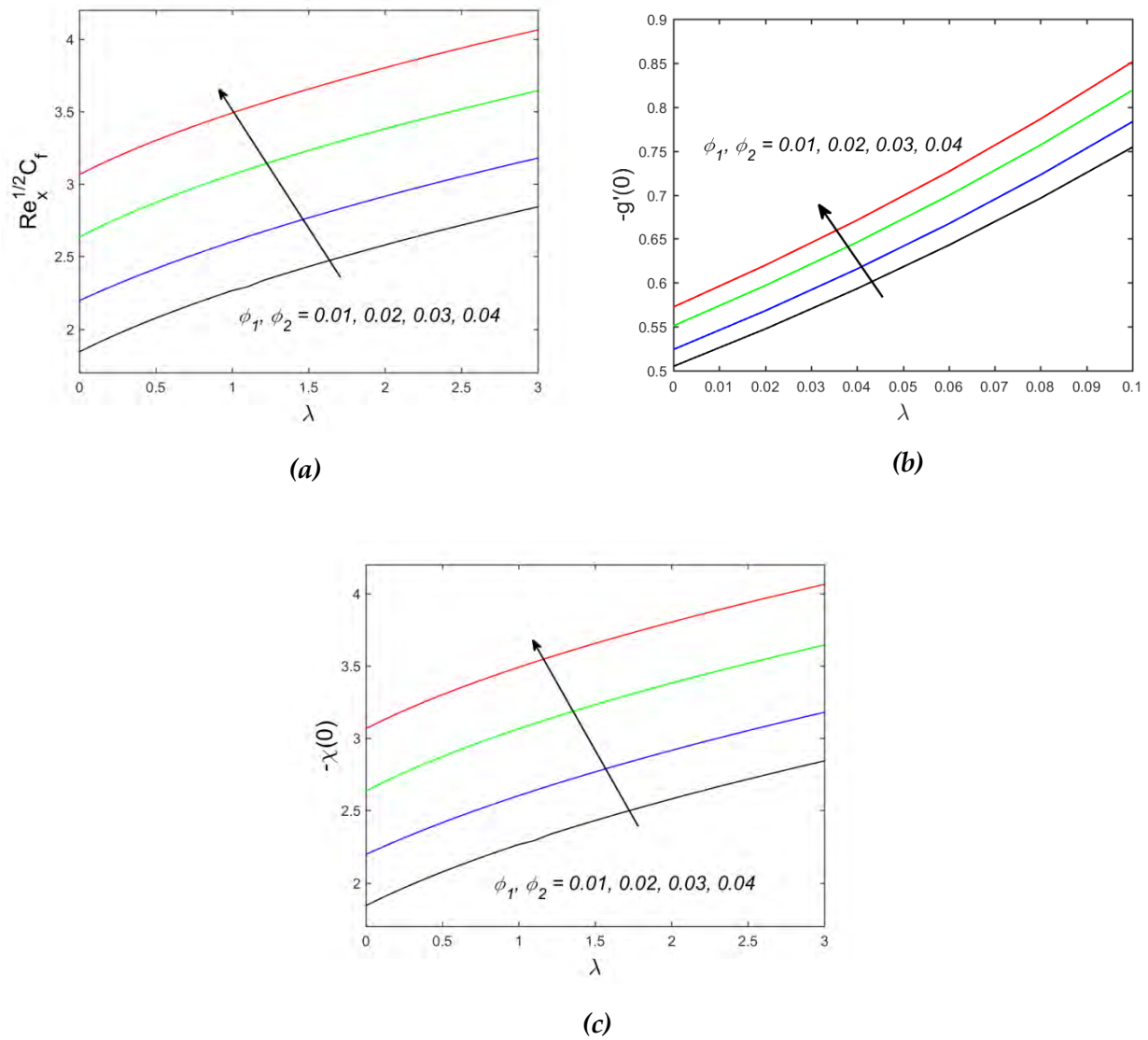
Fig. 7.7: Skin friction, local Sherwood number, and local microorganism number variation with ϕ_1, ϕ_2 ***and with*** λ ***.***
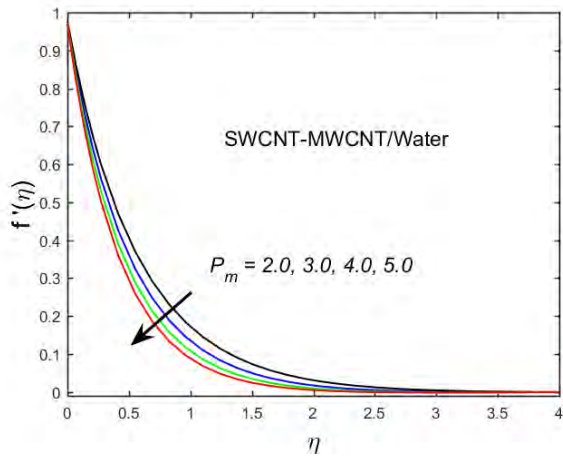
7.4 Concluding Remarks

The main finding of the present result as given below:

➢ The solid volume fraction parameter show dual behavior on linear and angular velocity while microorganism and concentration field diminishes.

➢ The temperature profile is a boosting function of solid volume fraction.

➢ The $\theta(\eta)$ shows the decreasing behavior for S_1, and K.

➢ Improving the values of solutal stratification parameter and Schmidt number, the concentration field decay while improves for activation energy parameter.

➢ As rises the Peclet number, bio - convection Schmidt number, and microorganism stratification parameters, the microorganism field decreases.

➢ The drag force, local Sherwood and microorganism number show growing performance as growing solid volume fraction and stretching parameter.

References

1. Choi, S. U., & Eastman, J. A. (1995). *Enhancing thermal conductivity of fluids with nanoparticles* (No. ANL/MSD/CP-84938; CONF-951135-29). Argonne National Lab., IL (United States).

2. Saleem, S., Qasim, M., Alderremy, A., & Noreen, S. (2020). Heat transfer enhancement using different shapes of Cu nanoparticles in the flow of water based nanofluid. *Physica Scripta*, *95*(5), 055209.

3. Lu, D., Ramzan, M., Ahmad, S., Chung, J. D., & Farooq, U. (2017). Upshot of binary chemical reaction and activation energy on carbon nanotubes with Cattaneo-Christov heat flux and buoyancy effects. *Physics of fluids*, *29*(12), 123103.

4. Hussain, S. T., Khan, Z. H., & Nadeem, S. (2016). Water driven flow of carbon nanotubes in a rotating channel. *Journal of Molecular Liquids*, *214*, 136-144.

5. Shahzadi, I., Nadeem, S., & Rabiei, F. (2017). Simultaneous effects of single wall carbon nanotube and effective variable viscosity for peristaltic flow through annulus having permeable walls. *Results in physics*, *7*, 667-676.

6. Sheikholeslami, M., M. Jafaryar, Ahmad Shafee, and Zhixiong Li. "Simulation of nanoparticles application for expediting melting of PCM inside a finned enclosure." *Physica A: Statistical Mechanics and its Applications* 523 (2019): 544-556.

7. Diglio, G., Roselli, C., Sasso, M., & Channabasappa, U. J. (2018). Borehole heat exchanger with nanofluids as heat carrier. *Geothermics*, *72*, 112-123.

8. Ahmed, Z., Nadeem, S., Saleem, S., & Ellahi, R. (2019). Numerical study of unsteady flow and heat transfer CNT-based MHD nanofluid with variable viscosity over a permeable shrinking surface. *International Journal of Numerical Methods for Heat & Fluid Flow*.

9. Akbar, N. S., Khan, Z. H., & Nadeem, S. (2014). The combined effects of slip and convective boundary conditions on stagnation-point flow of CNT suspended nanofluid over a stretching sheet. *Journal of Molecular Liquids*, *196*, 21-25.

10. Haq, R. U., Nadeem, S., Khan, Z. H., & Noor, N. F. M. (2015). Convective heat transfer in MHD slip flow over a stretching surface in the presence of carbon nanotubes. *Physica B: condensed matter*, *457*, 40-47.

11. Nasir, S., Islam, S., Gul, T., Shah, Z., Khan, M. A., Khan, W., Khan, A.Z., & Khan, S. (2018). Three-dimensional rotating flow of MHD single wall carbon nanotubes over a stretching sheet in presence of thermal radiation. *Applied Nanoscience*, *8*(6), 1361-1378.

12. Saba, F., Ahmed, N., Hussain, S., Khan, U., Mohyud-Din, S. T., & Darus, M. (2018). Thermal analysis of nanofluid flow over a curved stretching surface suspended by carbon nanotubes with internal heat generation. *Applied Sciences*, *8*(3), 395.

13. Chen, L. F., Cheng, M., Yang, D. J., & Yang, L. (2014). Enhanced thermal conductivity of nanofluid by synergistic effect of multi-walled carbon nanotubes and Fe2O3 nanoparticles. In *Applied mechanics and materials* (Vol. 548, pp. 118-123). Trans Tech Publications Ltd.

14. Madhesh, D., Parameshwaran, R., & Kalaiselvam, S. (2014). Experimental investigation on convective heat transfer and rheological characteristics of Cu–TiO2 hybrid nanofluids. *Experimental Thermal and Fluid Science*, *52*, 104-115.

15. Sundar, L. S., Singh, M. K., & Sousa, A. C. (2014). Enhanced heat transfer and friction factor of MWCNT–Fe3O4/water hybrid nanofluids. *International Communications in Heat and Mass Transfer*, *52*, 73-83.

16. Zadkhast, M., Toghraie, D., & Karimipour, A. (2017). Developing a new correlation to estimate the thermal conductivity of MWCNT-CuO/water hybrid nanofluid via an experimental investigation. *Journal of Thermal Analysis and Calorimetry*, *129*(2), 859-867.

17. Nadeem, S., Hayat, T., & Khan, A. U. (2019). Numerical study of 3D rotating hybrid SWCNT–MWCNT flow over a convectively heated stretching surface with heat generation/absorption. *Physica Scripta*, *94*(7), 075202.

18. Farooq, M., Ahmad, S., Javed, M., & Anjum, A. (2018). Chemically reactive species in squeezed flow through modified Fourier's and Fick's laws. *The European Physical Journal Plus*, *133*(2), 1-18.

19. Alamri, S. Z., Khan, A. A., Azeez, M., & Ellahi, R. (2019). Effects of mass transfer on MHD second grade fluid towards stretching cylinder: a novel perspective of Cattaneo–Christov heat flux model. *Physics Letters A*, *383*(2-3), 276-281.

20. Cattaneo, C. (1948). Sulla conduzione del calore. *Atti Sem. Mat. Fis. Univ. Modena*, *3*, 83-101.

21. Christov, C. I. (2009). On frame indifferent formulation of the Maxwell–Cattaneo model of finite-speed heat conduction. *Mechanics Research Communications*, *36*(4), 481-486.

22. Shah, Z., Tassaddiq, A., Islam, S., Alklaibi, A. M., & Khan, I. (2019). Cattaneo–Christov heat flux model for three-dimensional rotating flow of SWCNT and MWCNT Nanofluid with Darcy–Forchheimer porous medium induced by a linearly stretchable surface. *Symmetry*, *11*(3), 331.

23. Han, S., Zheng, L., Li, C., & Zhang, X. (2014). Coupled flow and heat transfer in viscoelastic fluid with Cattaneo–Christov heat flux model. *Applied Mathematics Letters*, *38*, 87-93.

24. Nadeem, S., Ahmad, S., Muhammad, N., & Mustafa, M. T. (2017). Chemically reactive species in the flow of a Maxwell fluid. *Results in physics*, *7*, 2607-2613.

25. Khan, U., Ahmad, S., Ramzan, M., Suleman, M., Lu, D., & Inam, S. (2019). Numerical simulation of Darcy–Forchheimer 3D unsteady nanofluid flow comprising carbon nanotubes with Cattaneo–Christov heat flux and velocity and thermal slip conditions. *Processes*, *7*(10), 687.

26. Tulu, A., & Ibrahim, W. (2020). MHD slip flow of CNT-ethylene glycol nanofluid due to a stretchable rotating disk with cattaneo–christov heat flux model. *Mathematical Problems in Engineering*, *2020*.

27. Tibullo, V., & Zampoli, V. (2011). A uniqueness result for the Cattaneo–Christov heat conduction model applied to incompressible fluids. *Mechanics Research Communications*, *38*(1), 77-79.

28. Kundu, P. K., Chakraborty, T., & Das, K. (2018). Framing the Cattaneo–Christov heat flux Phenomena on CNT-based Maxwell Nanofluid along stretching sheet with multiple slips. *Arabian Journal for Science and Engineering*, *43*(3), 1177-1188.

29. Makinde, O. D., Nagendramma, V., Raju, C. S., & Leelarathnam, A. (2017). Effects of Cattaneo-Christov heat flux on Casson nanofluid flow past a stretching cylinder. In *Defect and Diffusion Forum* (Vol. 378, pp. 28-38). Trans Tech Publications Ltd.

30. Gangadhar, K., Ramana, K. V., Makinde, O. D., & Kumar, B. R. (2018). MHD flow of a Carreau fluid past a stretching cylinder with Cattaneo-Christov heat flux using spectral relaxation method. In *Defect and Diffusion Forum* (Vol. 387, pp. 91-105). Trans Tech Publications Ltd.

31. Hayat, T., Qayyum, S., Imtiaz, M., & Alsaedi, A. (2017). Flow between two stretchable rotating disks with Cattaneo-Christov heat flux model. *Results in Physics*, *7*, 126-133.

32. Kumari, M., & Nath, G. (1984). Unsteady incompressible boundary layer flow of a micropolar fluid at a stagnation point. *International journal of engineering science*, *22*(6), 755-768.

33. Eringen, A. C. (2001). *Microcontinuum field theories: II. Fluent media* (Vol. 2). Springer Science & Business Media.

34. Lukaszewicz, G. (1999). *Micropolar fluids: theory and applications*. Springer Science & Business Media.

35. Nadeem, Sohail, Muhammad Naveed Khan, Noor Muhammad, and Shafiq Ahmad. "Mathematical analysis of bio-convective micropolar nanofluid." *Journal of Computational Design and Engineering* 6, no. 3 (2019): 233-242.

36. Nadeem, S., Rehman, A., Vajravelu, K., Lee, J., & Lee, C. (2012). Axisymmetric stagnation flow of a micropolar nanofluid in a moving cylinder. *Mathematical Problems in Engineering*, *2012*.

37. Balaram, M., & Sastri, V. U. K. (1973). Micropolar free convection flow. *International Journal of Heat and Mass Transfer*, *16*(2), 437-441.

38. Das, K. (2012). Slip effects on MHD mixed convection stagnation point flow of a micropolar fluid towards a shrinking vertical sheet. *Computers & Mathematics with Applications*, *63*(1), 255-267.

39. Maleki, H., Safaei, M. R., Alrashed, A. A., & Kasaeian, A. (2019). Flow and heat transfer in non-Newtonian nanofluids over porous surfaces. *Journal of Thermal Analysis and Calorimetry*, *135*(3), 1655-1666.

40. Senthil, K., Kalainathan, S., & Kumar, A. R. (2014). Bulk size crystal growth, spectral, optical, luminescence, thermal, mechanical, and dielectric properties of organic single crystal. *Journal of Thermal Analysis and Calorimetry*, *118*(1), 323-331.

41. Heydari, A., Akbari, O. A., Safaei, M. R., Derakhshani, M., Alrashed, A. A., Mashayekhi, R., ... & Nguyen, T. K. (2018). The effect of attack angle of triangular ribs on heat transfer of nanofluids in a microchannel. *Journal of Thermal Analysis and Calorimetry*, *131*(3), 2893-2912.

42. Alfvén, H. (1942). Existence of electromagnetic-hydrodynamic waves. *Nature*, *150*(3805), 405-406.

43. Ellahi, R., Alamri, S. Z., Basit, A., & Majeed, A. (2018). Effects of MHD and slip on heat transfer boundary layer flow over a moving plate based on specific entropy generation. *Journal of Taibah University for Science*, *12*(4), 476-482.

44. Ellahi, R., Bhatti, M. M., & Pop, I. (2016). Effects of hall and ion slip on MHD peristaltic flow of Jeffrey fluid in a non-uniform rectangular duct. *International journal of numerical methods for heat & fluid flow*.

45. Sheikholeslami, M., Shafee, A., Zareei, A., Haq, R. U., & Li, Z. (2019). Heat transfer of magnetic nanoparticles through porous media including exergy analysis. *Journal of Molecular Liquids*, *279*, 719-732.

46. Waqas, M., Farooq, M., Khan, M. I., Alsaedi, A., Hayat, T., & Yasmeen, T. (2016). Magnetohydrodynamic (MHD) mixed convection flow of micropolar liquid due to nonlinear stretched sheet with convective condition. *International Journal of Heat and Mass Transfer*, *102*, 766-772.

47. Ishak, A., Nazar, R., & Pop, I. (2008). Magnetohydrodynamic (MHD) flow and heat transfer due to a stretching cylinder. *Energy Conversion and Management*, *49*(11), 3265-3269.

48. Sheikholeslami, M., Ganji, D. D., Javed, M. Y., & Ellahi, R. (2015). Effect of thermal radiation on magnetohydrodynamics nanofluid flow and heat transfer by means of two phase model. *Journal of Magnetism and Magnetic Materials*, *374*, 36-43.

49. Haq, R. U., Nadeem, S., Khan, Z. H., & Akbar, N. S. (2015). Thermal radiation and slip effects on MHD stagnation point flow of nanofluid over a stretching sheet. *Physica E: Low-dimensional Systems and Nanostructures*, *65*, 17-23.

50. Nadeem, S., Haq, R. U., & Akbar, N. S. (2013). MHD three-dimensional boundary layer flow of Casson nanofluid past a linearly stretching sheet with convective boundary condition. *IEEE Transactions on Nanotechnology*, *13*(1), 109-115.

51. Su, X. H., & Zheng, L. C. (2011). Approximate solutions to MHD Falkner-Skan flow over permeable wall. *Applied Mathematics and Mechanics*, *32*(4), 401-408.

52. Yousif, M. A., Ismael, H. F., Abbas, T., & Ellahi, R. (2019). Numerical study of momentum and heat transfer of MHD Carreau nanofluid over an exponentially stretched plate with internal heat source/sink and radiation. *Heat Transfer Research*, *50*(7).

53. Bejan, A. (1979). A study of entropy generation in fundamental convective heat transfer. *Journal of heat transfer*, 718-725.

54. Bejan, A., & Kestin, J. (1983). Entropy generation through heat and fluid flow. *Journal of Applied Mechanics*, 475-475.

55. Bhatti, M. M., Sheikholeslami, M., Shahid, A., Hassan, M., & Abbas, T. (2019). Entropy generation on the interaction of nanoparticles over a stretched surface with thermal radiation. *Colloids and Surfaces A: Physicochemical and Engineering Aspects*, *570*, 368-376.

56. Feroz, N., Shah, Z., Islam, S., Alzahrani, E. O., & Khan, W. (2019). Entropy generation of carbon nanotubes flow in a rotating channel with hall and ion-slip effect using effective thermal conductivity model. *Entropy*, *21*(1), 52.

57. Shahsavar, A., Sardari, P. T., & Toghraie, D. (2019). Free convection heat transfer and entropy generation analysis of water-Fe3O4/CNT hybrid nanofluid in a concentric annulus. *International Journal of Numerical Methods for Heat & Fluid Flow*.

58. Hussien, A. A., Abdullah, M. Z., Yusop, N. M., Al-Kouz, W., Mahmoudi, E., & Mehrali, M. (2019). Heat transfer and entropy generation abilities of MWCNTs/GNPs hybrid nanofluids in microtubes. *Entropy*, *21*(5), 480.

59. Ellahi, R., Alamri, S. Z., Basit, A., & Majeed, A. (2018). Effects of MHD and slip on heat transfer boundary layer flow over a moving plate based on specific entropy generation. *Journal of Taibah University for Science*, *12*(4), 476-482.

60. Lu, D., Ramzan, M., Ahmad, S., Shafee, A., & Suleman, M. (2018). Impact of nonlinear thermal radiation and entropy optimization coatings with hybrid nanoliquid flow past a curved stretched surface. *Coatings*, *8*(12), 430.

61. Abbas, S. Z., Khan, M. I., Kadry, S., Khan, W. A., Israr-Ur-Rehman, M., & Waqas, M. (2020). Fully developed entropy optimized second order velocity slip MHD nanofluid flow with activation energy. *Computer methods and programs in biomedicine*, *190*, 105362.

62. Wang, J., Muhammad, R., Khan, M. I., Khan, W. A., & Abbas, S. Z. (2020). Entropy optimized MHD nanomaterial flow subject to variable thicked surface. *Computer methods and programs in biomedicine*, *189*, 105311.

63. Khan, M. I., Qayyum, S., Kadry, S., Khan, W. A., & Abbas, S. Z. (2020). Theoretical investigations of entropy optimization in electro-magneto nonlinear mixed convective second order slip flow. *Journal of Magnetics*, *25*(1), 8-14.

64. Merkin, J. H. (1994). Natural-convection boundary-layer flow on a vertical surface with Newtonian heating. *International Journal of Heat and Fluid Flow*, *15*(5), 392-398.

65. Lesnic, D., Ingham, D. B., & Pop, I. (1999). Free convection boundary-layer flow along a vertical surface in a porous medium with Newtonian heating. *International Journal of Heat and Mass Transfer*, *42*(14), 2621-2627.

66. Lesnic, D., Ingham, D. B., & Pop, I. (2000). Free convection from a horizontal surface in a porous medium with Newtonian heating. *Journal of Porous Media*, *3*(3).

67. Pop, I., Lesnic, D., & Ingham, D. B. (2000). Asymptotic solutions for the free convection boundary-layer flow along a vertical surface in a porous medium with Newtonian heating. *Hybrid Methods in Engineering*, *2*(1).

68. Nadeem, S., Ahmad, S., & Muhammad, N. (2017). Cattaneo-Christov flux in the flow of a viscoelastic fluid in the presence of Newtonian heating. *Journal of Molecular liquids*, *237*, 180-184.

69. Suleman, M., Ramzan, M., Ahmad, S., Lu, D., Muhammad, T., & Chung, J. D. (2019). A numerical simulation of silver–water nanofluid flow with impacts of newtonian heating and homogeneous–heterogeneous reactions past a nonlinear stretched cylinder. *Symmetry*, *11*(2), 295.

70. Xue, Q. Z. (2005). Model for thermal conductivity of carbon nanotube-based composites. *Physica B: Condensed Matter*, *368*(1-4), 302-307.

71. Yacob, N. A., Ishak, A., & Pop, I. (2011). Falkner–Skan problem for a static or moving wedge in nanofluids. *International Journal of Thermal Sciences*, *50*(2), 133-139.

72. Nadeem, S., Ahmad, S., & Muhammad, N. (2018). Computational study of Falkner-Skan problem for a static and moving wedge. *Sensors and Actuators B: Chemical*, *263*, 69-76.

73. Zaib, A., & Haq, R. U. (2019). Magnetohydrodynamics mixed convective flow driven through a static wedge including TiO2 nanomaterial with micropolar liquid: Similarity dual solutions via finite difference method. *Proceedings of the Institution of Mechanical Engineers, Part C: Journal of Mechanical Engineering Science*, *233*(16), 5813-5825.

74. Yih, K. A. (1999). MHD forced convection flow adjacent to a non-isothermal wedge. *International Communications in Heat and Mass Transfer*, *26*(6), 819-827.

75. Abbas, Z., Sheikh, M., Hasnain, J., Ayaz, H., & Nadeem, A. (2019). Numerical aspects of Thomson and Troian boundary conditions in a Tiwari–Das nanofluid model with homogeneous–heterogeneous reactions. *Physica Scripta*, *94*(11), 115220.

Turnitin Originality Report

CNTs based nanofluids over a stretchable surface   by Shafiq Ahmad .

From DRSM (DRSM L)

- Processed on 20-Oct-2021 11:54 PKT
- ID: 1678905179
- Word Count: 19109

Similarity Index
16%
Similarity by Source

Internet Sources:
  10%
Publications:
  13%
Student Papers:
  2%

Focal Person (Turnitin)
Quaid-i-Azam University
Islamabad

---

sources:

---

1   < 1% match (Internet from 09-Apr-2021)
https://iopscience.iop.org/article/10.1088/1402-4896/abcc9d

---

2   < 1% match (Internet from 08-Jan-2020)
https://iopscience.iop.org/article/10.1088/1402-4896/ab4067

---

3   < 1% match (Internet from 28-Sep-2021)
https://iopscience.iop.org/article/10.1088/1402-4896/abd790

---

4   < 1% match (Internet from 09-Apr-2020)
https://iopscience.iop.org/article/10.1088/1402-4896/ab5a36

---

5   < 1% match (Internet from 24-Apr-2020)
https://iopscience.iop.org/article/10.1088/1402-4896/ab03a8

---

6   < 1% match (Internet from 10-Mar-2021)
https://iopscience.iop.org/article/10.1088/2399-6528/aaafff

---

7   < 1% match (Internet from 16-Aug-2021)
https://iopscience.iop.org/article/10.1088/1402-4896/abbf1e

---

8   < 1% match (Internet from 13-Oct-2021)
https://iopscience.iop.org/article/10.1088/1402-4896/abd441

---

9   < 1% match (Internet from 25-Aug-2020)
https://www.hindawi.com/journals/jnm/2015/934367/

---

10   < 1% match (Internet from 05-Oct-2021)
https://www.hindawi.com/journals/aaa/2014/261630/

---

11   < 1% match (Internet from 25-Aug-2021)
https://www.hindawi.com/journals/sv/2021/9918988/

---

12   < 1% match (Internet from 10-Jun-2021)
https://www.hindawi.com/journals/mpe/2021/8407194/

---

13   < 1% match (Internet from 07-Oct-2020)
https://www.hindawi.com/journals/mpe/2013/632394/

---

14   < 1% match (Internet from 06-Aug-2021)
https://www.hindawi.com/journals/mpe/2021/6618395/

---

15   < 1% match (publications)
"Advances in Fluid Dynamics", Springer Science and Business Media LLC, 2021